LUMINESCENCE CHARACTERISTICS OF Te- AND

Bi-DOPED GLASSES AND GLASS-CERAMICS

Sasithorn Khonthon

A Thesis Submitted in Partial Fulfillment of the Requirements for the

Degree of Doctor of Philosophy in Ceramic Engineering

Suranaree University of Technology

Academic Year 2008

ลักษณะการเรืองแสงของแก้วและแก้วเซรามิกที่โด๊ปด้วยเทลลูเรียมและบิสมัท

นางสาวศศิธร คนทน

LUMINESCENCE CHARACTERISTICS OF Te- AND Bi-DOPED GLASSES AND GLASS-CERAMICS

Suranaree University of Technology has approved this thesis submitted in partial fulfillment of the requirements for the Degree of Doctor of Philosophy

Thesis Examining Committee

_____

(Assoc. Prof. Dr. Sutin Kuharuangrong)

Chairperson

_____

(Asst. Prof. Dr. Shigeki Morimoto)

Member (Thesis Advisor)

_____

(Asst. Prof. Dr. Sirithan Jiemsirilers)

Member

_____

(Assoc. Prof. Dr. Charussri Lorprayoon)

Member

_____

(Dr. Veerayuth Lorprayoon)

Member

_____   _____

(Prof. Dr. Pairote Sattayatham)   (Assoc. Prof. Dr. Vorapot Khompis)

Vice Rector for Academic Affairs   Dean of Institute of Engineering

ศศิธร คนทน : ลักษณะการเรืองแสงของแก้วและแก้วเซรามิกที่โด๊ปด้วยเทลลูเรียมและ บิสมัท (LUMINESCENCE CHARACTERISTICS OF Te- AND Bi-DOPED GLASSES AND GLASS-CERAMICS) อาจารย์ที่ปรึกษา : ผู้ช่วยศาสตราจารย์ ดร.ชิเกกิ โมริโมโต, 110 หน้า.

การศึกษาศูนย์กลางสี ศูนย์กลางการเรืองแสงใกล้รังสีใต้แดง (Near Infrared) และลักษณะ เฉพาะการเรืองแสงใกล้รังสีใต้แดงของแก้วและแก้วเซรามิกที่มีเทลลูเรียมและบิสมัท ตามหลัก สมดุลของปฏิกิริยารีดอกซ์ โดยเน้นศึกษาปัจจัยที่มีผลต่อสมดุลของปฏิกิริยารีดอกซ์ ซึ่งได้แก่ อุณหภูมิในการหลอม ส่วนผสมและการเติมสารช่วยรีดิวส์ (คาร์บอน) ในแก้วบอเรตและแก้วโซดา ไลม์ซิลิเกตที่มีบิสมัท

การศึกษาพบว่าสมดุลของปฏิกิริยารีดอกซ์มีผลอย่างมากต่อการเกิดศูนย์กลางสี ศูนย์กลาง การเรืองแสงใกล้รังสีใต้แดง และลักษณะเฉพาะการเรืองแสงใกล้รังสีใต้แดงของแก้วและแก้วเซรา มิกที่มีบิสมัทและเทลลูเรียม ในสภาวะออกซิไดซ์ ศูนย์กลางสีและศูนย์กลางการเรืองแสงใกล้รังสี ใต้แดงจะไม่เกิดขึ้น ทำให้การเรืองแสงใกล้รังสีใต้แดงไม่สามารถตรวจพบได้ ในทางตรงกันข้าม ในสภาวะรีดิวส์ เกิดสีเข้มขึ้น เนื่องจากการเกิดคอลลอยด์ของโลหะบิสมัท และไม่พบการเรืองแสง ใกล้รังสีใต้แดง เพราะฉะนั้นศูนย์กลางสีและศูนย์กลางการเรืองแสงใกล้รังสีใต้แดงจึงสามารถเกิด ได้ภายใต้สภาวะรีดิวส์อ่อนถึงปานกลางโดยพบการเรืองแสงใกล้รังสีใต้แดงอยู่ที่ประมาณ 1100-1300 นาโนเมตร ซึ่งศูนย์กลางสีและศูนย์กลางการเรืองแสงใกล้รังสีใต้แดงในแก้วที่มีเทลลูเรียม และบิสมัทน่าจะเป็นผลมาจากการเกาะกลุ่มของเทลลูเรียมและบิสมัทหรือกลุ่มของเทลลูเรียมและ บิสมัทที่สูญเสียอิเลคตรอน เช่น Te_2, Te_2^-, Bi_2, Bi_3, Bi_2^- เป็นต้น

การศึกษาครั้งนี้ เป็นครั้งแรกที่ได้พบวัสดุที่มีการเรืองแสงใกล้รังสีใต้แดงชนิดใหม่ในแก้ว และแก้วเซรามิกที่เติมเทลลูเรียม

สาขาวิชาวิศวกรรมเซรามิก	ลายมือชื่อนักศึกษา _____
ปีการศึกษา 2551	ลายมือชื่ออาจารย์ที่ปรึกษา _____

SASITHORN KHONTHON : LUMINESCENCE CHARACTERISTICS OF Te- AND Bi-DOPED GLASSES AND GLASS-CERAMICS. THESIS ADVISOR : ASST. PROF. SHIGEKI MORIMOTO, Ph.D., 110 PP.

NIR LUMINESCENCE CENTER/Te-DOPED GLASSES/Bi-DOPED GLASSES/ GLASS-CERAMICS/REDOX EQUILIBRIUM

The color center, near-infrared (NIR) luminescent center and NIR luminescent characteristics of Te- and Bi-containing glasses and glass-ceramics were investigated based on redox equilibrium. Particularly, the factors affecting the redox equilibrium, melting temperature, glass composition and addition of reducing agents (carbon), were investigated in detail in Bi-containing borate glasses and soda-lime-silicate glasses.

It was found that the formation of color center and NIR luminescent center and luminescent characteristic of Te- and Bi-containing glasses and glass-ceramics were strongly affected by redox equilibrium. In oxidized side, color center and NIR luminescent center were not formed, and hence NIR luminescence could not be detected. On the contrary, the darkening effect due to formation process of Bi metallic colloids, took place in strong reduced side, and also NIR luminescence was not observed. Therefore, the color center and NIR luminescent center can be formed under mild to medium reducing condition and the NIR luminescence centered at around 1100-1300 nm can be detected.

It is suggested that the color center and luminescent center in Te- and Bi-containing glasses is likely to be caused by Te- and Bi-clusters or electron trapped Te- and Bi-clusters, such as Te_2, Te_2^-, Bi_2, Bi_3, Bi_2^-, etc

New type NIR luminescent materials of Te-doped glasses and glass-ceramics which exhibit broad NIR luminescence were discovered for the first time to our knowledge.

School of <u>Ceramic Engineering</u>   Student's Signature _____

Academic Year 2008   Advisor's Signature _____

ACKNOWLEDGEMENTS

I would like to express my thanks and appreciation to my advisor, Asst. Prof. Dr. Shigeki Morimoto, for his consistent supervision, comments on several drafts and advices towards the completion of this study.

I would like to express my gratitude to all the teachers of the School of Ceramic Engineering for giving me good opportunity to study. I wish to express my special thanks to Dr.Veerayuth Lorprayoon and Assoc. Prof. Dr.Charussri Lorprayoon for their advice when I have any problem.

I also would like to thanks Dr.Yusuke Arai and Prof.Dr.Yasutake Ohishi, Research center for Advanced Photon Technology, Toyota Technological Institute, Nagoya, Japan, for NIR luminescence measurement.

Finally, most important, I appreciate the encouragement and support of family and also thank Mr.Chokchai Yatongchai and Ms.Pannee Lawudomphan for their help throughout my studying life at SUT.

Sasithorn Khonthon

TABLE OF CONTENTS

TABLE OF CONTENTS (Continued)

TABLE OF CONTENTS (Continued)

TABLE OF CONTENTS (Continued)

TABLE OF CONTENTS (Continued)

LIST OF TABLES

LIST OF FIGURES

LIST OF FIGURES (Continued)

LIST OF FIGURES (Continued)

FIGURE   **PAGE**

CHAPTER I

INTRODUCTION

Owing to rapid increase of information traffic in the telecommunication network, the development of the wavelength-division-multiplexing (WDM) network system becomes important. WDM point-to-point systems provide very large capacity between widely spaced (300 to 600 km) end terminals, in many network it is necessary to drop some traffic and decrease the capacity of the process (Trigg, 2006). Therefore, device for the WDM optical communication system, amplifiers and tunable lasers should be a key material, because the number of channels depends on the gain bandwidth of the amplifiers and tunable lasers source. In order to develop broadband amplifiers and broadly tunable laser sources for the efficient wavelength-division multiplexing system, it gradually becomes important to explore and synthesize new luminescent materials with larger FWHM (full widths at half maximum) emission in the telecommunication wavelength region, to fully utilize the wide window of silica glass fiber in the range of 1.2–1.65 µm (NIR) (Ren et al., 2007). Considerable efforts have been devoted to rare earth ions- and transition metal ions-doped materials.

Many attempts have been made on broadening and flattening of gain spectra of optical fiber amplifiers such as Er^{3+}-doped fiber amplifiers (EDFAs) has broadband light source operating in the 1.55 µm telecommunication band (wikipedia, WWW, 2007), Tm^{3+}-doped fiber amplifiers (TDFAs) can work in the range of 1.45-

1.50 µm (Sakamoto et al., 1995). Broadband tunable lasers such as $Ti^{3+}:Al_2O_3$ (Sapphire) is the most widely used crystal for wavelengths tunable lasers. It can be lased over the entire band from 600 to 1100 nm (VIS-NIR region) (Albrecht, Eggleston and Ewing, 1985), $Cr^{4+}:Y_3Al_5O_{12}(YAG)$ shows the output in the 1.2-1.5 µm (NIR region) at room temperature (Sorokina et al., 1999), $Cr^{4+}:MgSiO_4$ crystal can generate near infrared emission at 1.2-1.6 µm (Petricevic, Gayen, and Alfano, 1988) and were realized by using transition metal ions as active ions. The Ni^{2+} ion-doped Spinel transparent glass-ceramics is also promising materials as broad band near infrared tunable lasers (Suzuki, Murugan, and Ohishi, 2005 and Khonthon, Morimoto, and Ohishi, 2006)

Recently, Fujimoto and Nakatsuka (2001) discovered a new infrared luminescence from a Bi-doped silica glass with long life time. The spectroscopic properties of this new Bi-doped silica glass are different from previous Bi-luminescent materials (Blasse, 1997), and 1250 nm wide band luminescence is useful for optical amplifier of telecommunication with optical fiber. They proposed that this near infrared luminescence comes from Bi^{5+} ions, on the contrary Peng et al. (2004, 2005, 2007) estimated to be due to BiO or Bi cluster (molecule). The origin of NIR luminescence from Bi-doped glasses and glass-ceramics is still unknown.

Generally, the luminescence is the phenomenon in which the materials absorb the energy and emits UV-VIS and NIR light subsequently. In this process, the absorption center (color center) is regarded also as luminescence center. Luminescence is due to the addition of a luminogen or activator in the form of trace impurities such as transition metal or rare earth ions. In some case crystal lattice

defects provide localized level, like those of impurity, which play the part of the activator (Curie, 1963).

In addition, glass coloration in visible region is usually induced by impurities, such as transition metal ions, rare earth ions, nanometer sized semiconductor and metal particles. There are numerous other sources of visible coloration in glasses which are of interest. Included in this group are blue sulfur (S), pink-selenium (Se), and purple or green-tellurium (Te) glasses whose colors are associated with elemental clustering (Sigel, 1977).

The findings from elemental clustering reveal that the luminescence from sulfur was found in UV-VIS region but not in NIR region, and color centers of sulfur are S_2, S_2^- (Ahmed, Sharaf, and Codreate, 1997, Kowalak and Jankowska, 2003 and Asahi, 2006). Selenium has similar luminescent characteristics to sulfur and the color centers of selenium are Se_2, Se_2^- (Paul, 1975 and Guha, Leppert, and Risbud, 1998). Tellurium was found to have luminescence in UV-VIS region but no information in the NIR region and the color centers of tellurium are Te_2, Te_2^- and Te-metallic colloids (Lindner et al., 1996 and Konishi et al., 2003).

As mentioned previously, the new NIR luminescent materials, Bi-doped silica glass, have been discovered but its color center and luminescent center is still unknown. On the contrary, the color center of Te-doped glasses and crystals have been already identified, however, the NIR luminescence from Te-doped glasses and crystals has not been discovered yet.

Therefore, this research focuses the luminescence characteristics of Te- and Bi-doped glasses and glass-ceramics in relation to valence state and preparation conditions.

1.1   Research objective

The objectives of this research are to focus on the relationship between the change in valence state and accompanying optical properties such as the formation of color center and luminescent center of TeO_2 and Bi_2O_3 containing glasses and glass-ceramics.

1.   To investigate the relationship between valence state of Te and Bi ions and preparation conditions.

2.   To determine the optimum preparation condition

Experimental subject

Preliminary Research

1.   Confirmation and determination of NIR luminescence of Te- and Bi-doped soda-lime-silicate, zinc tellurium phosphate, lithium disilicate, spinel and aluminum phosphate glasses and glass-ceramics.

2.   Identification of color center and luminescence center of Te- and Bi-doped soda-lime-silicate, zinc tellurium phosphate, lithium disilicate, spinel and aluminum phosphate glasses and glass-ceramics.

Fundamental research.

Investigation of factors affecting on valence state and luminescence.

1.   Melting temperature.

   Bi: B_2O_3-Al_2O_3-ZnO-K_2O-Bi_2O_3 system of glass.

2.   Glass composition.

   Bi: B_2O_3-Al_2O_3-ZnO-K_2O-Bi_2O_3 system of glass.

3.   Reducing agent (Carbon addition).

   Bi: Soda-lime-silicate glass.

1.2   Scope and limitation of research

1.   Investigation of UV-VIS and NIR luminescence characteristics of Te- and Bi-clusters in glasses and glass-ceramics.

2.   Investigation of color center and NIR luminescence center of Te- and Bi-clusters in glasses and glass-ceramics.

3.   Investigation of formation of color center and NIR luminescence center of Te- and Bi-doped glasses and glass-ceramics based on redox reaction.

1.3   Expected results

1.   Establishment of basic technology for the preparation of elemental clustering of Te- and Bi-doped glasses and glass-ceramics.

2.   Identification of color center and luminescent center of Te- and Bi-doped glasses and glass-ceramics.

3.   Discovery of new NIR amplifiers and NIR tunable laser materials.

CHAPTER II

LITERATURE REVIEW

2.1   Luminescence

Luminescence is the emission of optical radiation (infrared, visible, or ultraviolet light) by matter. It represents the conversion of energy from one form to another, in this case, light. This phenomenon is to be distinguished from incandescence, which is the emission of radiation by a substance by virtue of its being at a high temperature (>500°C). Luminescence can occur in a wide variety of substances and under many different circumstances. Thus, atoms, various kinds of molecules, polymers, organic or inorganic crystals, amorphous substances or even biological units can luminesce under appropriate conditions. The common aspect to observe luminescence is when an atom or molecule emits a photon (a quantum of light), there is change in its electronic structure. When electrons are confined to a region of space that is defined by the position of the atomic centers of a molecule (or just the nucleus, in the case of an atom), a set of discrete energy levels is imposed on the system. In the case that some process delivers an appropriate amount of energy to the system, the electronic structure can be changed to an excited state. The release of this extra energy, and thus the way back to the initial state (ground state) can occur via the emission of a photon. Dependent on whether the spin quantum number of the electrons is change in the emission process or not, one may distinguish two different types of luminescence: fluorescence, in which emission occurs with no net change of

the spin quantum number, and phosphorescence, in which emission is accompanied by a change in the spin quantum number. These have the consequence that fluorescence is much shorter-lived (ca. 10^{-9}-10^{-7} s) as compared with phosphorescence (ca. 10^{-3}-10 s). However, to life apply this rule correctly; the spin state of the system under investigation has to be known in detail, which is, especially for complex systems, rarely the case.

Another way to get some sort of order in the widespread phenomenon of light emission of matter is to distinguish the modes of luminescence production, that is, the way in which the electronic system is excited. Other common types of luminescence and their modes of production are as follows: (Halpern, 2005)

2.1.1 Radioluminescence (or scintillation) is produced by ionizing radiation. Some polymers contain organic molecules that emit visible light when exposed to such radiation as x-ray, γ-ray, or cosmic ray, and thus act as detectors for high-energy radiation. Scintillators are organic molecules that emit visible light when they are excited by the decay products of certain radioactive isotopes such as ^{3}H (tritium), ^{14}C, and ^{18}O, and are used in many biomedical applications.

2.1.2 Electroluminescence is produced by the exposure of atoms or molecules to an electric field or plasma. An example is the gas-discharge tube. These are lamps that are filled with a gas such as neon, argon, xenon, nitrogen, etc. or the vapor of metals such as mercury or sodium. The lamps contain electrodes, which are connected to an electrical power supply. The applied voltage is high enough to ionize the atoms and produce a low-pressure plasma, or ionic (current-carrying) gas. The recombination of metal ions and electrons in the plasma leads to the production of electronically excited states of the atoms and hence the emissions of light, usually in

the form of very narrow lines throughout the electromagnetic spectrum. The common fluorescence lamp is a discharge tube in which electronically excited mercury atoms transfer this energy to a material called a phosphor, which are coated the inside surface of the tube. The phosphor, after being excited by collisions with electrons or light produced by atoms or molecules, emits most of the observed light. Another example is lightning, in which the static electricity generated by a moving air mass ionizes (removes electrons from) the nitrogen and oxygen molecules. Charge recombination produces nitrogen molecules in an excited electronic state, which release this energy by emitting radiation as visible light. The Northern Lights (aurora borealis) also represents an example of this type of luminescence. Electroluminescence is produced by the familiar light-emitting diode, which is constructed from a pair of aluminum-gallium-arsenide (AlGaAs) sheets in contact with each other. One contains impurities that add electrons, while the other has deficiencies of electrons. When an electric current flows between the sheets, electrons are promoted to a higher energy level (the conduction band), and the subsequent of these electrons to a lower level (the charge-depleted sites) result in the emission of light, often in the red region of the spectrum.

2.1.3 Chemiluminescence is produced as a result of a chemical reaction usually involving an oxidation-reduction process, in which, simply viewed, electronic charge is transferred from one species to another with the resultant formation of an excites state. One common example is the luminol reaction. When luminol, an amino-substituted phthalazine derivative, is treated with base and an oxidizing agent such as hydrogen peroxide, nitrogen molecules are produced along with the emission of blue light. This light comes from the excited state of a product, the aminophthalate

molecule. In this example, the light emitted represents the conversion of chemical energy to optical energy.

2.1.4 Bioluminescence is the result of certain oxidation processes (usually enzyme-catalyzed) in biological systems. The firefly and its larva, the glowworm, are well-studied examples: light emission for the firefly serves as a mating signal. These organisms produce a molecule called luciferin and an enzyme known as luciferase. When these molecules are in the presence of oxygen and adenosine phosphate, yellow-green light is produced with very high efficiency. Many other organisms such as bacteria, fungi, and certain marine species are bioluminescent. It is thought that chemiluminescence is a now-defunct evolutionary mechanism that was developed by some anaerobic organisms for the disposal of oxygen, which can be toxic to organisms.

2.1.5 Thermoluminescence (TL) is light produced when a substance, previously exposed to ionizing radiation, is heated. Many natural substances, such as quartz and feldspar, are exposed to ionizing radiation produced by radioactive decay of the isotopes of elements such as potassium, thorium and uranium that are present in their immediate environment (and also from cosmic rays). As a result of this exposure, electrical charges are gradually placed in low-energy sites in the solid called traps. When this substance is heated, these (opposite) charges recombine; producing luminescence whose intensity reflects the number of stored-up charges. If in some past event the material became heated, either through geological processes or anthropological activities, the accumulated charge pairs are depleted (the "clock is reset"), and their population again increases with time. Deliberate exposure of the sample to heat at some later time produces TL, which can be used to date it.

Alternatively, this light can be released by exposing the sample to light in a technique called Optically Stimulated Luminescence.

2.1.6   Triboluminescence is light emitted when a solid is subjected to friction, such as when it is scratched, ground, or rubbed. The luminescence produced by some minerals in this way is akin to thermoluminescence, except that a mechanical stimulus, rather than bulk heating, causes the effect. In other cases involving organic solids, such as sucrose, the frictional forces result in charge separation, which, in turn, leads to the production of electronically excited nitrogen molecules that emit light (similar to what is seen in lightning). Crushing candy products that contain wintergreen flavor (salicylate), causes a bright blue triboluminescent response. In this case the excited nitrogen (or other species) transfers its energy to the salicylate it to fluoresce.

Although there is a wide range of circumstances in which luminescence is observed, there is one common to this phenomenon. For solid state materials charge recombination produces the excited state of the emitting species. In the case of atoms or molecules, luminescence results from the transition between discrete energy levels.

The luminescence is due to the addition of a luminogen or activator in the form of a trace impurity. For example, in phosphorescent sulphides, copper, manganese, bismuth. In some cases crystal lattice defects provide localized levels, like those of impurity, which play the part of the activator.

Stimulated emission (laser action) requires an inverted ion population of the excited species (Siegman, 1994) and has been achieved for a large number of ions and transitions at wavelengths ranging from the far infrared to soft x-ray. Solid-state lasers incorporate many different transition-metal ions, organic dyes, and color center in

inorganic and organic crystalline and amorphous hosts. Lasing is produced principally by optical pumping. In semiconductor-junction laser materials, a large electron current creates excited electron and hole states and induces laser action (Yariv, 1989).

2.2   Glasses and Glass-ceramics system

2.2.1   Soda-lime glass

Soda-lime glass or soda-lime-silicate glass is perhaps the least expensive and the most widely used of all glasses made commercially. Most of the beverage containers, glass windows, and incandescent and fluorescent lamp envelopes are made from soda-lime glass. It has good chemical durability, high electrical resistivity, and good spectral transmission in the visible region. Because of its relatively high coefficient of thermal expansion ($\sim100 \times 10^{-7}/°C$), it is prone to thermal shock failure, and this prevents its use in a number of applications. Large scale continuous melting of inexpensive batch materials such as soda ash (Na_2CO_3), limestone ($CaCO_3$) and sand at 1400-1500°C make it possible to form the products at high speeds inexpensively.

Soda-lime glass contains about 72% SiO_2, 14% Na_2O, 10% CaO, and 2% Al_2O_3 (Wikipedia, www, 2008) (The sum of these comes to 98%, implying the presence of small quantities of other oxides.) In soda-lime glass, sodiumT (Na^+) and calcium (Ca^{2+}) ions are inserted into the silicate ion structure such that the tetrahedrons of silicon and oxygen atoms are stretched. The glass transition temperature (T_g) is about 550°C and the melting point is about 1000°C.

Whereas pure SiO_2 glass does not absorb UV light, soda-lime glass does not allow light at a wavelength of shorter than 400 nm (UV light) to pass. The disadvantages of soda-lime glass are that not resistant to high temperatures and sudden thermal changes. For example, everybody has experienced a glass breaking down when pouring liquid at high temperature, e.g. to make tea. Some of the use of soda-lime glass is primarily used for bottles, jars, everyday drinking glasses, and window glass (Lenntech, www, 2008).

2.2.2 Lithium silicate glass and glass-ceramics

Simple silicate glass-ceramics are composed of alkali and alkaline earth silicate crystal whose properties dominate that of the glass-ceramics. The most important ones are lithium silicate, both lithium metasilicate ($Li_2O \cdot SiO_2$) and lithium disilicate ($Li_2O \cdot 2SiO_2$).

Lithium silicate glass-ceramics consist of two composition group. The first group based on lithium disilicate ($Li_2O \cdot 2SiO_2$) crystal, nucleated with P_2O_5, develops high thermal expansion glass-ceramics which match the thermal expansion of several nickel based superalloys, and are used in variety of high strength hermetic seals, connectors, and feedthroughs (Headley and Loehman, 1984).The second group based on lithium metasilicate ($Li_2O \cdot SiO_2$), photosensitively nucleated by colloidal silver, produces a variety of chemically machined materials which are useful as fluidic devices, display screens, lens arrays, and other patterned devices (Pinkney, 2001).

The composition of lithium silicate glass-ceramics typically comprises 70-85SiO_2, 10-15Li_2O, 3-10Al_2O_3, 1-5P_2O_5 wt%. The glasses phase separate on heat treatment and lithium orthophosphate (Li_3PO_4) crystals precipitate as the first phase.

Lithium metasilicate (Li_2SiO_3) and/or lithium disilicate (Li_2SiO_5) then form, the latter predominating with further heat treatment.

Lithium metasilicate crystallization was found to precede lithium disilicate crystallization as a metastable phase in some silicate glasses. Hench, Freiman and Kinser (1971) determined that lithium metasilicate crystal was formed before lithium disilicate in two glass composition of 30 and 33 mol% Li_2O, but the amount of lithium metasilicate was extremely small and it disappeared on further heat treatment.

Soares et al. (2003) studied the early crystallization stage of lithium disilicate glasses using TEM and XRD techniques. Three lithium silicate glasses close to the $Li_2O \cdot 2SiO_2$ composition were heat treated at ~T_g = 454°C, two distinct crystalline phases, stable lithium disilicate (Li_2SiO_5) and metastable lithium metasilicate $Li_2O \cdot SiO_2$ coexist up to 120 h at 454°C (crystalline fraction<1 vol%). For longer treatment (240-600 h) only the stable phase $Li_2O \cdot 2SiO_2$ was observed.

Morimoto (2006) investigated the effect of K_2O on crystallization in Li_2O-SiO_2 glass. He has found that a small amount of K_2O affected the mechanism of phase separation and crystallization process, and K_2O suppressed the crystallization of $Li_2O \cdot 2SiO_2$, but promote the precipitation of $Li_2O \cdot SiO_2$ crystal in Li_2O rich continuous phase containing K_2O.

Lithium disilicate glass-ceramics nucleated with P_2O_5 are characterized by high body strength, 140-210 MPa, good fracture toughness, ≈ 3 MPa·m$^{1/2}$, and moderate high thermal expansion coefficient, 80-130x10^{-7} °C^{-1} (Pinkney, 2001)

Morimoto and Waraporn Emem (2004) studied the properties of $77.7SiO_2 \cdot 2.2Al_2O_3 \cdot 18.8Li_2O \cdot 1.2P_2O_5$ (mol%). They found that the transparent

glass-ceramics can be obtained by heat treatment below 800°C. The main crystalline phase is $Li_2O \cdot 2SiO_2$. The percent crystallinity and crystal size range from 60 to 70% and from 20 to 60 nm, respectively. The density of glass-ceramics increases with increasing heating temperature and time of crystallization. Fracture strength of transparent glass-ceramics increases linearly with crystal size ranging 20-60 nm.

2.2.3 Spinel glass and glass-ceramics

Spinel have cubic crystal structures with the general chemical formula AB_2O_4, where A is a tetrahedrally coordinated, typically divalent metal, such as zinc, magnesium, iron, or manganese, and B is an octahedrally coordinated, usually trivalent metal, such as aluminum, iron, or chromium. Glass-ceramics based on spinel compositions ranging from gahnite ($ZnAl_2O_4$) toward spinel ($MgAl_2O_4$) can be crystallized from glasses in the SiO_2-Al_2O_3-ZnO-MgO system, with ZrO_2 and/or TiO_2 as nucleating agents. (Beall and Duke, 1969, Pinckney, 1999). These glass-ceramics can be made highly transparent, with sipnel crystals in the order of 10-50 nm in size.

2.2.4 Aluminum phosphate glass and glass-ceramics

Phosphorus is network-forming element, and P_2O_5 is known to be formed as a glass by itself. The properties of glass such as the viscosity and refractive index depend on the parent crystalline form, the melting time and the cooling rate. In both crystals and glasses, the basic unit of structure is the PO_4 tetrahedron. The P_2O_5 glass is significantly less rigid (or is more fluid) compared to SiO_2 glass. The rigidity of the structure is increased by the addition of alkalis or alkaline earths. The extent of glass formation of phosphate glasses with alkali and alkaline earth is generally larger than in the silicates or the borates (Varshneya, 1993). In the crystalline form, analogous allotropic forms of $AlPO_4$ exist for all allotropic forms of silica (including

high and low forms). $AlPO_4$ can only be brought to glassy state by vapor phase condensation by Varshneya, Busbey and Soules (1985) suggested that with the addition of Al_2O_3 to P_2O_5, the size of tetrahedral AlO_4-PO_4 clusters continue to grow; however, full connectivity is still not obtained even at the stoichiometric $AlPO_4$ composition, allowing structural rearrangement, and thus crystallization, to occur. Experimental problems in the melting of $AlPO_4$ are augmented because of the rapid volatilization of P_2O_5.

A phosphate glass containing lead and indium have been fabricated as optical fibers and lenses. They have a high index of refraction and the ability to bend light at high angles. It is also chemically stable and durable. In addition, it has a low melting point and is transparent over a wide range of wavelengths. Perhaps the most important characteristic of phosphate glass is readily to dissolve rare-earth elements, and hence phosphate glasses can be used in developing new optically active devices such as fiber-optic amplifiers and new lasers (Oak Ridge National Laboratory, www, 2008).

Aboud and Stoch (1997) investigated crystallization behavior in the glass system SiO_2-P_2O_5-Al_2O_3-MgO-Na_2O. This is a mixed network glass, in which $[AlPO_4]$ tetrahedra substitute for pairs of $[SiO_4]$ tetrahedra, leading to increased thermal stability and reduced crystallization ability. Crystallization of SiO_2---$AlPO_4$ network glass is accomplished through reconstruction and depolymerization of the glass network as temperature and/or time of heat treatment are increased. The first phase to crystallize is $AlPO_4$-high cristobalite type, followed by the formation of spherulitic $Mg_3(PO_4)_2$ which is grown on the $AlPO_4$ crystals.

Morimoto (2006) investigated phase separation and crystallization in the system of SiO_2-Al_2O_3-P_2O_5-B_2O_3-Na_2O glasses. He found two phases, one of which rich in Al_2O_3-P_2O_5-SiO_2 forms continuous phase first and then tridymite type $AlPO_4$ crystals precipitate and grow in this phase. Highly transparent glass-ceramics comparable to glass can be successfully obtained by controlling heat treatment precisely. The crystal size and percent crystallinity of these transparent glass-ceramics are 20-30 nm and about 50%, respectively.

2.2.5 Zinc tellurium phosphate glass

Tellurite glasses and phosphotellurite glasses have drawn much attention as promising candidates for "new glass", i.e. glasses for new application, because they exhibit the following various unique or functional properties. Their low glass transition temperature (~400°C) is attractive for use in lead-free adhesive or soldering glasses (Mizuno, 1991). Their coloration from pale green to dark-red-brown is applicable to optical filter (Hasegawa and Kawakubo, 1957). Tellurite glass with transition metal doping shows thermochromism based on the high thermal expansion coefficient (Inoue et al., 1995). As the host materials for rare earth ions, their high refractive indices (~2.0) and the low phonon vibration allow large radiation transition rate that is useful for optically functional glasses (Tanabe, Hirao, and Soga, 1990). The large refractive index dispersion is also advantageous for non-linear optical properties (Kim, Yoko, and Sakka, 1993). The ionic conductions of guest cations are increased by the addition of P_2O_5 into tellurite glasses (Jayasinghe et al., 1995)

Konishi et al. (2003) investigated the glass formation and color generation in the P_2O_5-TeO_2-ZnO system of glasses. They found that the color of glasses varied from clear, green to deep red depending on the composition, and the

color became deeper with increasing TeO_2 content and melting temperature. The transmission spectra show that the transmittance is significantly lower for glass melting at 1200°C than that for glass melted at 1000°C. The origin of reddish coloration was induced by metallic Te-colloidal particles.

2.3   Oxidation-reduction equilibrium in glass

Oxidation is the loss of an electron and reduction is the reverse:

$$Fe^{3+} + electron \xrightarrow{\text{reduction}} Fe^{2+} \tag{2.1}$$

The simultaneous occurrence of oxidation and reduction is commonly known as a "redox process". When a metal, M forms an oxide MO_x, it can be visualized that the metal electrons are transferred to the empty 2p orbitals of the oxygen atom and thus the elementary steps of the reaction can be hypothetically written as:

$$M \longrightarrow M^{2+} + electrons \qquad \text{(oxidation)} \tag{2.2}$$

$$xO + 2x \text{ electrons} \longrightarrow xO^{2-} \text{ (reduction)} \tag{2.3}$$
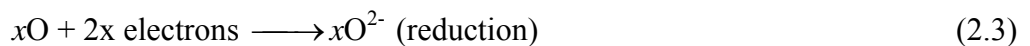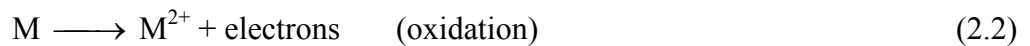
The redox reaction in glass melt may be written in different ways, for example the redox reaction of ferrous and ferric iron, the reaction may be written in terms of the pure oxide as:

$$2FeO \text{ (glass)} + O_2 \text{ (glass)} \longleftrightarrow 2Fe_2O_3 \text{ (glass)} \tag{2.4}$$
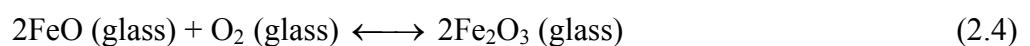
$$K = [\alpha_{(Fe_2O_3)}]^2/[\alpha_{(FeO)}]^2 \cdot [p_{(O_2)}] \tag{2.5}$$

where K is the redox equilibrium constant, α is the activity of oxide in glass, pO_2 is partial pressure of oxygen. The redox reaction may also be written in terms of the ionic species present in the system as:

$$4Fe^{2+} \text{ (glass)} + O_2 \text{ (glass)} \longleftrightarrow 4Fe^{3+} \text{ (glass)} + 2O^{2-} \text{ (glass)} \qquad (2.6)$$
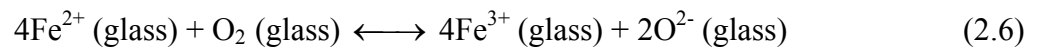
When a redox oxide is introduced into a glass melt, it distributes itself into different states of oxidation depending upon the time and temperature of melting, the glass composition, the furnace atmosphere and batch composition.

2.3.1 Effect of melting temperature on the redox equilibrium in glasses

The oxidation-reduction equilibrium in glass usually moves toward the reduced side with increasing temperature. This can be explained by using standard thermodynamic data.

The redox equilibrium constant, K, is related to the temperature of reaction by the Van't Hoff isochore:

$$\frac{d \ln K}{dT} = \frac{\Delta H}{RT^2} \qquad (2.7)$$

where ΔH is the enthalpy, R is the gas constant and T is the absolute temperature. On integration

$$\ln K = -\frac{\Delta H}{RT} + I \qquad (2.8)$$

where I is the integration constant.

From above equation, the plot of the ratio: log [(concentration of oxidized form)/(concentration of the reduce form)] against reciprocal of absolute temperature (1/T) should give a straight line, with slope equivalent to $-\Delta H/R \times 2.303$. The slope of the lines is positive, indicating that these reactions are exothermic and that they will proceed towards the reduced side at higher temperature.

2.3.2 Effect of glass composition on the redox equilibrium in glasses

All experiments on redox equilibria reported that the proportion of the redox ion in the higher oxidation state increases with the basicity. Comparing these results with equation (2.6) for the redox equilibrium in glasses, the conclusion must be that oxygen ion activity decreases with increasing basicity. This apparent paradox is resolved by recognizing that the concentration equilibrium constant K, which was measured in these cases, varies with composition. Further, transition metal ions occur as different complexes in glass, and not free ions as written in equation (2.6). When redox equilibria are written in terms of these complexes, instead of free ions, a satisfactory qualitative correlation may be obtained between the oxygen ion activity and the redox equilibrium. Finally, the more basicity of alkali oxide and the greater its concentration, the more redox reaction (equation 2.6) will move to the right side and higher valence state will be formed. For example:

$$1/2Cr_2O_3 + 3/4O_2 + R_2O \leftrightarrow [CrO_4]^{2-} + 2R^+ \qquad (2.9)$$
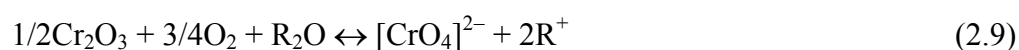
The basicity of glasses can be evaluated according to Duffy's optical basicity scheme (Duffy, 1996).

2.3.3 Effect of additives on the redox equilibrium in glasses

In the glass melting, it also has the main ingredients such as soda-lime silicate glasses are sand, sodium carbonate, limestone, dolomite, and minerals containing alumina. In addition to melting aids such as borates and fluorspar there are two other groups of supplementary raw materials in use; those which have a reducing effect and those which are oxidizing. Carbon and calumite slag are widely used as reducing agents and sulfate and nitrate of alkaline metal for oxidizing agent. These materials act as oxidizing agents or reducing agents directly to opponent materials.

$$2Bi_2O_3 + 3C \rightarrow 4Bi + 3CO_2 \qquad\qquad (2.10)$$

$$2BiO + C \rightarrow 2Bi + CO_2 \qquad\qquad (2.11)$$
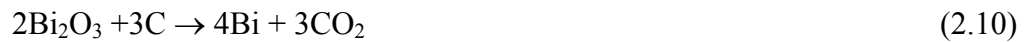
2.4 Characterizations

2.4.1 Electron Spin Resonance: ESR

Electron spin resonance is a spectroscopic technique for studying chemical species that have one or more unpaired electrons, such as organic and inorganic free radicals or inorganic complexes possessing a transition metal ion. A great number of materials contain such paramagnetic entities, which may occur either as electrons in unfilled conduction bands, electrons trapped in radiation damaged sites, or as free radicals, various transition, bi-radical, triplet states, impurities in semi-conductors, as well as other types.

(1) Origin of an ESR signal

Every electron has a magnetic moment and spin quantum number $s = 1/2$, with magnetic components $m_s = +1/2$ and $m_s = -1/2$ (Wikipedia, www, 2008).

In the presence of a strong magnetic field B_0, the individual magnetic moment arising via the electron "spin" of the unpaired electron can be oriented either parallel ($m_s = -1/2$) or anti-parallel ($m_s = +1/2$) to the applied field, as shown in Figure 2.1

An unpaired electron can move between the two energy levels by absorption or emitting electromagnetic radiation of energy with the equation is;

$$\Delta E = h\nu = g.\mu.B_0 \quad\quad (2.12)$$

Where: ΔE; energy difference between the two spin states

h; Planck constant (6.6261×10^{-34} J.s)

ν; microwave frequency

g; the electron's so-called g-factor (that give information about a paramagnetic center's electronic structure)
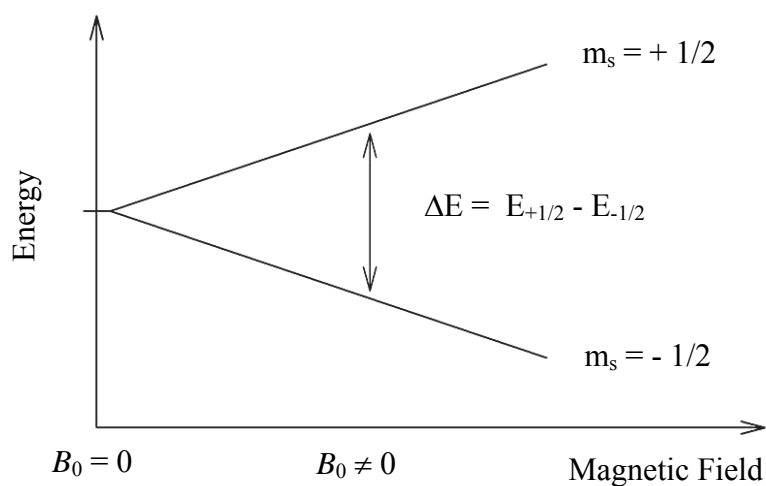
Figure 2.1   The diagrams for two spin states as a function of applied field, B_0.

(Wikipedia (2008) Electron paramagnetic resonance [On-line])

μ; the Bohr magneton (9.2740×10^{-24} J.T^{-1})

B_0; the applied magnetic field.

In principle, ESR spectra can be generated by either varying the photon frequency incident on a sample while holding the magnetic field constant, or doing the reverse. In practice, it is usually the frequency which is kept fixed. A collection of paramagnetic centers, such as free radicals, is exposed to microwaves at a fixed frequency. By increasing an external magnetic field, the gap between the $m_s = +1/2$ and $m_s = -1/2$ energy states is widened until it matches the energy of the microwaves, as represented by the double-arrow in Figure 2.1. At this point the unpaired electron has the absorption of energy which is monitored and converted into a spectrum. ESR spectra are recorded and reported only as first derivative, as represented in Figure 2.2
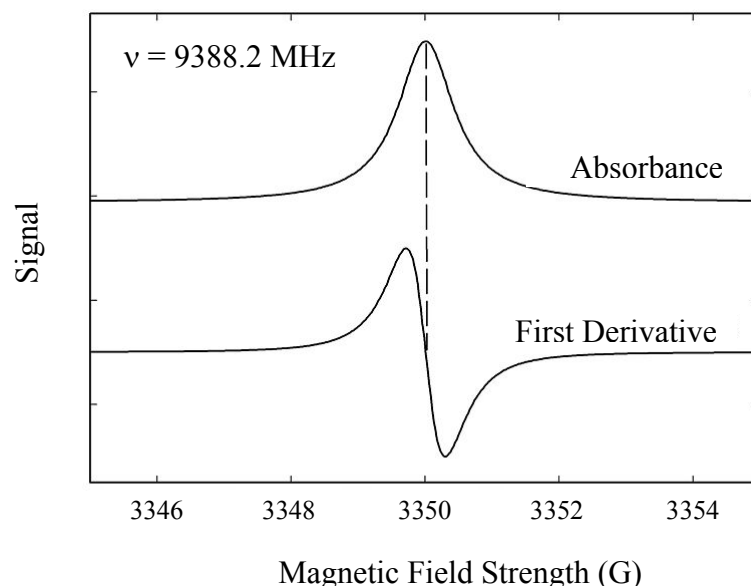
Figure 2.2   ESR spectra are recorded and published as first derivative.

(Wikipedia (2008) Electron paramagnetic resonance [On-line])

(2) Electron Spin Resonance (ESR) applications.

ESR spectroscopy is used in various branches of science, such as chemistry and physics, for the detection and identification of free radicals and paramagnetic centers (Wikipedia, www, 2008).

ESR signal can be identified and studied the both radicals formed in chemical reaction and the reaction themselves, such as H, OH and HO_2 are produced from frozen water (solid H_2O).

ESR signal can be detected in electrochemical system and in material exposed to UV light.

ESR technique can detect color center of transition metals in polycrystalline and glassy solids.

2.4.2 X-ray Photoelectron Spectroscopy: XPS

(1) Introduction

X-ray photoelectron spectroscopy is a quantitative spectroscopic technique that measures the elemental composition of the surface (1-10 nm usually), empirical formula of pure materials, chemical state and electronic state of the elements in the surface that exist within a material (Wikipedia, www, 2008).

Surface analysis by XPS is accomplished by irradiating a sample with soft X-rays and energy analyzing the electrons emitted and this gives a spectrum with a series of photoelectron peaks. Photoelectrons are collected and analyzed by the electron spectrometer of emission intensity versus electron binding energy (Hong Kong Paptist University, www, 2008). The binding energy of the peaks is characteristic of each element. Quantitative data can be obtained from the peak

heights or areas and identification of chemical states often can be made from the exact position and separations of the peaks, as well as from certain spectral contours.

(2) Principle of the Technique

X-ray photoelectron spectroscopy (XPS) is a surface analytical technique, which is based upon the photoelectric effect. Each atom in the surface has core electron with the characteristic binding energy that is conceptually, not strictly, equal to the ionization energy of that electron. When an X-ray beam directs to the sample surface, the energy of the X-ray photon is adsorbed completely by the core electron of an atom. The energy of a photon is given by the Einstein relation: (Queen Mary University, www, 2008)

$$E = h\,\nu \tag{2.13}$$

where h - Planck constant (6.6261×10^{-34} J.s)

ν - frequency (Hz) of the radiation

If the photon energy, $h\nu$, is large enough, the core electron will then escape from the atom and emit out of the surface by the photoelectric effect. The process of photoelectric effect is shown schematically in Figure 2.3, where an electron from the K shell is ejected from the atom (a 1s photoelectron). The photoelectron spectrum will reproduce the electronic structure of an element quite accurately since all electrons with a binding energy less than the photon energy will feature in the spectrum.

Ejected *K* electron
(1s electron)

Vacuum

Fermi

Valence band

$L_{2,3}$

Incident

L_1

X-ray
(*h*ν)

K
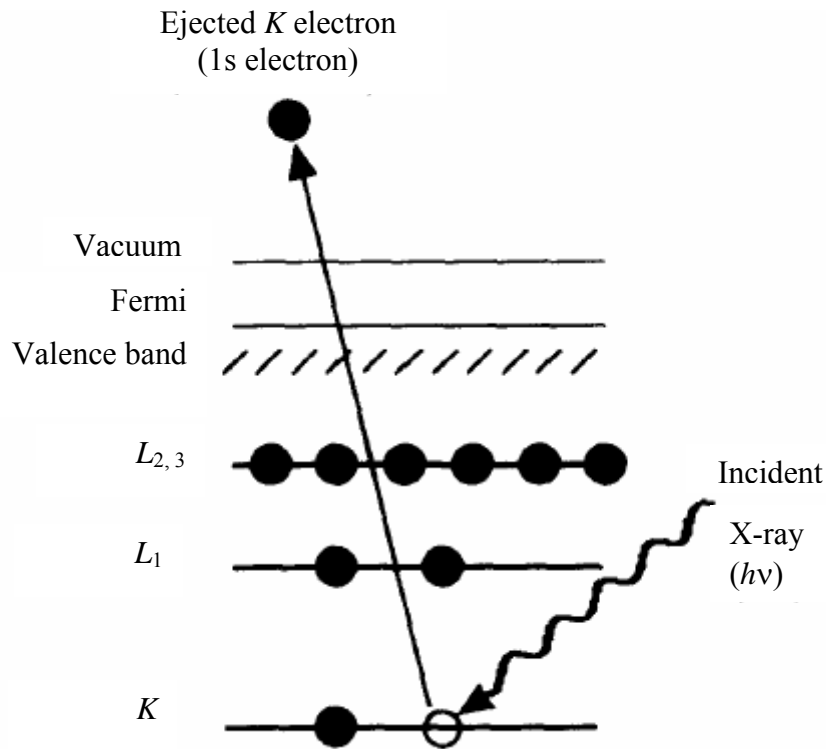
Figure 2.3   Schematic diagram of the photoelectric effect, showing

photoionization of an atom by the ejection of a 1s electron. (John F.

and John Wolstenholme, 2003)

Photoelectrons are emitted with a specific kinetic energy which is

measured by an electron analyzer. This kinetic energy is given by,

$$E_K = h\nu - E_B - \phi \tag{2.14}$$

Where E_k is the kinetic energy of photoelectron, which can be measured by the energy

analyzer; $h\nu$ is the X-ray photon energy (for monochromatic Al Kα, $h\nu = 1486.6$ eV

or MgKα, $h\nu = 1253.6$ eV); E_B is the binding energy of the atomic orbital from which

the electron originated; and ϕ is the work function induced by analyzer, about 4-5 eV.

The core electron of an element has a unique binding energy, which seems like a "fingerprint". Thus almost all elements except for hydrogen and helium can be identified via measuring the binding energy of its core electron. Furthermore, the binding energy of core electron is very sensitive to the chemical environment of element. The same atom is bonded to the different chemical species, lead to the change in the binding energy of its core electron.

The sample is irradiated with X-rays of energy hv, which interact with the electrons in the sample via the photoelectron effect. The energy of the emitted photoelectrons is then analyzed by the electron spectrometer and the data presented as a graph of intensity (usually expressed as counts or counts/s) versus electron energy - the X-ray induced photoelectron spectrum.

(3) Experimental Details

The basic requirements for a photoemission experiment XPS are: (Queen Mary University, 2008)

- An x-ray source The x-ray source is a standard which can be configured with AlKα or MgKα, of which the photo energies are 1486.6 eV and 1253.6 eV, respectively

- An electron energy analyzer

- A high vacuum environment

(4) XPS spectrum and analysis

The XPS technique is highly surface specific due to the short range of the photoelectrons that are excited from the solid. The energy of the photoelectrons leaving the sample are determined using a concentric hemispherical analyzer (CHA)

and gives a spectrum with a series of photoelectron peaks as a plot of electron binding

energy versus the number of electrons in fixed (shown in Figure 2.4).
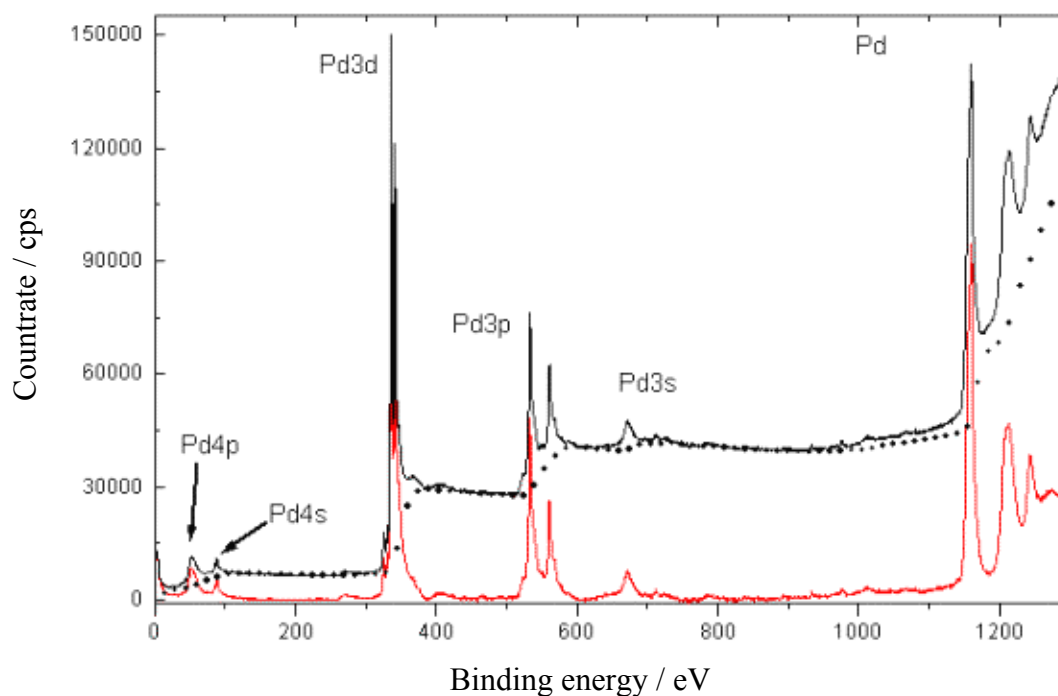
Figure 2.4   XPS spectrum of Pd. (Cain Department of Chemical Engineering of

LSU, www, 2008)

The binding energy of the peaks is characteristic of each element.

The peak areas can be used to determine the composition of the materials surface. The

shape of each peak and the binding energy can be slightly altered by the chemical

state of the emitting atom. Furthermore, the intensity of the peaks is related to the

concentration of the element within the sampled region. Several types of peaks are

observed in XPS spectra. Some are fundamental to the technique, and are always

observed. Others are dependent upon the exact physical and chemical nature of the

sample. The following describes the various spectral features that likely to be encountered.

- Photoelectron Lines.

The most intense photoelectron lines are usually relatively symmetrical and are typically the narrowest lines observed in the XPS spectrum, such as peak 3d of Pd as shown in Figure 2.5

- Auger Lines

These are groups of lines. In XPS spectrum, Auger lines are four main series, such as KLL, LMM, MNN and NOO series, identified by specifying the initial and final vacancies in the Auger transition. Core type Auger lines usually have at least one component of intensity and width similar to the most intense photoelectron line.
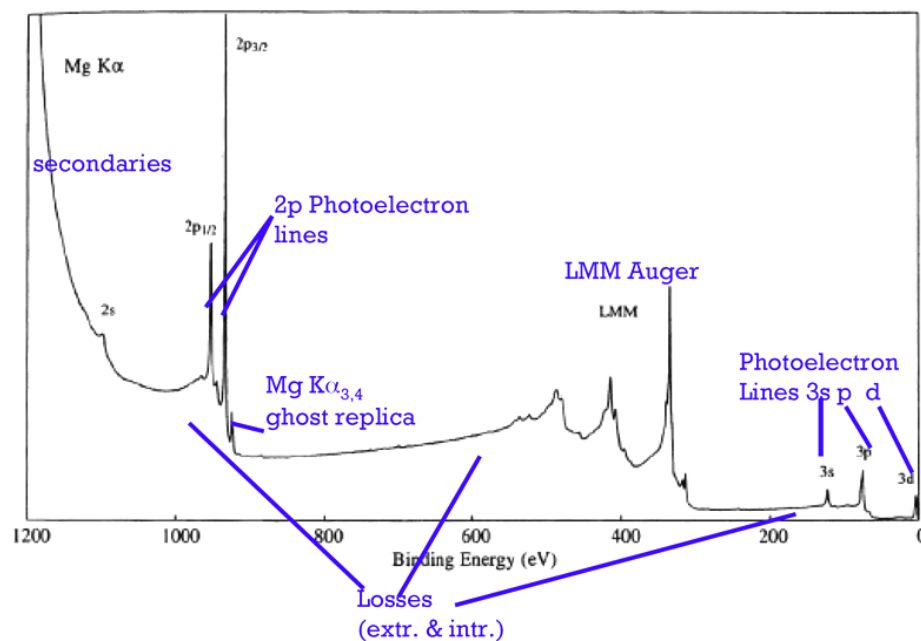
Figure 2.5   Auger Lines of a copper foil by MgKα x-ray. (Technical University of

Vienna, www, 2008)

- X-ray Satellites

The x-ray emission spectrum used for irradiation exhibits not only the characteristic x-ray, but some minor x-ray components at higher photo energies. For each photoelectron peak is a family of minor peaks at lower binding energies, with intensity and spacing characteristic of the x-ray anode material. The pattern is shown in Figure 2.6
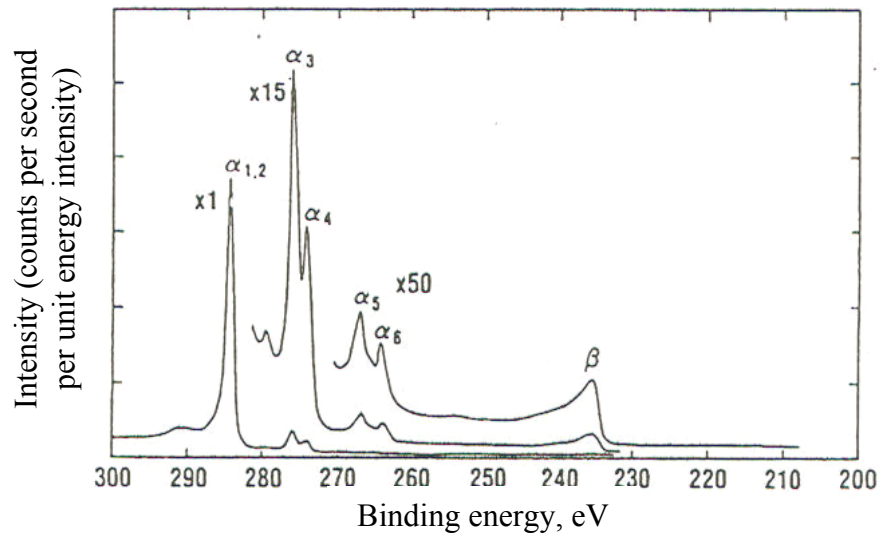
Figure 2.6   Mg x-ray satellites (C1s graphite spectrum). (C.D. Wagner et al, 1979)

- X-ray Ghosts

Occasionally x-radiation from an element other than the x-ray source anode material impinges upon the sample, resulting in small peaks corresponding to the most intense spectral peaks. These lines can be due to Mg impurity in the Al anode or Cu from anode generation of x-ray photos in aluminum foil x-ray window.

- Shake-Up Lines

Photoelectric processes are simple ones, leading to the formation of ions in the ground state. There is a finite probability that the ion will be left in an excited state. In this event, the kinetic energy of the emitted photoelectron is reduced. This result in the formation of a satellite peak a few electron volts lower in kinetic energy (higher in binding energy) than the main peak. The pattern of shake-up satellites for Cu is shown in Figure 2.7.
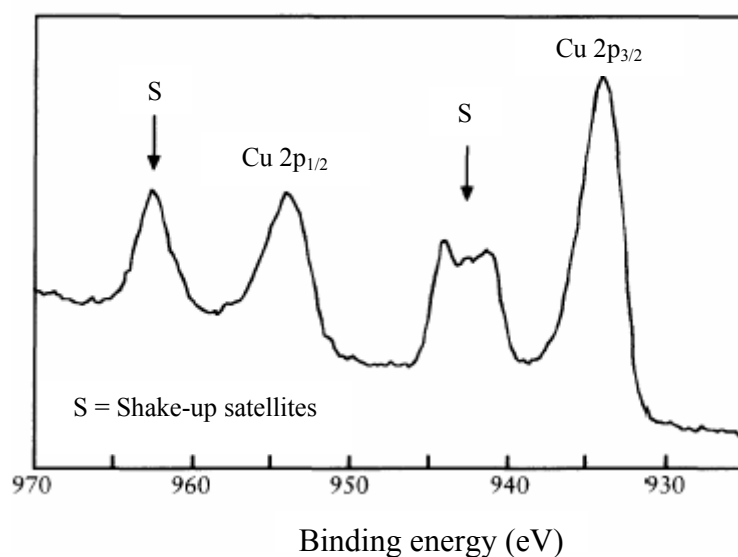
Figure 2.7   Shake-up satellites for Cu 2p spectrum from CuO. (Watts, F., J. and Wolstenholme, J., 2003)

- Multiplet Splitting

Multiplet splitting of a photoelectron peak may occur in a compound that has unpaired electrons in the valence band, and arises from different spin distributions of the electrons of the band structure. This results in a doublet of the core level peak being considered; multiplet splitting effects are observed for Mn, Cr

(3s levels), Co, Ni ($2p_{3/2}$ levels), and the 4s levels of the rare earths. The $2p_{3/2}$ spectrum of nickel shows multiplet splitting for NiO, as shown in Figure 2.8.
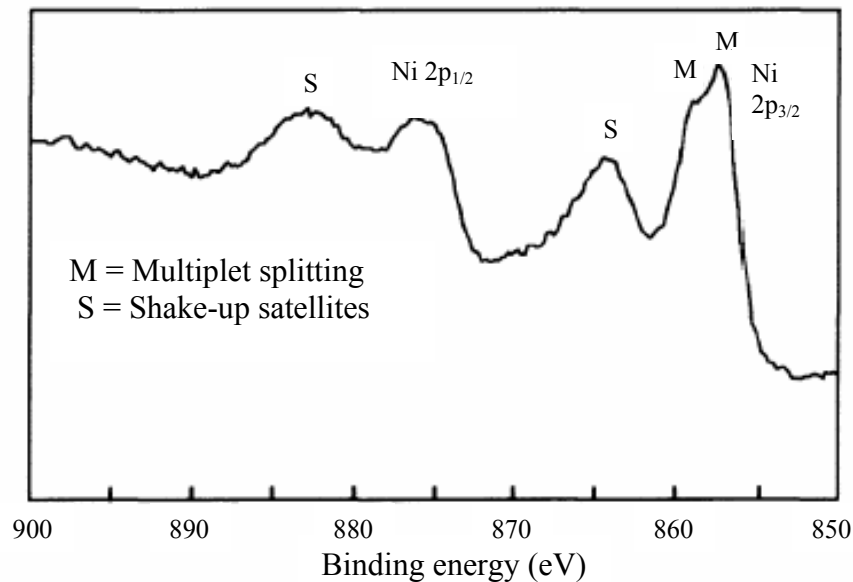
Figure 2.8   Multiplet splitting for the Ni $2p_{3/2}$ spectrum of NiO. (Watts, F., J. and Wolstenholme, J., 2003)

(5) Typical Analytical Applications (Hong Kong Paptist University, www, 2008)

- Elemental Analysis: Atomic abundance of all elements (except H and He) on metals, insulators, powders, etc

- Chemical state information (e.g. identification oxidation state)

- Quantitative analysis

- Angle dependent XPS measurement for non-destructive depth profiling

2.5   Literature reviews

Lindner et al. (1996) studied the color centers of Te-doped ultramarine-type zeorite. They found that the UV-VIS spectrum of Te-doped blue ultramarine showed three absorption bands at 16500 (606 nm), 20800 (481 nm) and 25000 cm^{-1}(400 nm). For the green product, the latter band was observed again together with a rather broad absorption bands at around 23000 cm^{-1} (435 nm), and they also found the broad luminescence at 11600 cm^{-1} (862 nm) and 17800 cm^{-1} (562 nm) under the excitation of 457 nm light. The absorption band at 16500 cm^{-1} (606 nm) and 23000 cm^{-1} (435 nm) can be assigned to $^2\pi_g \rightarrow {}^2\pi_u$ transition of Te_2^- and $^3\Sigma_g \rightarrow {}^3\Sigma_u$ transition of Te_2, respectively. Thus the color of Te-doped ultramarine-type zeorite was generated by Te_2 and Te_2^- species.

Srivastava (1998) reported that the visible luminescence centered at 628 nm was detected from Bi^{2+}:$CaBPO_3$ crystal prepared under the reducing condition at 1000°C, and assigned to $^2P_{3/2} \rightarrow {}^2P_{1/2}$ transition of Bi^{2+} ions.

Guha, Leppert, and Risbud (1998) investigated the electronic state of Se_2^- molecules in borosilicate glasses by ESR technique. They found two ESR signals at g = 4.3 (~150 mT) and g = 2.006 (~350 mT), and the former may be due to Fe^{3+} and the latter Se_2^- centers, respectively. Nistor et al. (2000) studied the electron-hole recombination in $PbCl_2$ crystals by ESR measurement. They found the ESR signal at g~2.05 similar to that of the molecular Cl_2^- defects (Vk-type center or hole trapped center) in alkali halide crystals.

Fujimoto and Nakatsuka (2001) investigated the NIR luminescence of Bi-doped silica glass. They found that the color of this glass was reddish-brown which exhibits NIR luminescence at 1120 nm, 1140 nm and 1250 nm under the excitation of

500 nm, 700 nm, and 800 nm, respectively. They could not find the luminescence from Bi^{3+} ions reported previously. They estimated that these luminescence might come from Bi^{5+} ions, where the transition between ground state $^1S_0$ and the exited state $^3D_{3,2,1}$ and $^1D_2$.

Konishi et al. (2003) reported the color generation in the ternary P_2O_5-TeO_2-ZnO system of glasses. They found that the color of these glasses varied from clear, green and deep red depending on the glass composition and melting temperature. The color became deeper with increase in TeO_2 content and melting temperature. The absorption band was observed at around 550 nm in the red glass. The XPS spectrum showed two peaks which reveal the existence of two bonding states of Te^{4+} and Te/Te^{2-}. They concluded that the red coloration of P_2O_5-TeO_2-ZnO system of glasses was considered to be due to metallic Te colloidal particles.

Peng et al. (2004) investigated the NIR luminescence characteristics of Bi- and Al- co-doped germanate glasses prepared by conventional melt-quench method. They found five absorption bands at 370, 500, 700, 800 and 1000 nm and broad NIR luminescence centered at 1300 nm with a FWHM of 320 nm pumped by 808 nm laser. The fluorescent life-time decreased with increase in the Bi_2O_3 concentration in glass. They proposed that the source of luminescence was different from that of Bi^{3+}-doped glasses. Peng et al. (2007) also investigated NIR luminescence from ZnO-Al_2O_3-SiO_2 glasses and glass-ceramics. They found that the colors of samples turns from light reddish brown to deep reddish brown and the transmittance decreases in turn with increase in heat treatment temperature for crystallization. Three absorption bands at around 500, 700 and 800 nm were observed and the broad NIR luminescence centered at 1300 nm was also detected. And no NIR luminescence was detected in the

glass with higher Na_2O content which shows the typical absorption spectrum of Bi^{3+} ions. Finally, they concluded that the NIR luminescence from Bi-doped glasses might come from BiO or Bi clusters.

Sanz et al. (2006) studied an influence of the melting condition of heavy metal oxide glasses containing Bi_2O_3 on the color generation. They found that the colors of glasses change from pale yellow to deep brown, turned to deeper at the higher temperature. Furthermore, they observed the nano-particles of metallic Bi by TEM in glasses melted above 1000°C. This effect has to be related to a redox process, reduction of Bi^{3+} to lower oxidation state in the glass melt during melting.

CHAPTER III

EXPERIMENTAL

3.1 Starting materials

Raw materials used in this research are listed in Table 3.1.

Table 3.1   Raw materials used in this research.

Raw materials	Chemical formula	Make	Remarks
Silica sand	SiO_2	Rayong sand, Thailand	–
Silica	SiO_2	Kojundo Chemicals	99.9%
Alumina	Al_2O_3	Sumitomo Chemicals Ind.	A-21
Lithium carbonate	Li_2CO_3	Merck	Reagent grade
Sodium carbonate	Na_2CO_3	Carlo Erba	"
Potassium carbonate	K_2CO_3	Carlo Erba	"
Calcium carbonate	$CaCO_3$	Carlo Erba	"
Magnesium carbonate, basic	*	Riedel-de Haen	" MgO: 40%
Zinc oxide	ZnO	Carlo Erba	"
Phosphoric acid	H_3PO_4	Carlo Erba	" 85% Solution
Boric acid	H_3BO_3	UNIVAR	"
Titanium oxide	TiO_2	Riedel-de Haen	"
Zirconium oxide	ZrO_2	Riedel-de Haen	"
Tellurium oxide	TeO_2	Fluka	"
Bismuth oxide	Bi_2O_3	Fluka	"
Activated carbon	C	Fluka	"

*: $3MgCO_3 \cdot Mg(OH)_2 \cdot 3H_2O$

3.2   Sample preparation

3.2.1   Preliminary research: Te and Bi doped glasses and glass-ceramics

This research was undertaken to detect the color center and luminescence center in Te- and Bi-doped glasses and glass-ceramics.

- Glass Melting

The compositions of glasses such as Spinel: Sp, soda-lime-silicate: SL, zinc tellurium phosphate: ZTP, lithium disilicate: L·2S, aluminum phosphate: $AlPO_4$ studied are shown in Table 3.2. High purity silica sand, alumina and reagent grade chemicals of Li_2CO_3, Na_2CO_3, K_2CO_3, $CaCO_3$, H_3PO_4, H_3BO_3, MgO, ZnO, TiO_2, ZrO_2, TeO_2, Bi_2O_3 and carbon were used as raw materials. The addition of a slight amount of carbon produces a mild reducing condition.

Table 3.2   Glass compositions (wt%) studied.

Name	SiO_2	Al_2O_3	ZnO	MgO	CaO	Na_2O	K_2O	TeO_2	Bi_2O_3*	Carbon*
Te-Sp	46.9	26.54	10.59	5.25	TiO_2:1.75, ZrO_2:8.93			0.2*	–	–
Te-SL	72	2	–	4	8	13	1	1.6*	–	0.08
Te-ZTP	P_2O_5: 50.06, ZnO: 35.87							14.07	–	–
Bi-L·2S	80	4	–	P_2O_5: 3, Li_2O: 13.0				–	6.0	–
Bi-AlPO$_4$	28.07	23.82	P_2O_5:33.17, B_2O_3: 4.07 , Na_2O: 10.86					–	6.0	–
Bi-Sp	46.9	26.54	10.59	5.25	TiO_2:1.75, ZrO_2:8.93			–	6.0	–

*: excess wt%

Batches corresponding to 25 g of glass were mixed thoroughly and melted in a 50 cc Pt/Rh10 or alumina crucibles under appropriate condition in an electric furnace in air. After melting they were poured onto iron plate and pressed by

another iron plate. Glasses were heat treated for nucleation and crystallization under various conditions. The melting conditions of glasses and heat treatment conditions for nucleation and crystallization of glass-ceramics are shown in Table 3.3

The glasses and glass-ceramics were cut into the size of $2\times2\times0.1\text{-}0.2$ cm^3 and then polished optically into about 1-2 mm in thickness for optical measurement.

Table 3.3 Melting conditions, heat treatment conditions for crystallization of glass-ceramics.

Name	Melting condition (°C–h)	Heat treatment (°C–h)
Te-Sp	1600-1 Pt/Rh10	800-10, 1000-5
Te-SL	1450-1 Pt/Rh10	*
Te-ZTP	1200-1 alumina	*
Bi-L·2S	1450-1 Pt/Rh10	500-10, 600-5
Bi-AlPO$_4$	1600-1 Pt/Rh10	500-10, 600-5
Bi-Sp	1600-1 Pt/Rh10	800-10, 1000-5

*: can not be treated to be glass-ceramics due to having not crystalline phase in the composition.

3.2.2 Fundamental research

This research was carried out to find factors affecting on valence state and NIR luminescence based on redox reaction in glasses.

3.2.2.1 Effect of melting temperature: Bi-containing borate glasses.

The glasses of composition $63B_2O_3 \cdot 9Al_2O_3 \cdot 9ZnO \cdot 9K_2O \cdot 10Bi_2O_3$ (mol%) were prepared by melting at various temperatures. Reagent grade chemicals of H_3BO_3, Al_2O_3, ZnO, K_2CO_3 and Bi_2O_3 were used as raw materials. Batches corresponding to 25 g of glass were mixed thoroughly and melted in 50 cc alumina crucible under various conditions in an electric furnace in air. The melting conditions of glasses are shown in Table 3.4. After melting they were poured onto iron plate and pressed by another iron plate. Then they were annealed at 450°C for 30 min and cooled slowly to room temperature in the furnace. Glasses were polished optically into about 1.5-2 mm in thickness for optical measurement. Hereafter, these glasses are referred to as Bi-1000, Bi-1100, Bi-1200, Bi-1300 and Bi-1400, respectively. The Bi-1400 glass was also melted under strong reducing condition by adding 2.0% of carbon (hereafter denotes Bi-1400 C2.0).

Table 3.4 Melting conditions.

No.	Melting condition/(°C–min.)
Bi-1000	1000-40
Bi-1100	1100-20
Bi-1200	1200-20
Bi-1300	1300-15
Bi-1400	1400-15
Bi-1400 C2.0	1400-15

3.2.2.2 Effect of glass composition: Bi-containing borate glasses.

Four glasses were prepared and their compositions were expressed by $90[10Al_2O_3 \cdot (80-X) B_2O_3 \cdot 10ZnO \cdot XK_2O] \cdot 10Bi_2O_3$ (mol%, X=0, 10, 20, 30). Reagent grade chemicals of H_3BO_3, Al_2O_3, ZnO, K_2CO_3 and Bi_2O_3 were used as raw materials. Batches corresponding to 25 g of glass were mixed thoroughly and melted in 50 cc alumina crucibles at 1200°C for 20 min in an electric furnace in air. After melting they were poured onto iron plate and pressed quickly by another iron plate. Then they were annealed at 450°C for 30 min and cooled slowly to room temperature in the furnace. Glasses were ground and polished optically into about 1.5-2 mm in thickness for optical measurement. Hereafter, glasses are referred to as X-0, X-10, X-20 and X-30, respectively.

3.2.2.3 Effect of reducing agent: Bi-doped soda-lime- silicate glass.

The compositions of glasses studied are $72SiO_2 \cdot 2Al_2O_3 \cdot 4MgO \cdot 8CaO \cdot 13Na_2O \cdot 1K_2O \cdot 0.5Bi_2O_3 \cdot C$ (wt%, C=0, 0.5, 1.0, 1.5), and hereafter, these glasses are referred to as C-X. In order to control the melting atmosphere, carbon was added to batches.

High purity silica (99.9%), alumina and reagent grade chemicals of Na_2CO_3, K_2CO_3, $MgCO_3$, $CaCO_3$, Bi_2O_3 and carbon were used as raw materials. Batches corresponding to 25 g of glass were mixed thoroughly and melted in 50 cc alumina crucibles at 1450°C for 1 h in an electric furnace in air. After melting they were poured onto an iron plate and pressed by other one. Then they were annealed at 650°C for 30 min and cooled slowly in the furnace. The C-1.0 glass was also annealed at 550°C for 0 min and cooled slowly in the furnace (hereafter denotes

C-1.0*). The glass transition point (T_g), softening point (T_{soft}) and thermal expansion coefficient (α) of these glasses are 550°C, 730°C and 90×10^{-7}/K, respectively.

The glasses were cut and polished optically into about 1.5-2 mm thickness for optical measurements.

3.3   Characterization

3.3.1   X-ray Diffraction (XRD) analysis

Crystalline phases, percent crystallinity and crystal size were examined by powder X-ray diffraction (XRD) using Bruker AXS Model D5005 under the condition of Cu-K$_\alpha$ radiation at 40 kV and 40 mA., slit system; $1°-1°$, scan; step scan $0.02°$/step, 0.1 sec./step. In some case, the step scan method (very slow scan) was applied for the detection of very small amount of crystals, less than 1 wt%. The condition is; Cu-K$_\alpha$ radiation at 40 kV-40 mA., slit system; $1°-1°$, scan; step scan $0.1°$/step, 100 sec. /step

Crystal size was calculated using Scherrer's equation.

$$d = 0.9\lambda \, / \, \beta \cdot Cos\theta \tag{3.1}$$

where d is the crystal size (nm), λ the wavelength of X-ray (0.154 nm), β the true half width (radian) and θ the diffraction angle (degree). The true half width was determined by Jones method (Nitta, 1975), and α-Quartz was used as a standard (Appendix I).

Percent crystallinity was determined using Ohlberg and Strickler's method (Ohlberg and Strickler, 1962) and was calculated using by next equation.

$$Percent\ crystallinity\ (\%) = [(Ig - Ix)/\ (Ig - Ic)]\ x\ 100 \qquad (3.2)$$

Where *Ig* is the background intensity of glass, *Ix* that of the specimens and *Ic* that of

the crystal at $2\theta = 23°$. The calibration curve was obtained using mixtures of α-Quartz

and parent glass at various ratios, and showed a good linearity (Appendix II).

3.3.2 Scanning Electron Microscopy (SEM) Analysis

The fractured surface of glasses and glass-ceramics were etched by

0.5% HF solution for 1 min at room temperature. The chemically etched samples

were coated with conductive material (Au) using Ion Sputtering Device (JEOL, JFC-

110E). The surface structures of glasses and glass-ceramics were observed by

scanning electron microscope (SEM) using JEOL, JSM 6400.

3.3.3 Electron Spin Resonance (ESR) Analysis

The electron spin resonance spectra were measured using JEOL JES

RE-2X at room temperature. Microwave unit: X band, frequency: 8.8-9.6 GHz,

cavity: cylindrical, operating in TE_{011} mode and ESR software: use ES-IPRIT

program.

3.3.4 Optical Analysis

The absorption spectra were measured with Cary 1E ultraviolet-visible

(UV-VIS) spectrometer in the range of 300 nm to 800 nm at room temperature.

The luminescence spectra in UV-VIS region were measured with

Perkin–Elmer Luminescence Spectrometer LS50B at room temperature.

The luminescence spectra in NIR region (1000 nm to 1700 nm) were

measured under the excitation of 974 nm laser diode at room temperature (Prof.

Ohishi Lab., TTI, Nagoya, Japan). Emission from the sample was dispersed by a

single monochromator (blaze, 1.0 μm; grating, 600 grooves/mm; resolution, 3 nm) and detected by an InGaAs photodiode, as shown in Figure 3.1.
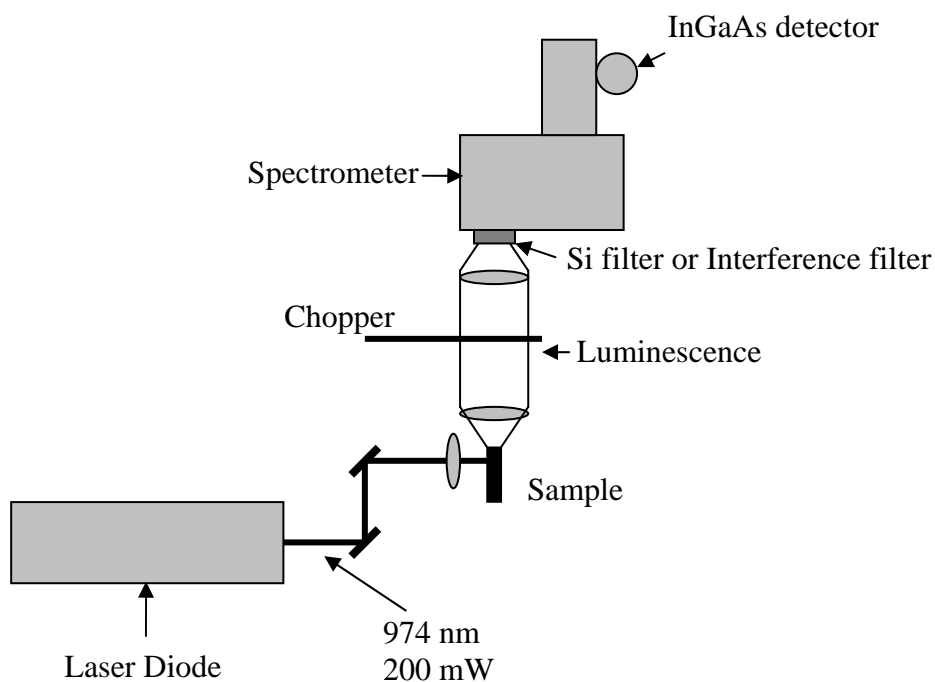
Figure 3.1   Optical setup for NIR luminescence measurement.

3.3.5   X-ray Photoelectron Spectroscopy Analysis

The X-ray photoelectron spectroscopy (XPS) measurement was performed with monohromatized Mg-Kα radiation at acceleration voltage of 15 kV with electron shower for Bi $4f_{5/2}$ and $4f_{7/2}$ (National Synchrotron Research Center, Thailand). The shift of the energy scale was corrected with a reference of C1s binding energy of residual hydrocarbon at 284.6 eV.

The research procedure is shown in Figure 3.2.

```
┌─────────────────────────────────────────────────────┐
│         Determination of Glass Composition          │
└─────────────────────────────────────────────────────┘
                          ↓
┌─────────────────────────────────────────────────────┐
│            Determination of Raw Materials           │
│                  Batch Preparation                  │
└─────────────────────────────────────────────────────┘
                          ↓
              ┌──────────────────────┐
              │        Mixing        │
              └──────────────────────┘
                          ↓
          ┌───────────────────────────────┐
          │            Melting            │
          │    Pt/Rh or Alumina Crucible  │
          │    1000-1600°C, 15-120 min.   │
          └───────────────────────────────┘
                          ↓
              ┌──────────────────────┐
              │        Casting       │
              │      Iron Plate      │
              └──────────────────────┘
                          ↓
          ┌───────────────────────────────┐
          │           Annealing           │
          │       450-700°C, 30 min.      │
          └───────────────────────────────┘
                          ↓
          ┌───────────────────────────────┐
          │         Heat Treatment        │
          │       500-1000°C, 5-10 h      │
          └───────────────────────────────┘
                          ↓
┌─────────────────────────────────────────────────────┐
│                 Sample Preparation                  │
│  1. Plate samples for optical measurement           │
│    Grinding, polishing                              │
│    (SiC powder, CeO2 powder)                        │
│  2. Powder samples                                  │
│    Pulverizing (> #100)                             │
└─────────────────────────────────────────────────────┘
         Plate                      Powder
        ↙                                  ↘
┌──────────────────────┐      ┌──────────────────────┐
│   Characterization   │      │   Characterization   │
│ 1. Absorption spectra│      │ 1. XRD               │
│ 2. Luminescence      │      │ 2. SEM               │
│    spectra           │      │ 3. ESR               │
│ 3. XPS               │      │                      │
└──────────────────────┘      └──────────────────────┘
```
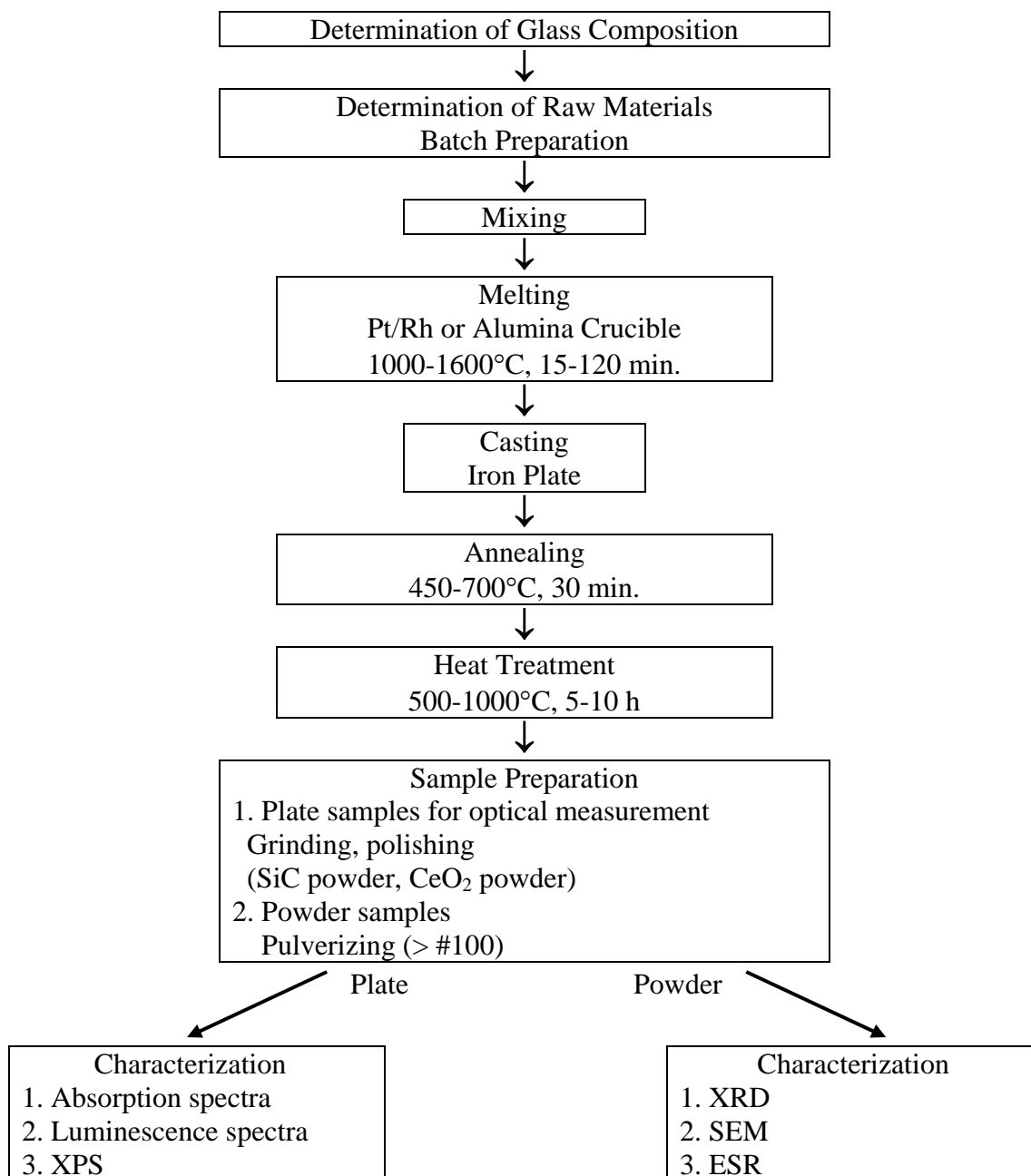
Figure 3.2 Flow sheet of experimental procedure.

CHAPTER IV

RESULTS AND DISCUSSION

4.1   Te- and Bi-doped glasses and glass-ceramics

4.1.1   Results

4.1.1.1   XRD analysis

Some glasses are able to convert to transparent glass-ceramics based on lithium disilicate ($Li_2O \cdot 2SiO_2$, JCPDS 40-0376) for L·2S, tridymite type $AlPO_4$ (JCPDS 051-1674) for $AlPO_4$ and spinel [(Mg,Zn)Al_2O_4, JCPDS 01-070-5187] crystals for Spinel upon heat treatment. Figure 4.1 shows XRD patterns of these transparent glass-ceramics. The crystalline phases, crystal size and percent crystallinity are summarized in Table 4.1. The percent crystallinity and crystal size are ranging 45-70±5% and 15-25±5 nm, respectively. All glass-ceramics are highly transparent.

4.1.1.2   Appearance and absorption spectra.

(a)   Te-doped glasses and glass-ceramics

Appearance of samples are pale green for Te-SL, brilliant purple for Te-ZTP and brown-pink for Te-Sp glass-ceramics, and absorption spectra are shown in Figure 4.2 (a). Three absorption bands are observed at around 377, 444 and 625 nm for green Te-SL glass. For Te-ZTP glass, the strong absorption band at 537 nm with a shoulder at around 420 nm appears. On the contrary, the shoulder at around 420 nm is observed in Sp glass-ceramics.
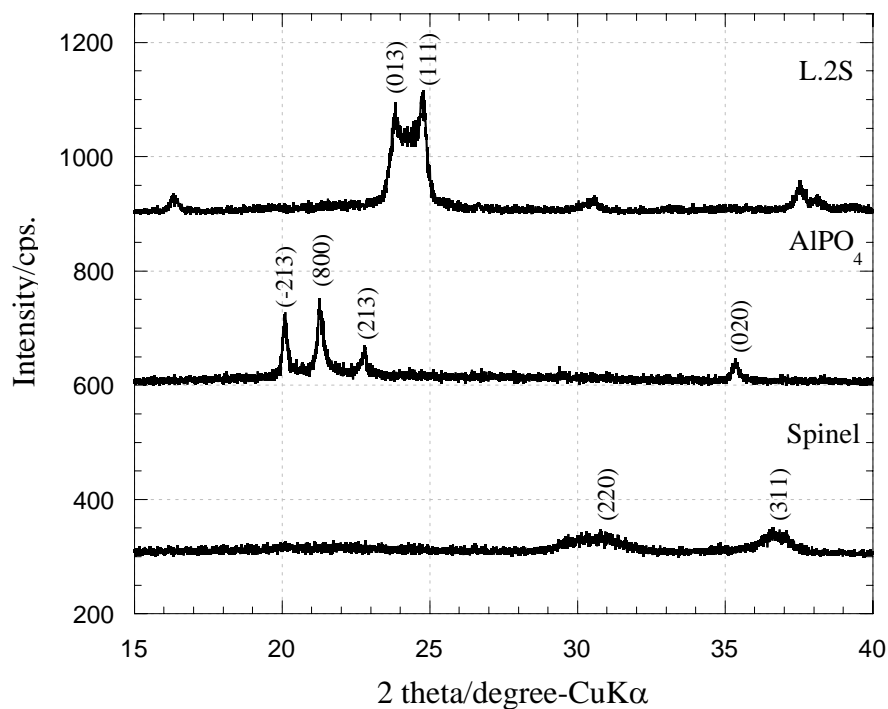
Figure 4.1   XRD patterns of transparent glass-ceramics.

Table 4.1   Appearance, Crystalline phases, Crystal size and Percent crystallinity.

Name	Appearance*	Crystals		
		Phases	Percent (wt %)	Size (nm)
Te-Sp	Pale brown Brown-pink	Spinel	45±5	15±5
Te-SL	Pale green	No crystallization		
Te-ZTP	Brilliant pink	No crystallization		
Bi-L·2S	Pale yellow Pale brown	Lithium disilicate	70±5	25±5
Bi-AlPO$_4$	Brown Brown black	AlPO$_4$	50±5	20±5
Bi-Sp	Pale pink Pink	Spinel	45±5	15±5

*: upper=glass, lower=glass-ceramics

The absorption bands may be classified into four bands, and they are summarized in Table 4.2. The absorption bands were analyzed with Gaussian distribution.

For green Te-SL glass, the absorption band at 440 nm is ascribed to $^3\Sigma_g \rightarrow {}^3\Sigma_u$ transition of Te_2 color center and the absorption band at 625 nm can be assigned to $^2\pi_g \rightarrow {}^2\pi_u$ transition of Te_2^- color center (Lindner et al., 1996). The 377 nm band may relate to exciton transition (Lindner et al., 1996). The strong absorption band at 537 nm of Te-ZTP glass seems to be due to colloidal metallic Te (Konishi et al., 2003). Actually, many particle of about 200 nm in diameter are observed in Te-ZTP glass, and a small particle was also detected in Te-Sp glass-ceramics as shown in Figure 4.3(a). This indicates that TeO_2 was reduced to metallic Te. This pink color generation might be due to the surface plasmon resonance absorption of Te colloids (Konishi et al., 2003)

(b)   Bi-doped glasses and glass-ceramics

Appearance of samples are yellow-brown for Bi-L·2S glass-ceramics, deep brown for Bi-AlPO$_4$ glass-ceramics and pale pink to pink for Bi-Sp glass and glass-ceramics, and their absorption spectra are shown in Figure 4.2(b). Two absorption bands at around 480 nm and 700 nm appear in pink Sp glass and glass-ceramics. This spectral pattern is the same as those reported previously (Fujimoto and Nakatsuka, 2001 and Peng et al., 2004). On the contrary, no specific absorption band can be detected in Bi-L·2S and Bi-AlPO$_4$ glass-ceramics. Figure 4.3(b) shows that particles of 100-200 nm in diameter precipitated in Bi-AlPO$_4$ glass-ceramics, while no particles can be detected in Bi-Sp glass-ceramics. These particles

may be colloidal metallic Bi (Sanz et al., 2006). This indicates that Bi_2O_3 was reduced to metallic Bi in Bi-AlPO$_4$ glass-ceramics.

The absorption spectra of Bi-doped glasses and glass-ceramics were analyzed with Gaussian distribution, and they are shown in Table 4.2.

Table 4.2 Absorption bands analyzed by Gaussian distribution.

Name	Band I nm	Band II nm	Band III nm	Band IV nm
Te-SL	377	444	(526)*	625
Te-ZTP	375	417	537	(600)*
Te-Sp G.C.	-	420 (448)*	(556)*	(599)*
Bi-L·2S G.C.	-	-	-	-
Bi-AlPO$_4$ G.C.	-	-	-	-
Bi-SpG.	(370)*	480	-	700
Bi-SpG.C.	(370)*	480	-	700

*: very weak

4.1.1.3   Luminescence in UV-VIS and NIR region.

Figure 4.4 shows UV-VIS luminescence of Te- and Bi-doped glasses and glass-ceramics at room temperature. The strong and structured blue luminescence was observed in Te-doped glasses and glass-ceramics. The weak sub luminescence band is detected in red region. The intensity of these luminescence bands seems to be proportional to TeO$_2$ content in samples.
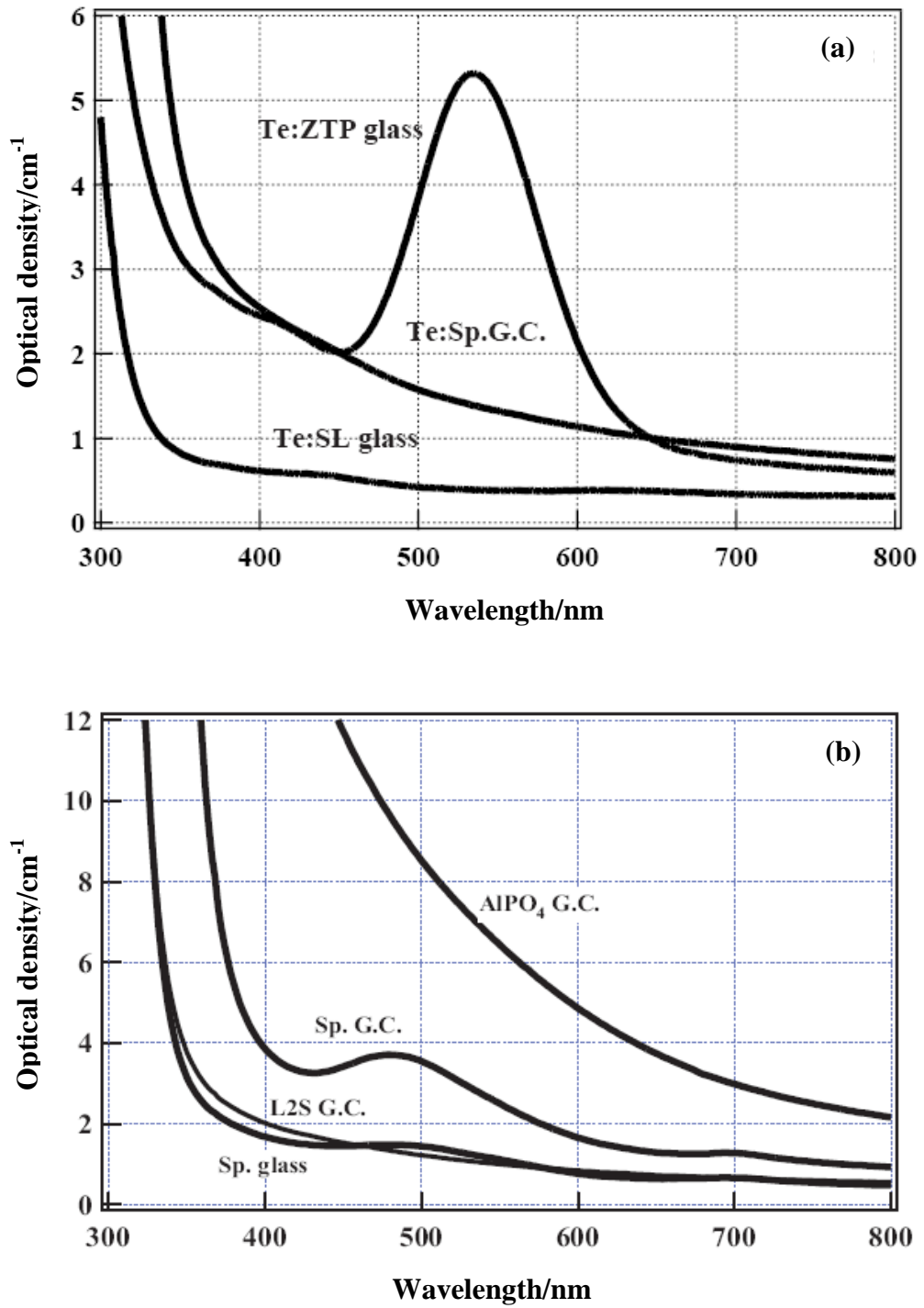
Figure 4.2   Absorption spectra of Te- and Bi-doped glasses and glass-ceramics. (a)

Te-doped glasses and glass-ceramics, (b) Bi-doped glasses and glass-
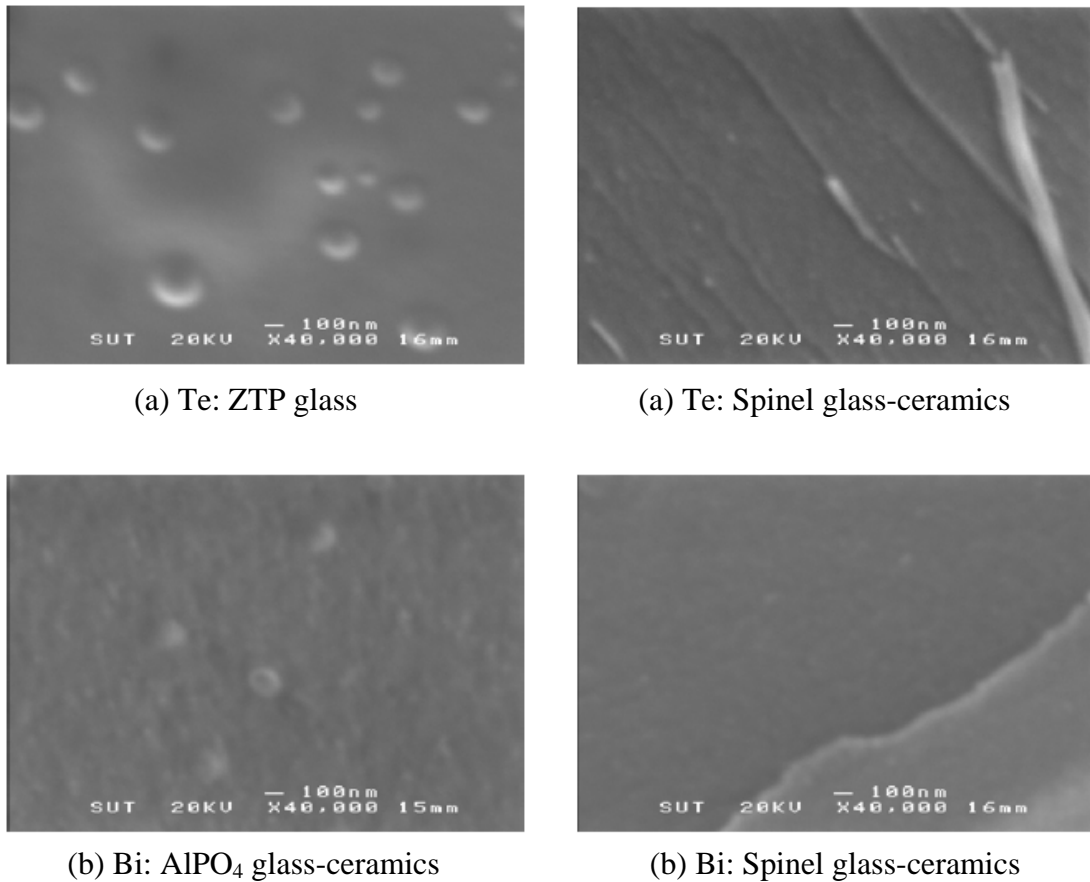
ceramics. (G.C.: glass-ceramics)

(a) Te: ZTP glass

(a) Te: Spinel glass-ceramics

(b) Bi: AlPO$_4$ glass-ceramics

(b) Bi: Spinel glass-ceramics

Figure 4.3   SEM photos of Te- and Bi-doped glasses and glass-ceramics. (a) Te-doped glass and glass-ceramics, (b) Bi-doped glass-ceramics.

In Bi-doped L·2S glass-ceramics and Sp glass, strong blue luminescence is detected with weak luminescence band at around 800 nm. On the contrary, a very weak and structured blue luminescence is observed in AlPO$_4$ and Sp glass-ceramics, and red luminescence disappears. The luminescence intensity decreases markedly by the heat treatment for crystallization in Sp glass. It is well known that the blue luminescence of Bi-containing glass is derived from Bi^{3+} ions in materials (Steen, 1981 and Blasse, 1997)
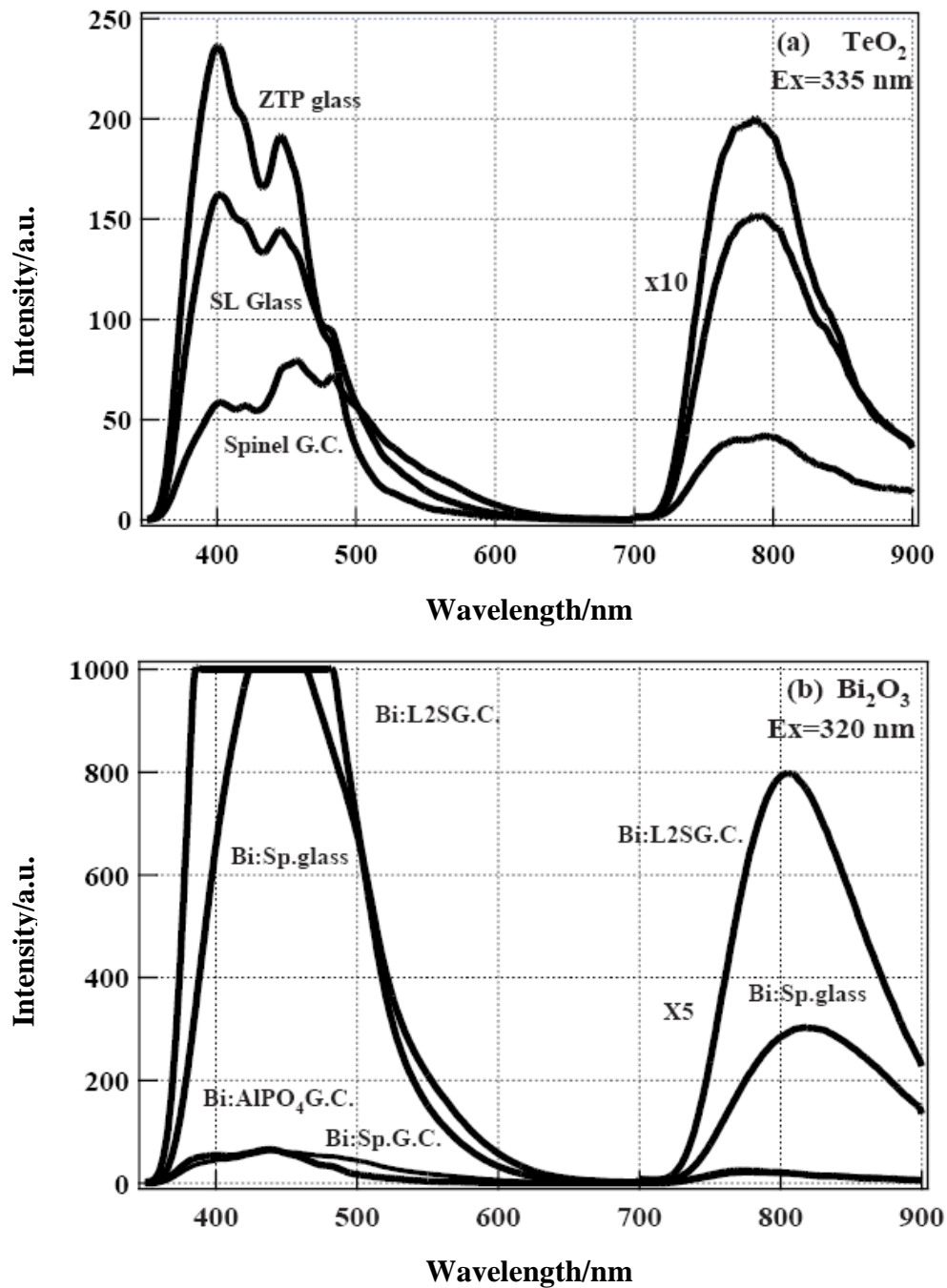
Figure 4.4   UV-VIS emission spectra of Te- and Bi-doped glasses and glass-

ceramics at room temperature. (a) Te-doped glasses and glass-ceramics.

The intensity has been multiplied by 10 times in the range of 700-900

nm, (b) Bi-doped glasses and glass-ceramics. The intensity has been

multiplied by 5 times in the range of 700-900 nm.

Figure 4.5 shows the NIR luminescence spectra of Te- and Bi-doped glasses and glass-ceramics under the excitation of 974 nm laser diode at room temperature. A broad NIR luminescence at around 1200 nm can be observed in all Te-doped glasses and glass-ceramics. It should be noted that a weak and rather sharp luminescence can also be detected at around 1020 nm in Te-Sp glass-ceramics.

On the other hand, pink colored Bi-Sp glass and glass-ceramics exhibit NIR luminescence at around 1100 nm with a shoulder at around 1450 nm. However, no NIR luminescence can be observed in other two Bi-doped glass-ceramics (L·2S and $AlPO_4$ glass-ceramics).

4.1.1.4   ESR spectra

In order to determine the luminescent center of Te- and Bi-doped glasses and glass-ceramics, the ESR spectra were measured. The ESR spectra are shown in Figure 4.6. Two ESR signals were detected, g~4.7 and g~2.0 for both Te- and Bi-doped glasses and glass-ceramics. The ESR signals at g~4.7 may be derived from impurities, such as Fe^{3+} ion in the sample (Elvers and Weissmann, 2001).

It is noteworthy that ESR spectrum of Bi-doped Sp glass and glass-ceramics is identical with that of Te-doped Sp glass-ceramics. The ESR signal at g~2.0 can also be observed in Bi-Sp glass and Sp glass-ceramics which exhibit NIR luminescence. However, the ESR signals at g~2.0 can not be detected in Bi-$AlPO_4$ G.C. and Bi-L·2S G.C. which do not exhibit NIR luminescence, and hence this ESR signal is strongly related to NIR luminescence.
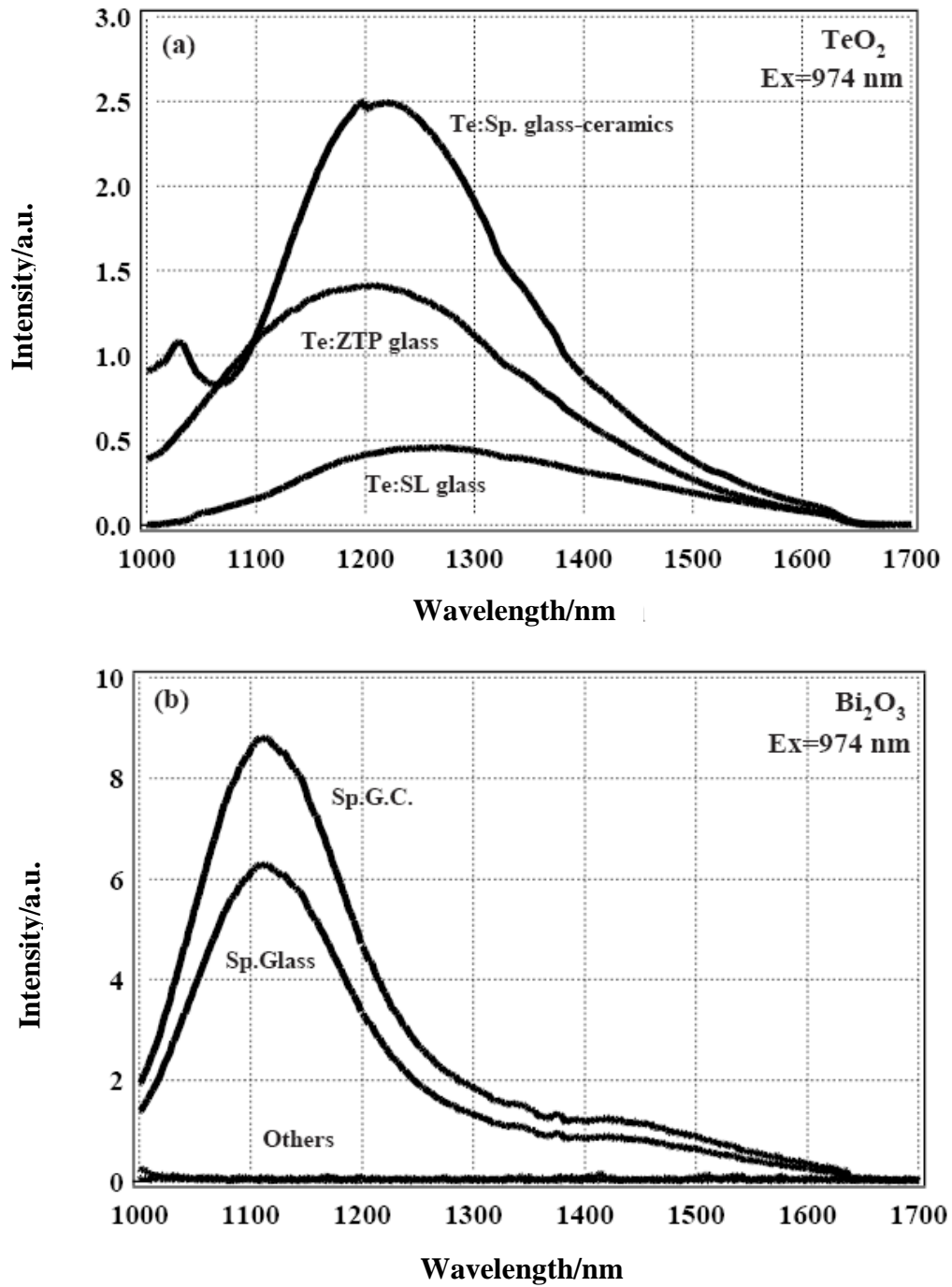
Figure 4.5   NIR luminescence spectra of Te- and Bi-doped glasses and glass-

ceramics under the excitation of 974 nm laser diode at room

temperature. (a) Te-doped glasses and glass-ceramics, (b) Bi-doped
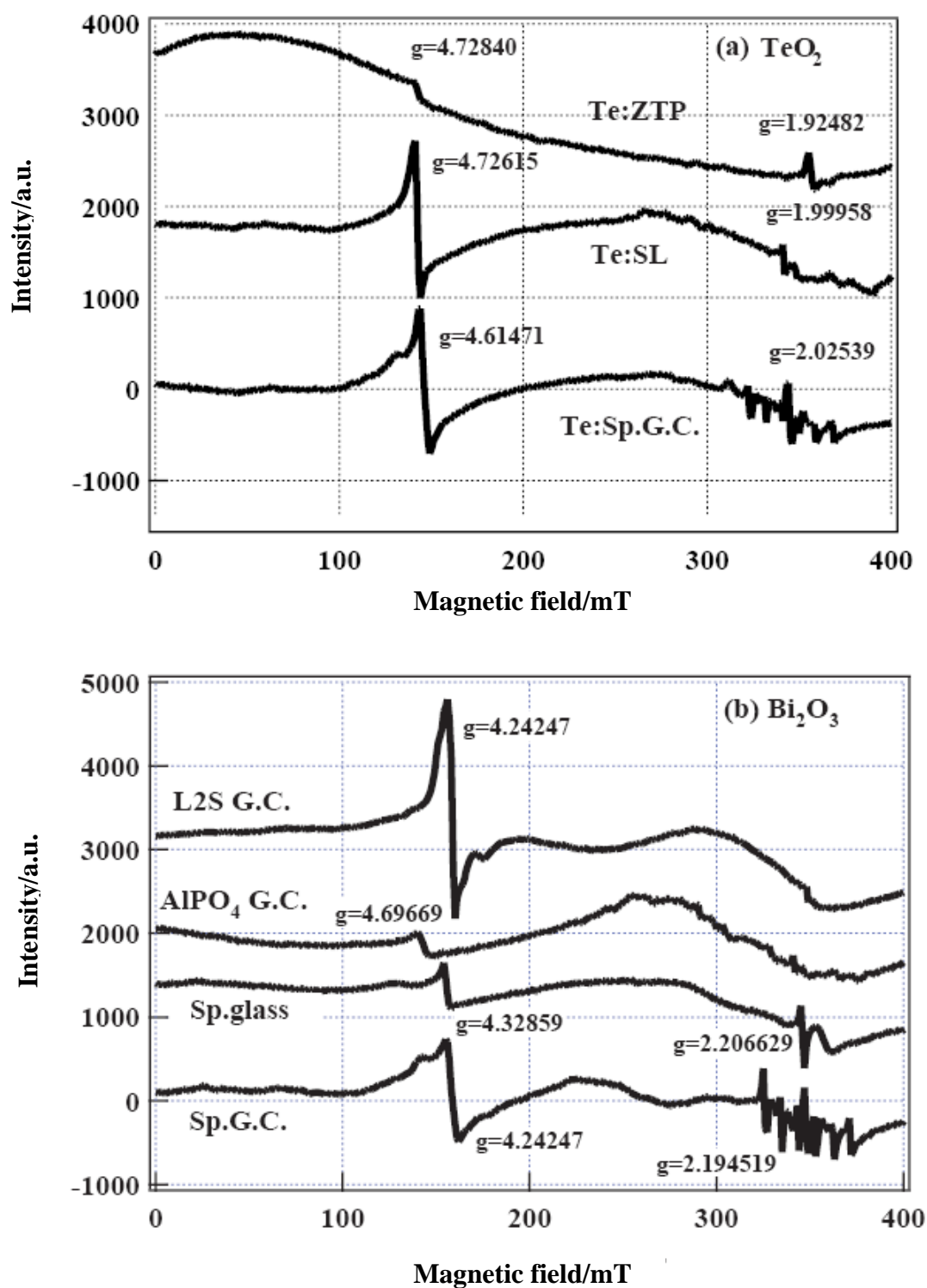
glasses and glass-ceramics.

Figure 4.6 ESR spectra of Te- and Bi-doped glasses and glass-ceramics. (a) Te-doped glasses and glass-ceramics, (b) Bi-doped glasses and glass-ceramics.

4.1.2 Discussion

4.1.2.1 Te-doped glasses and glass-ceramics

It was found that colorations of Te-doped glasses and glass-ceramics might be due to elemental clustering of Te, such as Te_2 and Te_2^-. The dimer of Te cluster is believed to be stable species (Willey et al., 1995 and Nagaya et al., 2002). In glasses and glass-ceramics, it is clear that TeO_2 was reduced to elemental Te during melting, and they aggregated to colloidal size. This colloidal metallic Te results in the pink coloration of ZTP glass. However, the NIR luminescence does not seem to be due to colloidal Te because the NIR luminescence is not proportional to the amount of colloidal Te.

In ESR spectra shown in Figure 4.6(a), two ESR signals were detected, g~4.7 and g~2.0. The ESR signals at g~4.7 may be derived from impurities, such as Fe^{3+} ion in the sample. The ESR signals at g~2.0 of SL and Sp glass-ceramics have fine structure. This signal often appears in halide crystals and it is assigned to self-trapped hole or V_k center (Dong et al., 1999 and Nistor et al., 2000). This means that ESR signal at g~2.0 is derived from halogen molecular ion, X_2^-. The similar ESR spectrum was obtained in Se-doped borosilicate glass and it is believed to be due to Se_2^- ions (Guha, Leppert, and Risbud, 1998). Since Te clustering such as Te_2^-/Te_2 exists in Te-doped glasses as mentioned previously, ESR signals at g~2.0 can be assigned to Te_2^- ions. The NIR luminescent intensity seems to be proportional to the intensity of g~2.0 signals of ESR spectra.
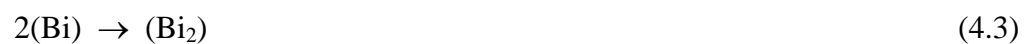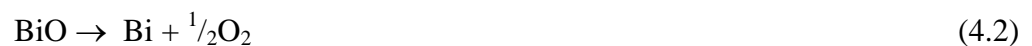
4.1.2.2 Bi-doped glasses and glass-ceramics

The origin of the pink coloration and NIR luminescence of

Bi-doped glasses and glass-ceramics are not clear yet. Here, the origin of the coloration and NIR luminescence of Bi-doped glasses and glass-ceramics will be discussed.

It is well known that the blue luminescence of Bi-containing glass is derived from Bi^{3+} ions in materials (Blasse, 1997), therefore a large amount of Bi^{3+} ions present in Bi-L2S glass-ceramics and Bi-Sp glass. On the contrary, Bi^{3+} ion scarcely exists in Bi-AlPO$_4$ glass-ceramics and Bi-Sp glass-ceramics. This indicates that Bi^{3+} ion was reduced to lower valence state by further heat treatment for crystallization in Bi-AlPO$_4$ glass-ceramics and Bi-Sp glass-ceramics.

The darkening effect of high Bi_2O_3-containing glasses was reported (Sanz et al., 2006). When glasses containing a large amount of Bi_2O_3 were melted at higher temperature, brown-black glasses could be obtained, and nano-scale Bi particles were detected by transmission electron microscope (TEM) observation (Sanz et al., 2006). The nano-scale Bi particles can also be detected in this study (Figure 4.3(b)). This darkening effect was related to a redox process partially reducing Bi^{3+} ions to a lower valence state, and hence the next process may be given:

$$Bi_2O_3 \rightarrow 2BiO + {}^1/_2O_2 \qquad\qquad (4.1)$$

$$BiO \rightarrow Bi + {}^1/_2O_2 \qquad\qquad (4.2)$$

$$2(Bi) \rightarrow (Bi_2) \qquad\qquad (4.3)$$

$$n(Bi) \rightarrow (Bi)_n \qquad\qquad (4.4)$$

Here, (Bi) indicates elemental Bi, (Bi$_2$) the molecular Bi and (Bi)$_n$ the metallic colloidal Bi. Above reactions go to right side at higher temperature and reducing condition.

From the result mentioned previously, it is clear that Bi^{3+} ions (L·2S glass-ceramics) and colloidal metallic Bi (AlPO$_4$ glass-ceramics) are not responsible for pink coloration and NIR luminescence. The NIR luminescence can be observed only for pink Sp glass and glass-ceramics.

It should be noted that ESR spectrum of Bi-doped Sp glass-ceramics is identical with that of Te-doped Sp glass-ceramics. The ESR signal at g~2.0 can also be observed in Bi-Sp glass and Bi-Sp glass-ceramics which exhibit NIR luminescence. This ESR signal can not be detected in AlPO$_4$ and L·2S glass-ceramics which did not exhibit NIR luminescence. Therefore, it seems that the ESR signal at g~2.0 is strongly related to NIR luminescence and pink coloration. In analogy with Te-doped Sp glass and Sp glass-ceramics, this ESR signal may come from Bi molecular ions, Bi$_2^-$.

In Se-pink glasses, the analytical concentration of Se is usually few hundreds ppm, and the Se molecule or molecular ions contributing the color generation is believed to be few % of total Se presented in glasses (Paul, 1975). Therefore, the concentration of Te and Bi molecular ions in glasses and glass-ceramics may be very low, ~10-30 ppm.

4.2   Effect of melting temperature: Bi-containing borate glasses.

4.2.1   Results

4.2.1.1   Appearance and absorption spectra.

The colors of glasses change from pale yellow (Bi-1000) to black (Bi-1300, Bi-1400 and Bi-1400 C2.0) with increasing temperature as shown in Table 4.3. In Bi-1400 C2.0 glass, silver-white colored Bi metal (6-8 mm in diameter with 5 mm thickness) deposited at the bottom of crucible during melting.

Table 4.3   Appearance and absorption bands analyzed by Gaussian distribution.

No.	Appearance	Absorption bands/nm		
		Band I	Band II	Band III
Bi-1000	Faint yellow-green	-	-	-
Bi-1100	Pale pink-red	460	490	-
Bi-1200	Orange-red	460	-	-
Bi-1300	Black	-	-	-
Bi-1400	Black	-	-	-
Bi-1400 C2.0	Black, Bi metal	-	-	-
Ren et al.(2006,2007)		~460	-	-
Fujimoto et al. (2001,2004), Peng et al. (2005,2007), Khonthon et al. (2007)		-	~490	~710

Figure 4.7 shows SEM photos of black colored glasses (Bi-1300, Bi-1400 and Bi-1400 C2.0). Many spherical particles of smaller than 1 μm are observed, and the shape of these particles becomes to be more clear and distinct with increasing melting temperature and reducing condition. These particles must be metallic Bi colloids (Sanz et al., 2006).
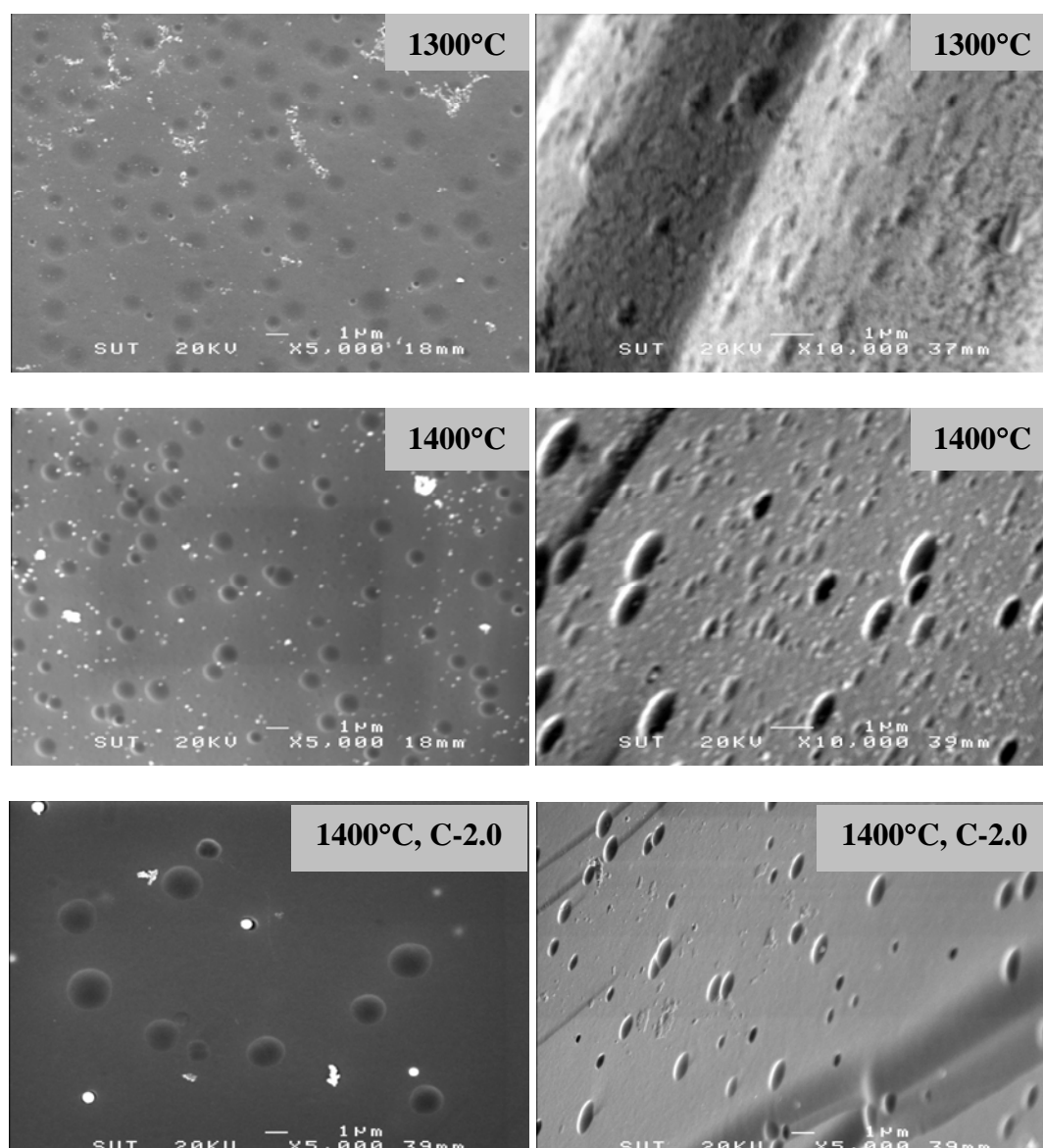
Figure 4.7   SEM photos of black-colored Bi containing borate glasses.

XRD patterns of Bi-1400 C2.0 glass are shown in Figure 4.8. These XRD patterns were obtained by step scan XRD method (very slow scan). It is clearly seen that two peaks can be detected at $2\theta = 27.2°$ and $2\theta = 38.1°$. These two diffraction peaks can be assigned to (012) and (104) planes of Bi metal (JCPDS 00-001-0688 or 00-005-0519), and therefore it is concluded that the particles observed

in SEM photos could be metallic Bi colloids. Thus, Bi_2O_3 is partially reduced to metallic Bi colloids by melting at higher temperature and strong reducing condition. However, it is considered that the amount of metallic Bi colloids might be very low, less than 1 wt%. The darkening effect (black coloration) of Bi-containing glasses is confirmed to be the formation process of metallic Bi colloids.
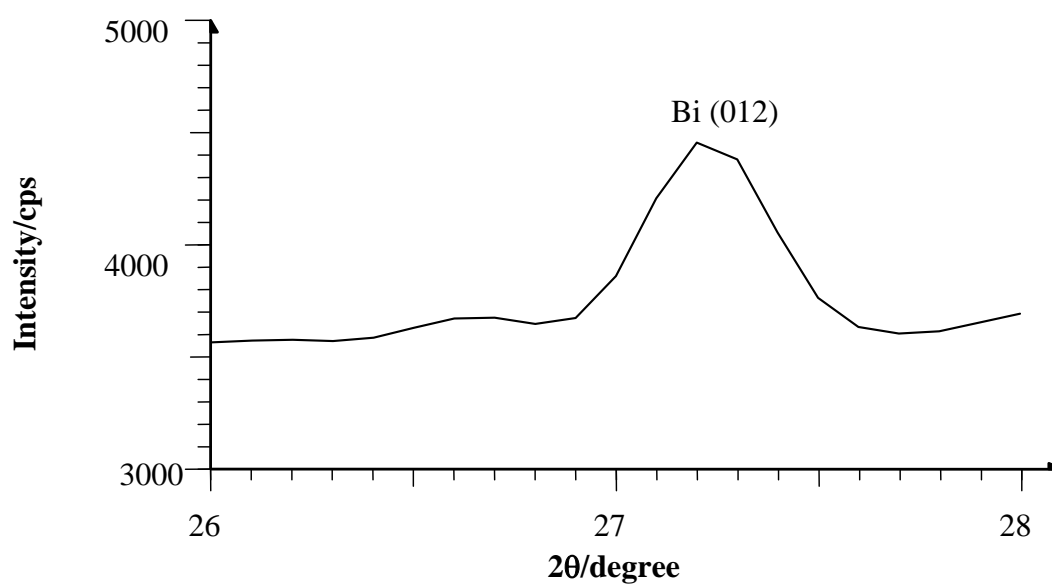

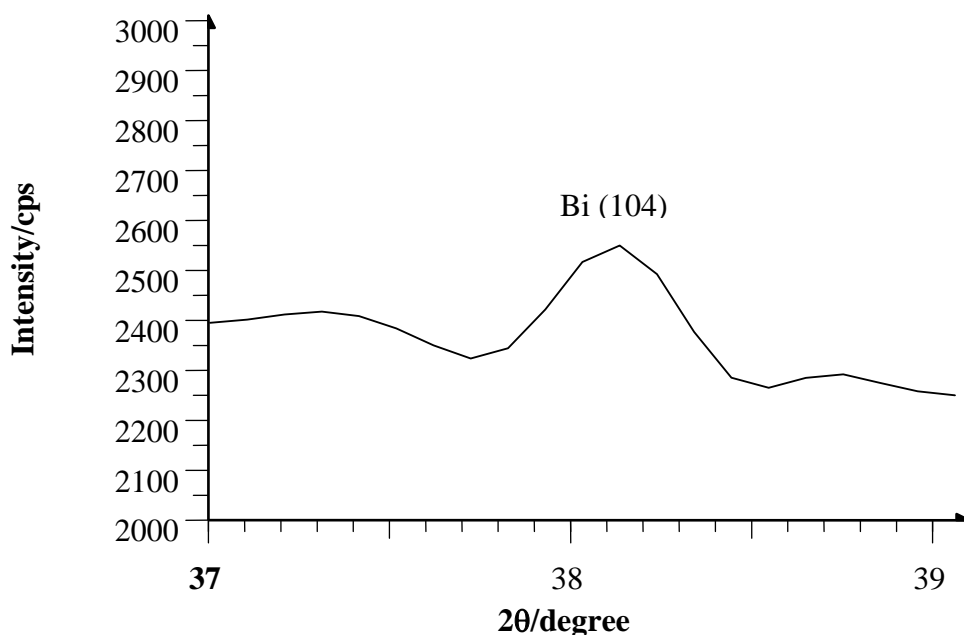**Figure 4.8** XRD patterns of Bi-1400 C2.0 glass.

Figure 4.8 XRD patterns of Bi-1400 C2.0 glass (cont.)

Figure 4.9 shows absorption spectra of Bi-containing glasses. The absorption spectra for black colored glasses could not be measured because of their very deep black coloration. The characteristic absorption band was not observed in Bi-1000 glass. On the other hand, the simple absorption band is observed at around 460 nm in Bi-1100 and Bi-1200 glasses. These spectral patterns are quite similar to those reported previously (Ren et al., 2006 and 2007). On the contrary, however, Peng et al. (2005 and 2007), Suzuki et al. (2004) and Khonthon et al. (2007) have observed different spectral patterns, in which there were two absorption bands, ~490 nm and ~710 nm in their glasses. This indicates that the different types of color centers may be present in glasses discussed here.
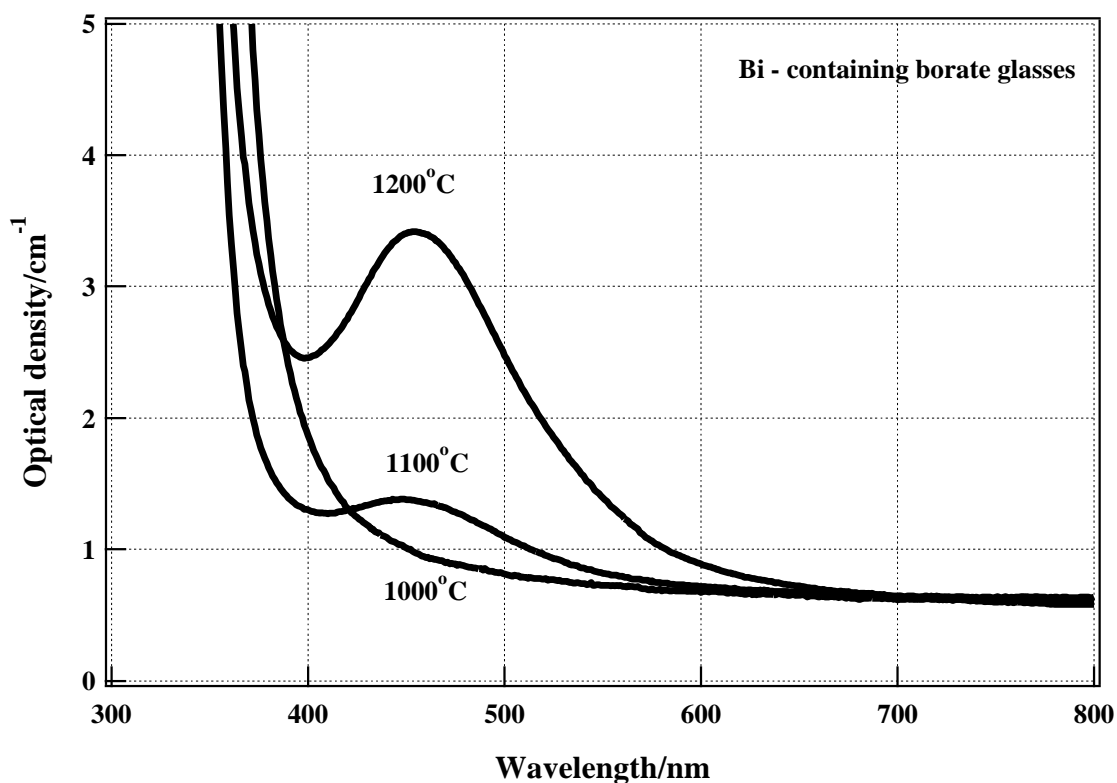
Figure 4.9   Absorption spectra of Bi-containing borate glasses.

4.2.1.2   NIR luminescence spectra

Figure 4.10 shows NIR luminescence spectra of glasses under the excitation of 974 nm laser diode at room temperature. Bi-1300, Bi-1400 and Bi-1400 C2.0 glasses do not exhibit NIR luminescence. On the other hand, the broad NIR luminescence centered at 1150 nm was detected in Bi-1100 and Bi-1200 glasses. The NIR luminescence intensity of Bi-1000 is very weak, while the intensity of NIR luminescence of Bi-1200 glass is the highest. From previous results (Section 4.1) and XRD result, it is clear that Bi^{3+} ion and metallic Bi colloids are not responsible for the generation of NIR luminescence.
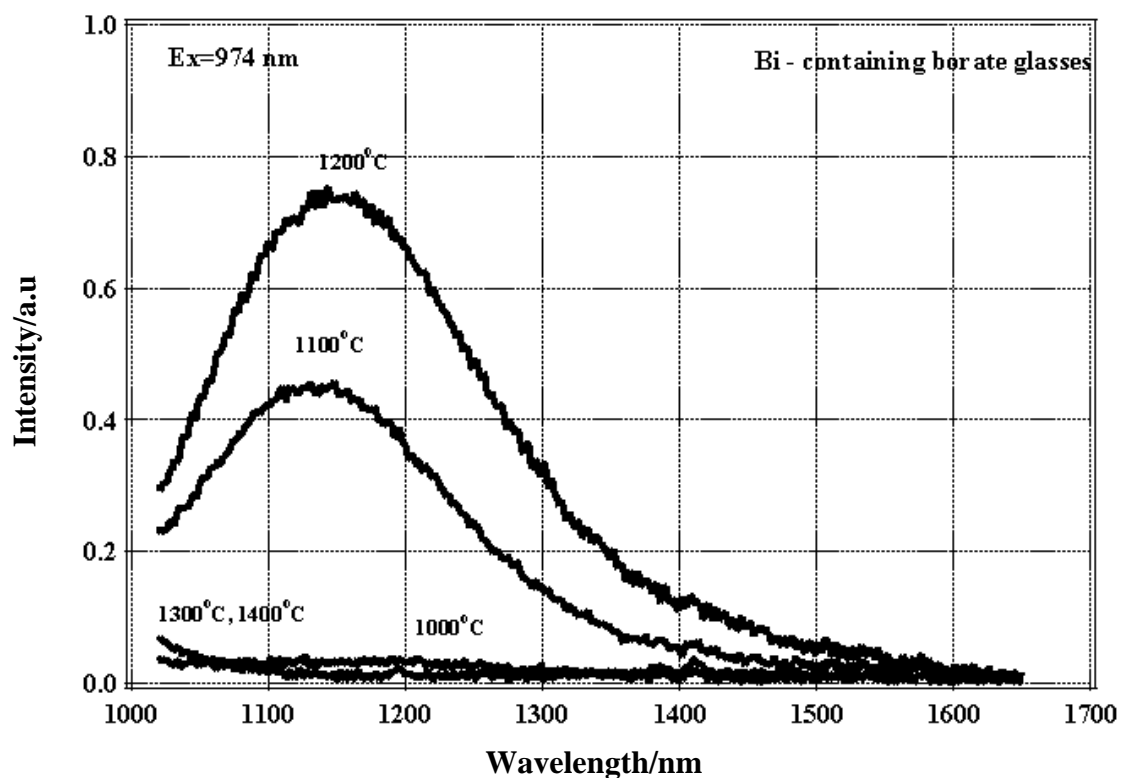
Figure 4.10   NIR luminescence spectra of Bi-containing borate glasses under the

excitation of 974 nm laser diode.

4.2.1.3   XPS spectra.

Figure 4.11 shows the XPS spectra of glasses. Two peaks of Bi $4f_{7/2}$ and Bi $4f_{5/2}$ were detected in all glasses. However, any signal can not be observed in lower energy side of these peaks, despite the peak position shifts slightly to lower energy side and half height width increases slightly with increasing melting temperature. This indicates that the considerable amount of lower valence species is not present in these glasses.
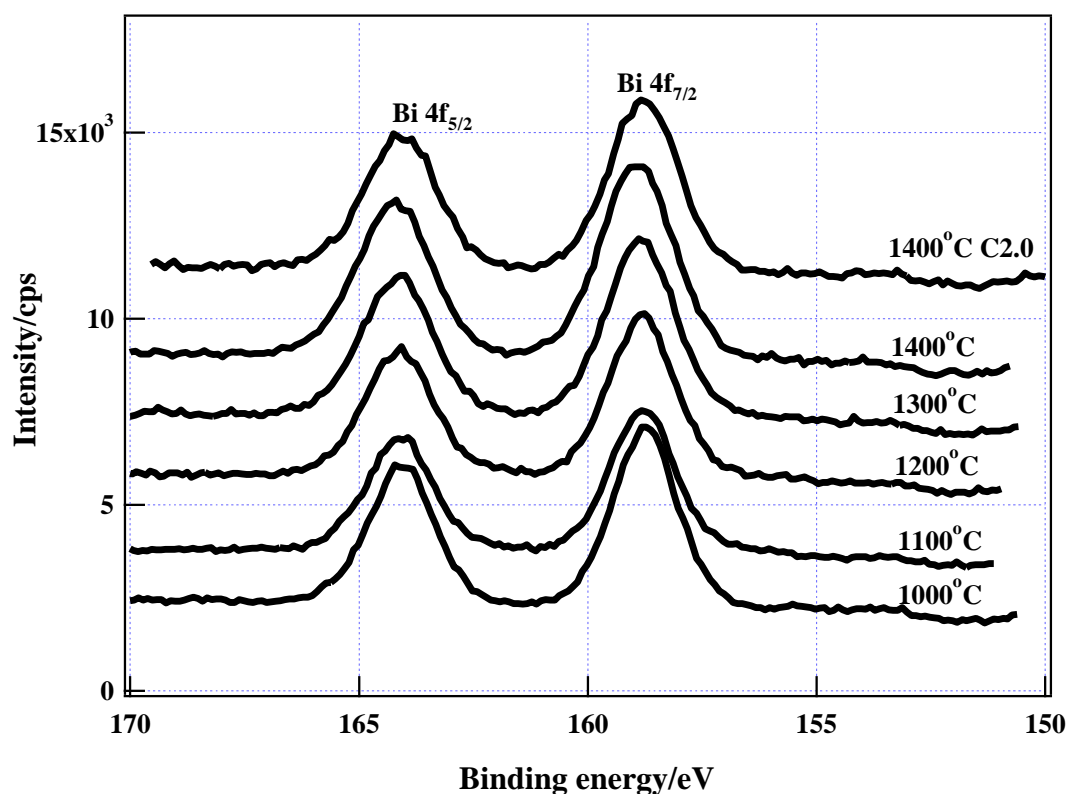
Figure 4.11 X-ray photoelectron spectra of Bi-containing borate glasses.

4.2.2 Discussion

It was found that the coloration and NIR luminescence characteristics were strongly affected by melting temperature. The color became deeper with increasing melting temperature and finally metallic Bi colloids precipitated being black color. NIR luminescence started to appear, reached the maximum and finally disappeared with increasing melting temperature.

Usually the valence state of metal ions moves toward lower side with increasing temperature (Paul, 1990). Thus, the change in valence state of Bi may be written by:

$$[I] \qquad [II] \qquad\qquad\qquad [III]$$

$$Bi^{3+} \rightarrow Bi^{2+} \rightarrow Bi, Bi_2, Bi_3, Bi_2^-, etc. \rightarrow (Bi)_n \qquad\qquad (4.5)$$
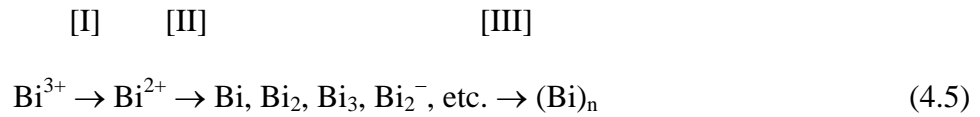
where Bi, Bi_2, Bi_3, Bi_2^-, etc. are Bi clusters and $(Bi)_n$ the metallic Bi colloids. This indicates that the redox equilibrium moves toward reduced side with increasing temperature, and the experimental results confirm this tendency.

As mentioned previously, Bi^{3+} ion and metallic Bi colloids do not contribute to the generation of NIR luminescence, and hence the coloration and the NIR luminescence of Bi-containing glasses might derive from intermediate species between Bi^{3+} ion and metallic Bi colloids. A well defined absorption bands and the NIR luminescence were observed in Bi-1200 glass, which is just before the beginning of darkening effect (black coloration, Bi-1300 glass). This process has often been observed in the formation of noble-metal colloid (Au, Ag) (Doremus, 1962). In this process, noble metal atoms were formed by the irradiation of UV light or heat treatment at first. Then reduced noble metal atoms gather together, grow and finally form metallic colloids by further heat treatment. Thus, the darkening effect of Bi-containing glasses can be interpreted as the process of metallic Bi colloids formation from atomic or molecular Bi. This process may correspond to [III] in equation 4.5.

Therefore, it was concluded that the color center and luminescent center is likely to be caused by Bi clusters, Bi, Bi_2, Bi_3, Bi_2^-, etc.

The absorption and NIR luminescence will be discussed in more detail in next section.

4.3 Effect of glass composition: Bi-containing borate glasses.

4.3.1 Results

4.3.1.1 Appearance and absorption spectra

The colors of glasses change from reddish-orange (X-0) to brown (X-30) with increasing amount of K_2O as shown in Table 4.4. X-20 and X-30 glasses were readily to crystallize/phase separate during casting.

Table 4.4   Appearance and absorption bands analyzed by Gaussian distribution.

Name	Appearance/by naked eye	Absorption bands/nm		
		Band I	Band II	Band III
X-0	Reddish-orange	455	497	-
X-10	Orange	456	-	-
X-20	Yellow-brown, partly crystallized	-	-	-
X-30	Brown, partly crystallized	-	-	-
Ren et al.(2006, 2007)		~460	-	-
Fujimoto et al. (2001, 2004), Peng et al. (2005, 2007), Khonthon et al. (2007)		-	~490	~710

Figure 4.12 shows absorption spectra of glasses. The strong absorption is observed in near ultra-violet (UV) to blue region of visible region for X-20 and X-30 glasses. The scattering due to crystallization/phase separation affects to increase transmission loss resulting in the strong absorption in 400-500 nm region. Two absorption bands at around 460 nm and 490 nm are observed in X-0 glass, while only one absorption band is detected at around 460 nm in X-10 glass. Although the

spectral pattern of X-0 glass is similar to that of Sp glass and Sp glass-ceramics (Section 4.1), that of X-10 glass is identical with those of Bi-1100 and Bi-1200 glasses (Section 4.2). The absorption bands at around 460 nm and 470 nm of X-0 and X-10 glasses are analyzed using Gaussian distribution as shown in Figure 4.13, and the result is summarized in Table 4.4. As shown in Table 4.4, these absorption bands might be separated into two bands, ~460 nm (Band I) and ~490 nm (Band II), and the former band is dominant in X-10 glass and the latter is dominant in X-0 glass. Thus, it seems that different color centers are present in these glasses.
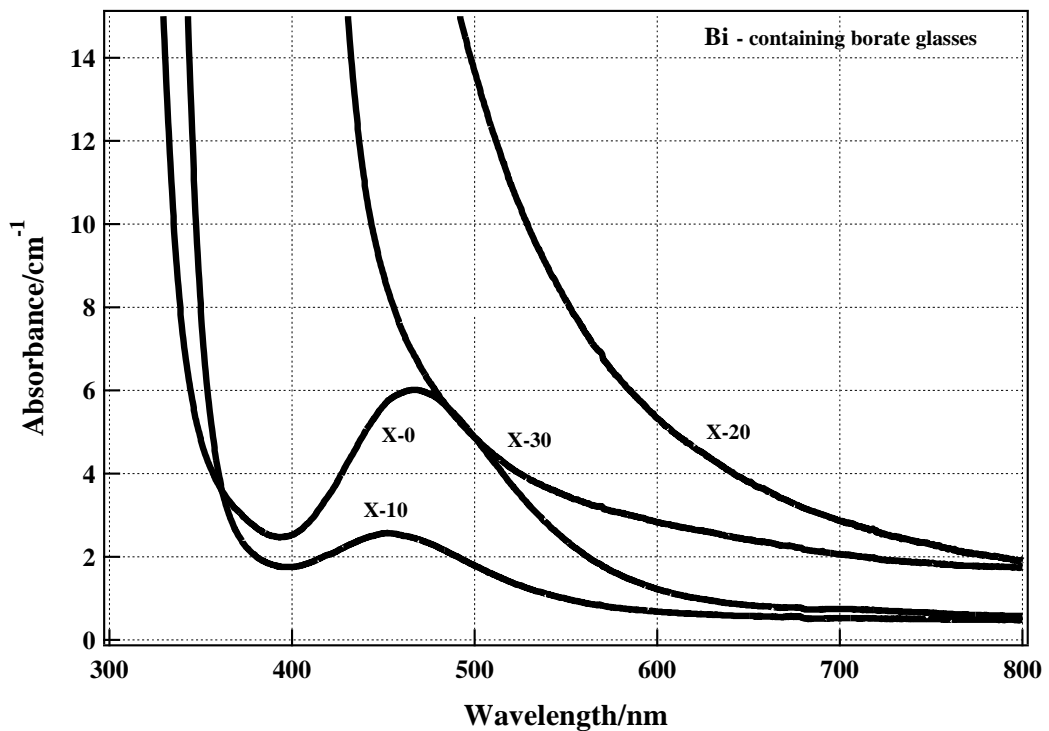

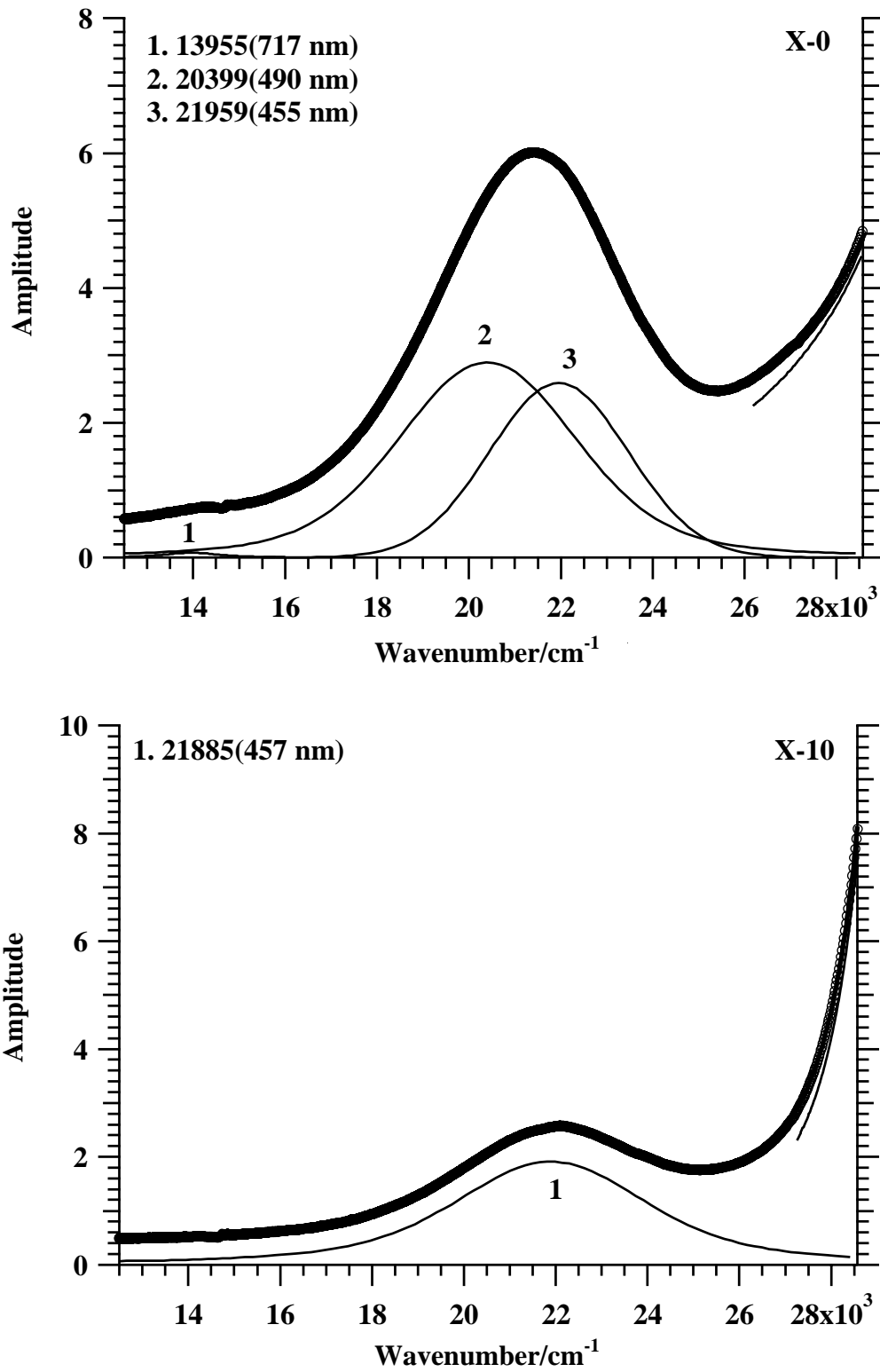**Figure 4.12**   Absorption spectra of Bi-containing borate glasses

Figure 4.13 Peak fitting of absorption bands of X-0 and X-10 glasses.

4.3.1.2 NIR luminescence spectra

Figure 4.14 shows NIR luminescence spectra of glasses under the excitation of 974 nm laser diode at room temperature. X-0 glass exhibits a relatively strong NIR luminescence centered at around 1100 nm, while a weak NIR luminescence can be detected centered at around 1150 nm in X-10 glass. The spectral pattern of X-10 glass is quite similar to those of Bi-1100 and Bi-1200 (Section 4.2). On the other hand, the spectral pattern of X-0 glass is similar to those of Sp glass and Sp glass-ceramics (Section 4.1).
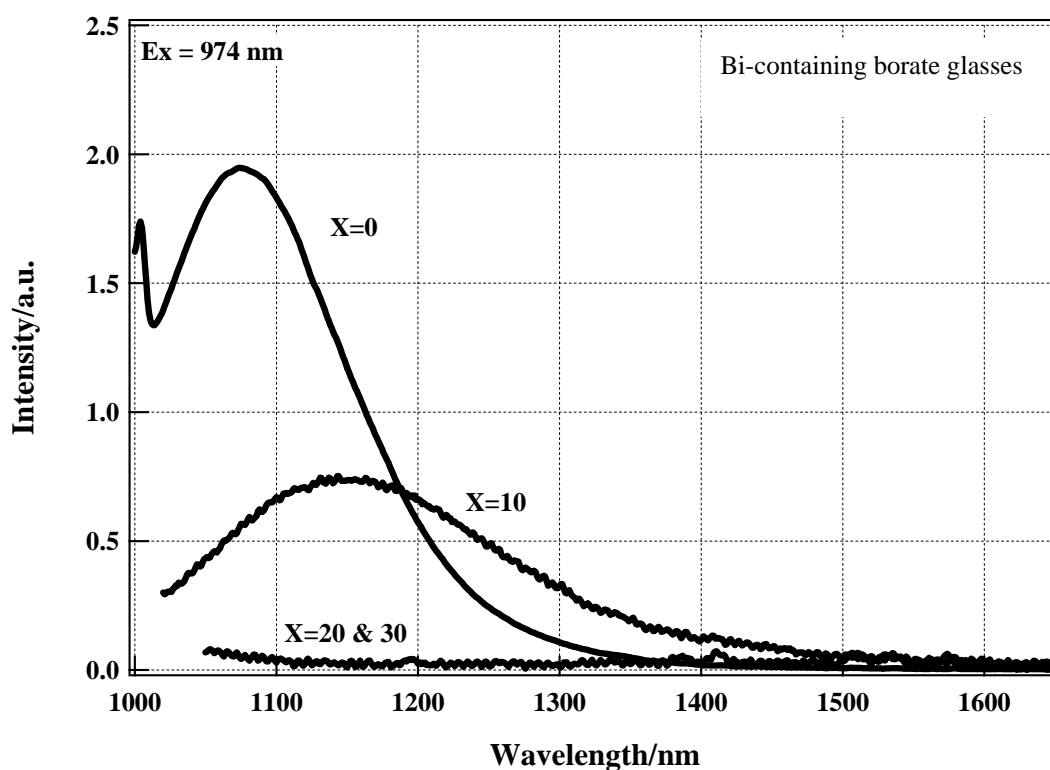

Figure 4.14 NIR luminescence spectra of Bi-containing borate glasses.

4.3.1.3   XPS spectra.

Figure 4.15 shows the XPS spectra of glasses. Two peaks of Bi $4f_{7/2}$ and Bi $4f_{5/2}$ were detected in all glasses. However, any signal can not be observed in lower energy side of these peaks, despite the peak position shifts slightly to lower energy side and half height width increases slightly with a decrease in X (K_2O content). This indicates that the considerable amount of lower valence species is not present in these glasses.
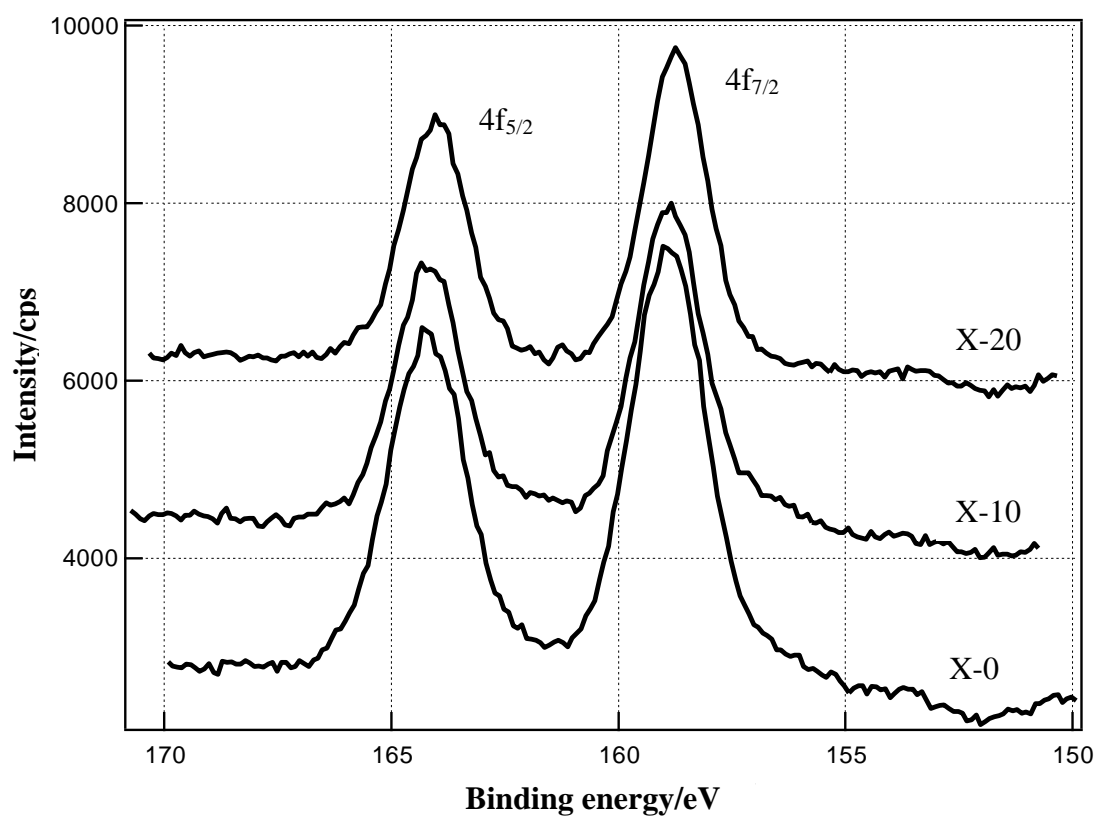

Figure 4.15 X-ray photoelectron spectra of Bi-containing borate glasses.

4.3.2 Discussion

It is well known that Bi^{3+} ions have a strong absorption in UV region (Srivastava, 1998 and 2002), and hence the absorption edge shift to longer wavelength with increasing amount of Bi^{3+} ions. This implies that the concentration of Bi^{3+} ions increases with increasing amount of K_2O (Figure 4.12).

As mentioned already, two absorption bands, ~460 and ~490 nm were observed in X-0 glass. Two different kind of spectral patterns have been reported previously in Bi-doped glasses. One is simple absorption band at around ~460 nm reported by Ren et al. (2005), and another is two absorption bands at around ~490 nm and ~710 nm reported by many researchers (Fujimoto and Nakatsuka, 2001, Suzuki et al., 2004 and Khonthon et al., 2007). The colors of these glasses are also different, orange in the former and reddish-orange to pink in the latter glasses. This suggests that two color centers are present in Bi-doped/Bi-containing glasses, for example, C1 center (~460 nm) and C2 center (~490 nm). The fraction of these color centers is strongly influenced by melting temperature, melting atmosphere and glass composition, i.e. redox equilibrium. The authors reported that the latter color center (C2 center) is likely to be caused by Bi cluster radicals or electron trapped Bi clusters, such as Bi_2^-, Bi_3^-, etc., by ESR measurement (Khonthon et al., 2007).

X-0 and X-10 glasses exhibit different NIR luminescence spectral patterns, difference in luminescence intensity and luminescence peak position. This result seems to be influenced by the concentration of luminescent center/color center. It is suggested that two color centers might be present in these glasses (X-0 and X-10). The NIR luminescence intensity of X-10 glass is much weaker than that of X-0 glass and the absorption band at around ~490 nm was not detected in X-10 glass. The NIR

luminescence spectra were analyzed using Gaussian distribution and are shown in Figure 4.16. Here, the NIR luminescence spectrum of Bi-1200 glass was used instead of that of X-10 glass (they have same spectral patterns, Figure 4.9 and 4.12). It is clearly seen that the NIR luminescence spectra is composed basically of two bands, ~1100 nm and ~1200 nm. In X-0 glass, only one band appears (~1100 nm), while two bands appear in Bi-1200 (same as X-10) glass. The C2 color center is dominant in X-0 glass, and therefore the band ~1100 nm may be derived from C2 color center. On the other hand, in Bi-1200 (X-10) glass, it seems that the position of NIR luminescence shifts to longer wavelength by the existence of C1 color center/luminescent center.

Generally, it is well known that the valence state of metal ions moves to higher side with increasing alkali content (Paul, 1990). The change in valence state of Bi may be written by:

$$Bi^{3+} \rightarrow Bi^{2+} \rightarrow Bi, Bi_2, Bi_3, Bi_2^-, \text{etc.} \rightarrow (Bi)_n \qquad (4.6)$$
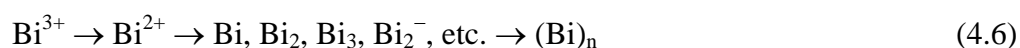
Higher R_2O Lower R_2O

This behavior of valence state of Bi is also confirmed here. High alkali containing glass, in which Bi^{3+} ion is dominant, do not exhibit the characteristic absorption band in UV-VIS region and NIR luminescence.

The Bi, Bi_2, Bi_3, Bi_2^-, etc species may be formed during reduction process of Bi_2O_3 to metallic colloids $(Bi)_n$ and they gather together and precipitate metallic $(Bi)_n$ colloids finally.

Here, the effect of glass composition on the redox equilibrium of Bi is discussed based on optical basicity scheme. Optical basicity is the measure of the basicity of glasses. According to Duffy's optical basicity scheme (Duffy, 1996), Λ values of these glasses were calculated, X-0:0.46, X-10:0.50, X-20:0.55 and X-30:0.59. Lower Λ value gives lower basicity (reduced side) and higher Λ value provides higher basicity (oxidized side). Murata and Mouri (2007) discussed the NIR luminescence characteristics of various Bi-doped glasses based on optical basicity scheme without reducing agents, and they reported that the generation of NIR luminescence was strongly affected by optical basicity of base glasses. They concluded that Λ of 0.4 was critical point (above 0.4 no NIR luminescence was observed). In this study, a relatively strong NIR luminescence was detected in X-0 glass, and its Λ value is close to 0.4. However, in X-10 glass (Λ-0.50), a weak NIR luminescence could be detected. Of course in this case, the redox equilibrium of glasses is influenced by not only optical basicity but also melting temperature, and hence a weak NIR luminescence could be detected in X-10 glass.
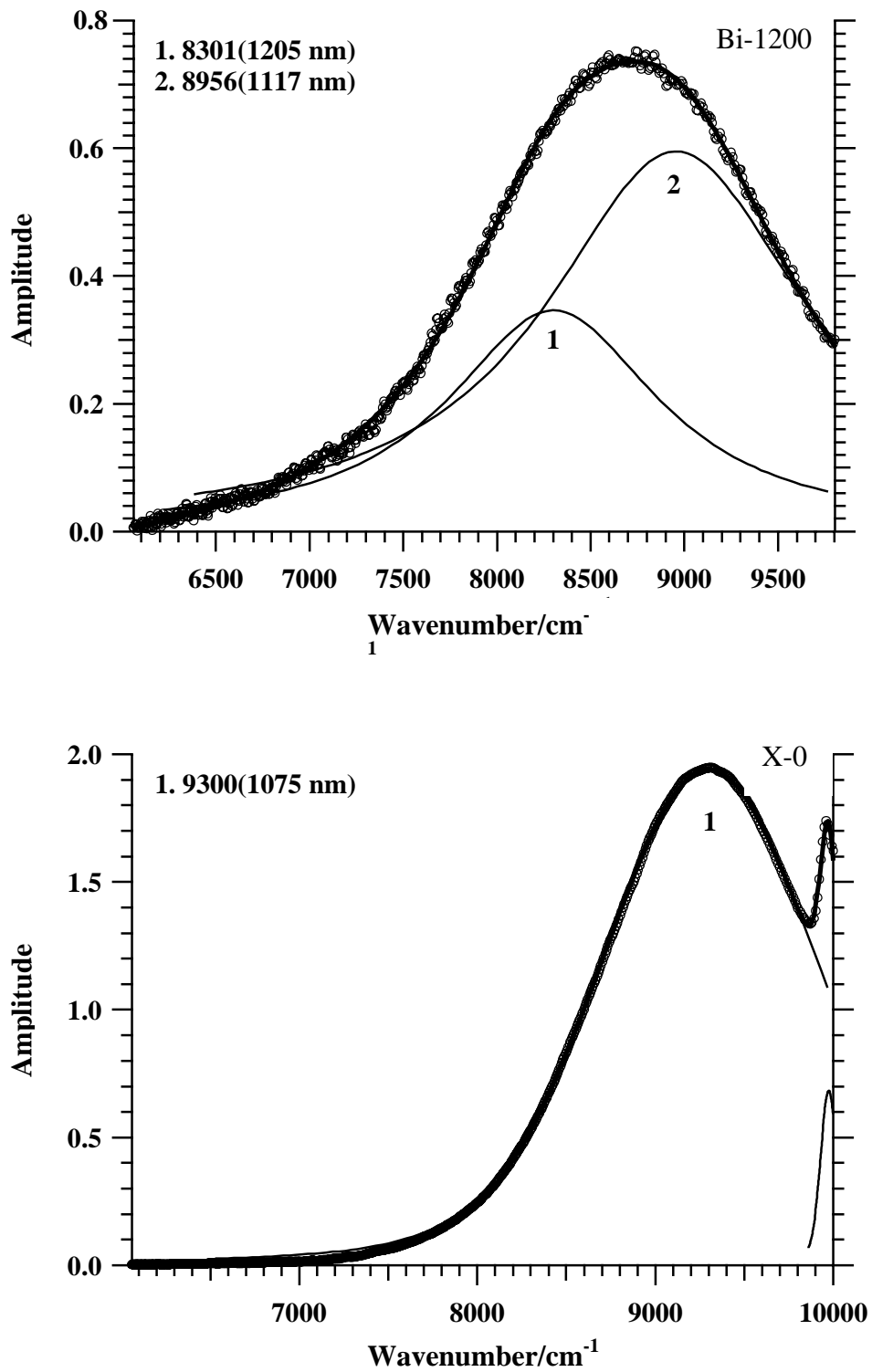
Figure 4.16   Peak fitting of NIR luminescence spectra of X-0 and X-10 (Bi-1200)

glasses.

4.4 Effect of reducing agent: Bi-doped soda-lime-silicate glass.

4.4.1 Results

4.4.1.1 Appearance and absorption spectra

The intensity of coloration changes systematically with the amount of carbon addition. The appearances of samples are colorless for C-0, C-0.5 and C-1.0* (550°C-0 min. annealing), brown for C-1.0 (650°C–30 min. annealing) and black-brown for C-1.5. The absorption spectra are shown in Figure 4.17. A weak absorption band at around 450 nm can be observed in C-0.5 and C-1.0* (550°C-0 min.) glasses. It should be noted that the color changes by the change of annealing condition (C-1.0* and C-1.0 glasses).
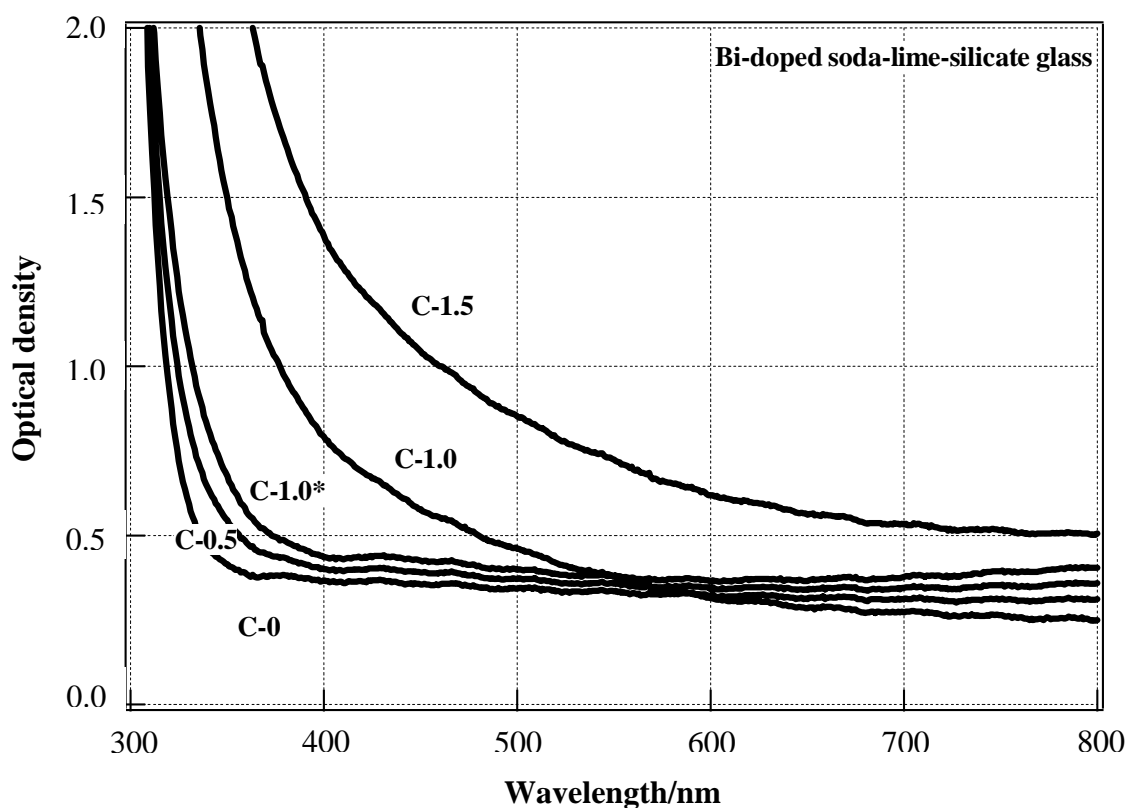
Figure 4.17 Absorption spectra of Bi-doped soda-lime-silicate glasses.

Figure 4.18 shows SEM photos of black colored C-1.0 and C-1.5 glasses. It is clearly seen that small particles of about 100 nm can be detected in these glasses. These particles could be colloidal metallic Bi (Section 4.2). This indicates that Bi_2O_3 was reduced to metallic Bi with increasing carbon content. It was already confirmed that the darkening effect (black coloration) was the formation process of Bi-metallic colloids (Section 4.2).
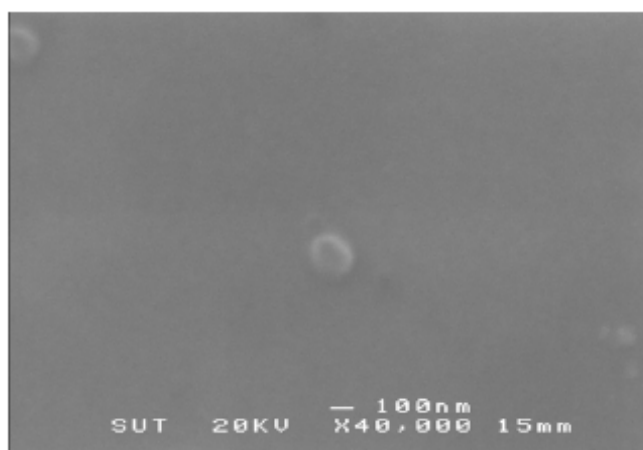
Bi-Soda-lime-silicate glass C-1.0
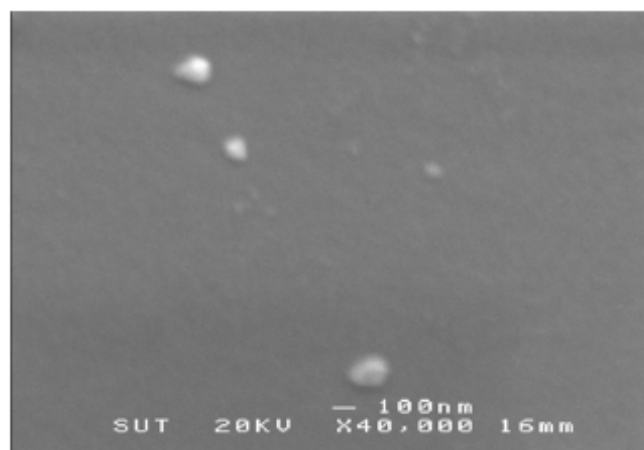
Bi-Soda-lime-silicate glass C-1.5

Figure 4.18   SEM photos of Bi-doped soda-lime-silicate glasses, C-1.0 and C-1.5.

4.4.1.2   Luminescence in VIS region

The UV-VIS luminescence spectra of glasses are shown in Figure 4.19 under the excitation of 300 nm at room temperature. Strong and broad luminescence bands were observed centered at 400 nm and 800 nm for C-0, C-0.5 and C-1.0* glasses. The emission intensity of 400 and 800 nm band decreases markedly with increasing the amount of carbon.

It is well known that UV-VIS luminescence at ~400 nm comes from Bi^{3+}, and it was assigned to $^3P_1 \rightarrow {}^1S_0$ transition (Srivastava, 1998 and 2002). The strong 400 and 800 nm bands observed in C-0, C-0.5 and C-1.0* glasses are derived from Bi^{3+} ions. Thus the concentration of Bi^{3+} in glasses decreased with increasing amount of carbon.
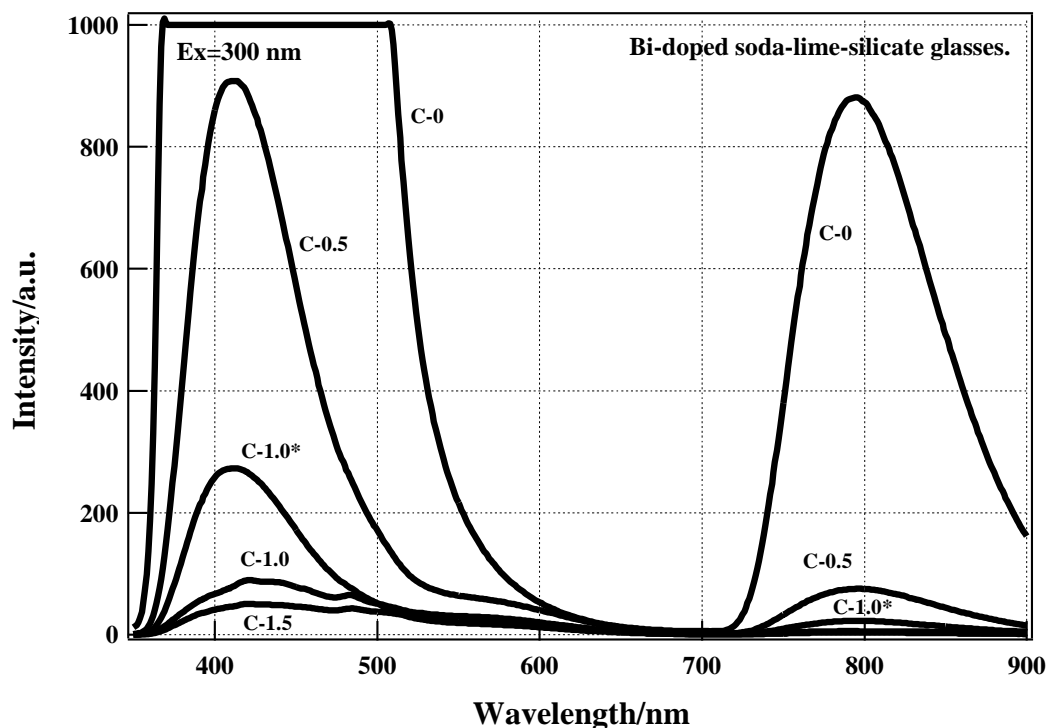
Figure 4.19   UV-VIS luminescence spectra of Bi-doped soda-lime-silicate glasses.

4.4.1.3   NIR luminescence spectra.

Figure 4.20 shows NIR luminescence spectra under the excitation of 974 nm laser diode at room temperature. The broad luminescent band centered at around 1200 nm is detected. The strongest luminescence was observed in C-0.5 glass, and the intensity of luminescence decreases with increasing amount of carbon. No NIR luminescence can be observed in C-0 glass. It should be noted that the different luminescent characteristics was observed in C-1.0* and C-1.0 glasses. The luminescent intensity of colorless C-1.0* is higher than that of brown colored C-1.0 glass. These glasses have a same batch composition but different annealing condition.

Figure 4.20   NIR luminescence spectra under the excitation of 974 nm laser diode.

4.4.2 Discussion

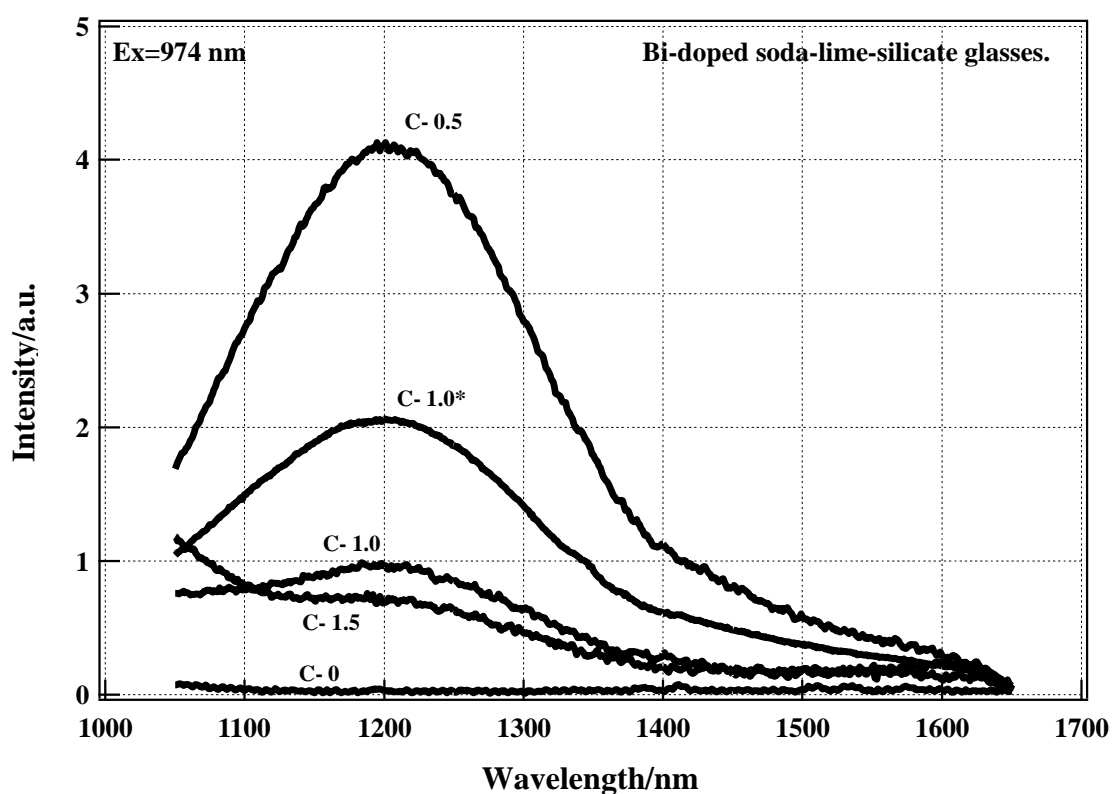A weak absorption band was observed at around 450 nm in C-0.5 and C-1.0* glasses. J. Ren et al. (2006) and Sumimiya et al. (2006) have also observed the absorption band at the same position. On the other hand, however, Fujimoto et al. (2001, 2004), Peng et al. (2004) and Khonthon et al. (2007) observed the absorption bands at different positions, around 500 nm and 700 nm. This suggests that there are different color centers.

The luminescence spectral patterns of these glasses are also different from that observed previously, in which the NIR luminescence centered at 1100 nm was detected in pink colored Bi-doped spinel glass-ceramics. In this case, as mentioned above, the color center might be different, and hence the NIR luminescence spectral pattern changes depending on the color center. Figure 4.21 shows Gaussian peak fitting of NIR luminescence spectra of C-0.5 glass, X-0 and X-10 glasses. In X-0 glass, basically the spectrum consists of one peak, ~1100 nm. On the other hand, three peaks can be observed in C-0.5 and X-10 glasses, ~1100 nm, ~1250 nm and ~1500 nm, and the second peak is relatively strong. The second band shifts slightly to longer wavelength compared with Bi-containing borate glass (X-0 glass, section 4.3). Therefore, it is considered that the color center at ~500 nm and ~700 nm contributes to the 1100 nm NIR luminescence.

It was observed that the glass annealed at lower temperature is less color and exhibits an intense luminescence than that annealed at higher temperature despite the same batch composition and melting condition (C-1.0* and C1.0 glasses). This result suggests the formation process of color center and luminescent center. As
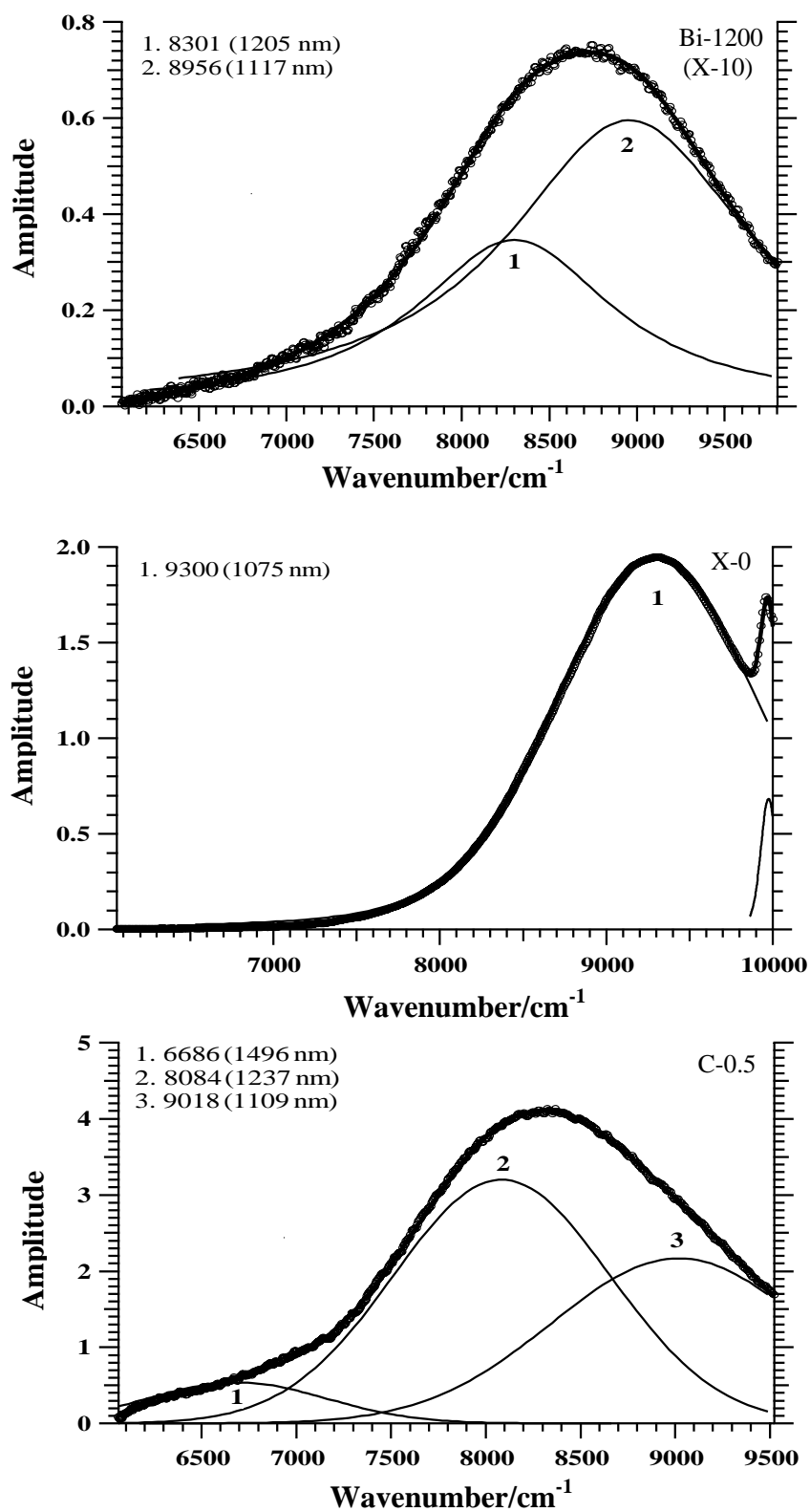
Figure 4.21   Peak fitting of NIR luminescence spectra of X-0, X-10 and C-0.5

glasses.

mentioned previously, Bi^{3+} ions and Bi colloids are dominant in C-0 glass (without carbon) and C-1.5 glass (highest carbon), respectively, and these species do not contribute to NIR luminescence. This change in valence state can exactly be considered as a redox reaction with carbon amount. As already shown in previous section (Section 4.2), the change in valence state of Bi may be written by:

$$\underset{[I]}{Bi^{3+}} \rightarrow \underset{[II]}{Bi^{2+}} \rightarrow \underset{[III]}{Bi, Bi_2, Bi_3,---} \rightarrow (Bi)_n \qquad (4.7)$$
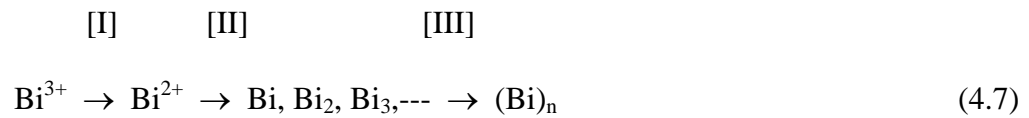
It seems that the phenomenon observed here may be the process [III]. Atomic or molecular Bi gathers together, grows and forms the Bi metallic colloids. This process is often observed in the formation process of noble-metal colloid (Rawson, 1980). Therefore, the glass becomes to be black in color and the NIR luminescence decreases with the formation of Bi colloid. Thus, the origin of color center and NIR luminescent center is likely to be caused by Bi cluster, such as Bi, Bi_2, Bi_3, Bi_4, etc., just before the beginning of darkening effect. The concentration of color center and luminescent center might be very low, ppm order like Se-pink glasses (Paul, 1975).

As mentioned in previous section (Section 4.3), the basicity (optical basicity) of glasses affected strongly the NIR luminescence characteristics of glasses. The optical basicity of soda-lime-silicate glass without carbon addition is calculated to be $\Lambda = 0.58$, which is much larger than critical value of 0.4 (Murata and Mouri, 2007). Therefore, the NIR luminescence could not be detected in C-0 glass even melted at 1450°C. However, the NIR luminescence started to appear and the reach the maximum at C-0.5 and decreased again with an increase in the amount of carbon addition. Thus, the effect of reducing agent is very large, and a suitable amount of

reducing agents enhances the NIR luminescence. This indicates that the higher concentration of color center and luminescent center, which could be Bi clusters such as Bi_2, Bi_2^-, etc., may be formed at that condition. And the colorless and transparent materials could also be obtained with lower Bi_2O_3 concentration (in this case only 0.5% compared with borate glasses).

In order to confirm the color center and luminescent center, the ESR spectra were measured. Figure 4.22 shows ESR spectra of glasses. Two ESR signals were observed at g~4.24 and g~2.0 in all glasses. The intensity of the ESR signal at g~4.24 decreased markedly with increasing amount of carbon. This signal is believed to be due to impurities, such as Fe^{3+} ion (Elvers and Wissmann, 2001). Thus the concentration of Fe^{3+} ion decreases with increasing amount of carbon addition.

On the contrary, ESR signal at g~2.0 was not detected in C-0 glass; the intensity of this signal reached the maximum at C-0.5 and decreased gradually with increasing amount of carbon addition. The authors (Khonthon, Morimoto and Ohishi, 2007) detected the ESR signal at g~2.0 in Bi-doped alkaline-earth alumino-silicate glass and glass-ceramics which exhibited NIR luminescence, and hence, this signal may relate to color center or luminescent center of Bi-doped glasses. Actually, the NIR luminescence intensity seems to be proportional to the intensity of ESR signal at g~2.0.
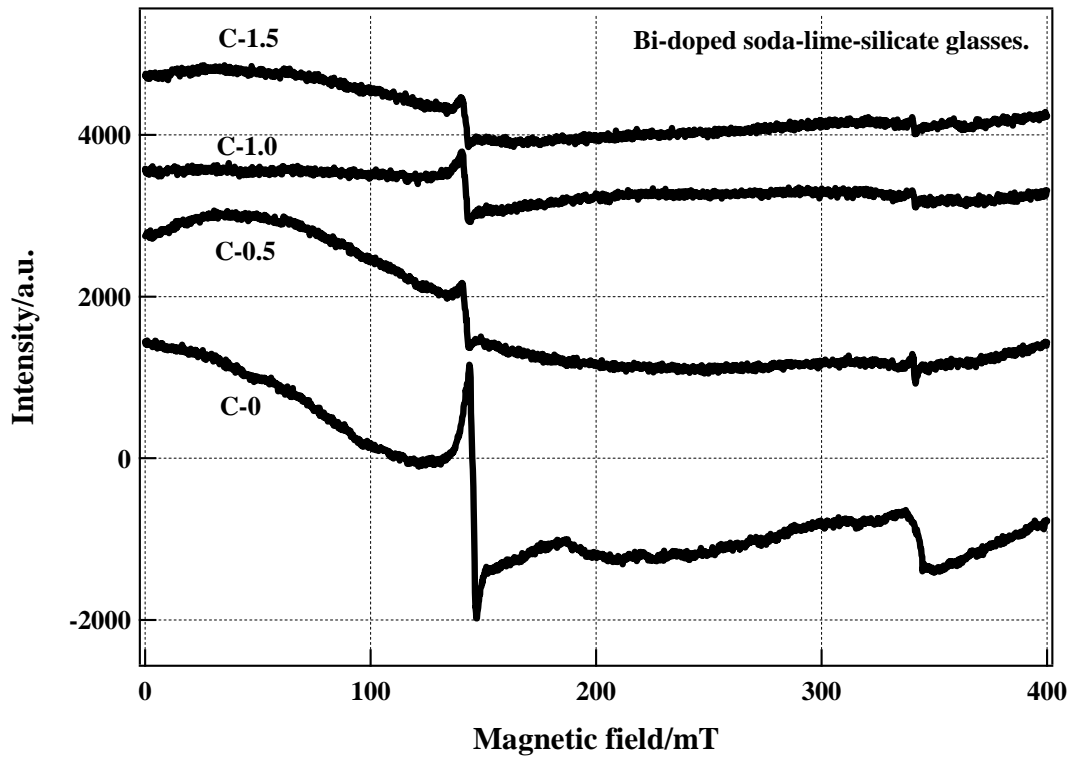
Figure 4.22   ESR spectra of Bi-doped soda-lime-silicate glasses.

CHAPTER V

CONCLUSION

The color center, near-infrared (NIR) luminescent center and NIR luminescent characteristics of Te- and Bi-containing glasses and glass-ceramics were investigated based on redox equilibrium. Particularly, the factors affecting the redox equilibrium, melting temperature, glass composition and addition of reducing agents (carbon), were investigated in detail in Bi-containing borate glasses and soda-lime-silicate glasses, and the formation of color center and NIR luminescent center was discussed.

5.1   Te- and Bi-doped glasses and glass-ceramics

5.5.1 The NIR luminescence centered at 1100-1300 nm were detected from various Te- and Bi-doped glasses and glass-ceramics under the excitation of 974 nm laser diode at room temperature.

5.1.2 In glasses and glass-ceramics which exhibited NIR luminescence, the characteristics ESR signals due to electron trapped clusters of Te and Bi, such as Te_2^- and Bi_2^- were detected at g~2.0 (~350 mT). This implies that this ESR signal relates strongly to the generation of the NIR luminescence, and therefore it is estimated that the NIR luminescent center might be the electron trapped clusters of Te and Bi, such as Te_2^- and Bi_2^-.

5.1.3 New type NIR luminescent materials of Te-doped glasses and glass-ceramics which exhibit broad NIR luminescence were discovered for the first time to our knowledge.

5.2   Effect of melting temperature: Bi-containing borate glasses

5.2.1 It was found that the formation of color center and NIR luminescence center and NIR luminescence characteristics were strongly affected by melting temperature. In the glasses melted at lower temperature, color center and NIR luminescent center were not formed, and hence the NIR luminescence could not be detected (or very weak). On the contrary, higher temperature melting induced black coloration (formation of Bi metallic colloids) and NIR luminescence also was not observed.

5.2.2 This darkening effect (black coloration) of Bi containing glasses is confirmed to be the formation process of Bi metallic colloids by XRD analysis of black colored glasses.

5.2.3 Glasses melted intermediate temperature appeared to be orange to pink in color and they exhibited NIR luminescence centered at around 1150 nm. Thus, the redox equilibrium moves to reduced side with increasing melting temperature.

5.2.4 The Bi clusters or electron trapped Bi clusters, such as Bi_2, Bi_3, Bi_2^-, etc., were formed just before the beginning of darkening effect (black coloration), and it is suggested that these species are strongly related to the coloration of glasses and the generation of NIR luminescence.

5.3   Effect of glass composition: Bi-containing borate glasses

5.3.1   It was found that the glass composition also affected strongly the formation of the color center and NIR luminescence center and NIR luminescence characteristics.

5.3.2   The color center and NIR luminescence center disappeared with increase in the amount of alkali content (increase in basicity of glass), and therefore NIR luminescence could not be detected in high alkali containing borate glasses.

5.3.3   The formation of color center and NIR luminescent center and NIR luminescence characteristics were discussed based on optical basicity scheme (measure of basicity of glasses, Λ). It was clarified that the color center and NIR luminescence center were not formed when the optical basicity Λ exceeds 0.5.

5.3.4   The absorption spectra and NIR luminescence spectra were analyzed by deconvolution method with Gaussian distribution. As a result, it was suggested that few color center and NIR luminescence center were present in glasses.

5.4   Effect of reducing agent: Bi-doped soda-lime-silicate glass

5.4.1   It was found that the addition of reducing agent also affected the formation of the color center and the NIR luminescence center and NIR luminescence characteristics.

5.4.2   The glass without carbon did not exhibit NIR luminescence, and the darkening effect (black coloration) (formation of Bi metallic colloids) took place and the NIR luminescence decreased in the glasses with higher amount of carbon. Therefore, the colorless and transparent glasses which exhibited NIR luminescence

could be obtained by melting under mild to medium reducing conditions despite lower concentration of Bi_2O_3 (0.5 wt%).

5.4.3   The annealing temperature also affected on the NIR luminescence characteristics. The higher annealing temperature (100°C above Tg) induced darkening effect (black coloration) and the NIR luminescence decreased. On the other hand, the glass annealed at lower temperature (~Tg) was colorless and transparent, and it exhibited higher NIR luminescence.

5.4.4   Thus, the NIR luminescence intensity reaches the maximum just before the beginning of darkening effect (black coloration), and therefore the color center and luminescent center are likely to be caused by Bi clusters or electron trapped Bi clusters, such as Bi_2, Bi_3, Bi_2^-, etc.

It was found that the formation of color center and NIR luminescent center and luminescent characteristic of Te- and Bi-containing glasses and glass-ceramics were strongly affected by redox equilibrium. In oxidized side, color center and NIR luminescent center were not formed, and hence NIR luminescence could not detected. On the contrary, the darkening effect (formation process of Bi metallic colloids) took place in strong reduced side, and also NIR luminescence was not observed. Therefore, the color center and NIR luminescent center can be formed under mild to medium reducing condition and the NIR luminescence can be detected.

It is suggested that the color center and luminescent center in Te- and Bi-containing glasses is likely to be caused by Te- and Bi-clusters or electron trapped Te- and Bi-clusters, such as Te_2, Te_2^-, Bi_2, Bi_3, Bi_2^-, etc.

REFERENCES

Aboud, T. and Stoch, L. (1997). Crystallization behavior in the glass system SiO_2-P_2O_5-Al_2O_3-MgO-Na_2O. **Journal of Non-crystalline Solids.** Vol.219: 149.

Ahmed. A.A., Sharaf, N.A., and Codrate Sr., R.A. (1997). Raman microprobe investigation of sulfur-doped alkali borate glasses. **Journal of Non-Crystalline Solids.** Vol.210: 59-69.

Albrecht, G.F., Eggleston, J.M., and Ewing, J.J. (1985). Measurements of Ti^{3+}:Al_2O_3 as a lasing material. **Optics Communications**. Vol.52: 401-404.

Asahi, T., et al. (2006). Preparation of Na_2S-B_2O_3-SiO_2 Glass System and Local Structure Analysis. **Journal of the Ceramic Society of Japan.** Vol.114: 697-704. [in Japanese].

Beall, H.G. and Duke, D.A. (1969). Transparent glass-ceramics. **Journal of Materials Science**. Vol.4: 340-352.

Beall, H.G. and Pinckney, L.R. (1999). Nanophase Glass-Ceramics. **Journal of the American Ceramic Society**. Vol.82: 5-16.

Blasse, G. (1997). Classical phosphors: A Pandora's Box. **Journal of Luminescence.** Vol.72-74: 129-134.

Curie, Daniel. (1963). **Luminescence in Crystal.** New York: 332.

Dong, Y., Ren, M., Mu, C., Lin, J-h., and Su, M-z. (1999). Luminescence center in Br^- rich $BaFBr$:O^{2-}. **Journal of Luminescence**. Vol.81: 231-235.

Doremus, R.H. (1962). **Diffusion in Non-Crystalline Silicate in Modern Aspects of Vitreous State.** Ed. J.D. Mackenzie, Butterworth, London. Vol.2: 1-71.

Duffy, J.A. (1996). Redox equilibria in glass. **Journal of Non-crystalline Solids**. Vol.196: 45-50.

Elvers, A. and Weibmann, R. (2001). ESR spectroscopy-an analytical tool for the glass industry. **Glastechnische Berichte-Glass Science and Technology.** Vol.74: 32-38.

Fujimoto, Y. and Nakatsuka, M. (2001). Infrared Luminescence from Bismuth-Doped Silica Glass. **Japanese Journal of Applied Physics.** Vol.40: L279-L281.

Fujimoto, Y. and Nakatsuka, M. (2004). Proceedings of XXth ICG, O-07-077, Kyoto, Japan.

Guha, S., Leppert, V-J., and Risbud, S-H. (1998). Identification of the electronic states of Se_2^- molecules embedded in borosilicate glasses and Se-based nanometer sized crystals. **Journal of Non-Crystalline Solids.** Vol.240: 43-49.

Halpern, A.M. (2005). Luminescence. **Encyclopedia of Physics**. 1349-1351.

Headley, T.J. and Loehman, R.E. (1984). The crystallization of Glass-ceramics by epitaxial-growth. **Journal of the American Ceramic Society**. Vol.67: 620.

Hench, L.L., Freiman, S.W., and Kinser, D.L. (1971). The Early stages of crystallization in a Li_2O-$2SiO_2$ Glass. **Physics and Chemistry of Glasses**. Vol.12: 58-63.

Hong Kong Paptist University. (2008). **X-ray Photoelectron Spectrometry (XPS)** [on-line]. Available: http://www.hkbu.edu.hk/~csar/xps.html.

Inoue, S., Shimizugawa, Y., Nukui, A., and Maeseto, T. (1995). Thermochromic property of tellurite glasses containing transition metal oxides. **Journal of Non-Crystalline Solids**. Vol.189: 36-42.

Khonthon, S, Morimoto, S, Arai, Y., and Ohishi, Y. (2007). Luminescence Characteristics of Te- and Bi-doped Glasses and Glass-ceramics. **Journal of the Ceramic Society of Japan.** Vol.115: 259-263.

Khonthon, S., Morimoto, S., and Ohishi, Y. (2006). Absorption and Emission Spectra of Ni-Doped Glasses and Glass-Ceramics in Connection with Its Co-Ordination Number. **Journal of the Ceramic Society of Japan.** Vol.114: 791-794.

Kim, S.H., Yoko, T., and Sakka, S. (1993). Linear and Nonlinear Optical Properties of TeO_2 Glass. **Journal of the American Ceramic Society**. Vol.76: 2486-2490.

Konishi, T., et al. (2003). Investigation of glass formation and color properties in the P_2O_5-TeO_2-ZnO system. **Journal of Non-Crystalline Solids.** Vol.324: 58-66.

Kowalak, S. and Jankowska, A. (2003). Application of zeolites as matrices for pigment. **Micoporous and mesoporous Materials.** Vol.61: 213-222.

Lenntech Water. (2008). **Glass** [on-line]. Available:
http://www.lenntech.com/Glass.htm

Lindner, G-G., Witke, K., Schlaich, H., and Reinen, D. (1996). Blue-green ultramarine-type zeolites with dimeric tellurium color centers. **Inorganica Chimica Acta.** Vol.252: 39-45.

Louisiana State University. (2008). **X-ray Photoelectron Spectroscopy** [On-line]. Available: http://www.che.lsu.edu/COURSES/4205/2000/Levy/paper.htm

Morimoto, S. (2006). Phase separation and crystallization in the system SiO_2-Al_2O_3-P_2O_5-B_2O_3-Na_2O glasses. **Journal of Non-crystalline Solids.** Vol.352: 756-760.

Morimoto, S. (2006). Effect of K_2O on the crystallization in Li_2O-SiO_2 system of glass. **Journal of the Ceramic Society of Japan.** Vol.114(2): 195-198.

Morimoto, S. and Waraporn Emem. (2004). Strength of Li_2O-SiO_2 system transparent glass-ceramics. **Journal of the Ceramic Society of Japan.** Vol.112: 259-262.

Murata, T. and Mouri, T. (2007). Matrix effect on absorption and infrared fluorescence properties of Bi ions in oxide glasses. **Journal of Non-crystalline Solids.** Vol.353: 2403-2407.

Nagaya, K., Oohata, A., Yamamoto, I., and Yao, M. (2002). Photoelectron spectroscopy of small tellurium clusters. **Journal of Non-Crystalline Solids**. Vol.312-314: 337-340.

Nistor, S.V., Stefan, M., Goovaerts, D., and Schoemaker, D. (2000). Eletron-hole recombination in $PbCl_2$:Tl crystals. **Journal of Luminescence**. Vol.87-89: 549-551.

Nitta, I. (1975). **X-ray Crystallography. Vol.I**. Maruzen, Tokyo: 489-495 [in Japanese].

Oak Ridge National Laboratory. (2008). **Phosphate Glass for Photonics** [on-line]. Available: http://www.ornl.gov/info/ornlreview/rev27-3/text/phoside2.htm

Ohlberg, S.M. and Strickler, D.W. (1962). Determination of Percent Crystallinity of Partly Devitrified Glass by X-Ray Diffraction. **Journal of the American Ceramic Society.** Vol.45: 170-171.

Paul, A. (1975). Mechanism of selenium pink coloration in glass. **Journal of Materials Science.** Vol.10: 415-422.

Paul, A. (1990). **Chemistry of Glass**. Chapman and Hall, London. 218-245.

Peng, M., et al. (2004). Bismuth- and aluminum-codoped germanium oxide glasses for super-broadband optical amplification. **Optics Letters.** Vol.29: 1998-2000.

Peng, M., et al. (2005). Investigations on bismuth and aluminum co-doped germanium oxide glasses for ultra-broadband optical amplification. **Journal of Non-Crystalline Solids.** Vol.351: 2388-2393.

Peng, M., et al. (2007). Bismuth-doped zinc aluminosilicate glasses and glass-ceramics with ultra-broadband infrared luminescence. **Optical Materials.** Vol.29: 556-561.

Petricevic, V., Gayen, S.K., and Alfano, R.R. (1988). Laser action in chromium-activated forsterite for near-infrared excitation: Is Cr^{4+} the lasing ion. **Applied Physics Letters**. Vol.53: 2590-2592.

Pinckney, L.R. (1999). Transparent high strain point spinel glass-ceramics. **Journal of Non-crystalline Solids.** Vol.225: 171-177.

Pinkney, L.R. (2001). Glass-ceramics. **Encyclopedia of Materials Science and Technology.** Vol.4: 3535-3540.

Queen Mary University. (2008). **Photoelectron Spectroscopy** [On-line]. Available: http://www.chem.qmul.ac.uk/surfaces/scc/ scat5_ 3.htm

Rawson, H. (1980). **Properties and Applications of Glass**. Elsevier Scientific Publishing, New York. 216-221.

Ren, J. et al. (2006). Effect of various alkaline-earth metal oxides on the broadband infrared luminescence from bismuth-doped silicate glasses. **Solid State Communications.** Vol.140: 38-41.

Ren, J. et al. (2007). Ultrabroad infrared luminescence from Bi-doped alumino-germanate glasses. **Solid State communications**. Vol.141: 559-562.

Sakamoto, T. et al. (1995). 1.4-µm-Band Gain Characteristics of a Tm-Ho-Doped ZBLYAN fiber Amplifier Pumped in the 0.8-µm Band. **IEEE Photonics Technology Letters**. Vol.7: 983-985.

Sanz, O., poniatowski, H-E., Gonzaro J., and Navarro, J.M-F. (2006). Influence of the melting conditions of heavy metal oxide glasses containing bismuth oxide on their optical absorption. **Journal of Non-Crystalline Solids.** Vol.352: 761-768.

Sigel Jr., G.H. (1977). **Glass I: Interaction with Eletromagnetic Radiation. Treatise on Materials Science and Technology. Vol.12**. Eds. Tomozawa, M. and Doremus, R.H. Academic Press, New York. 5-89.

Soares, JR., Zanotto, E.D., Fokin, V.M., and Jain, H. (2003). TEM and XRD study of early crystallization of lithium disilicate glasses. **Journal of Non-crystalline Solids**. Vol.331: 217-227.

Sorokina, T.I, Naumov, S., Sorokin, E., Wintner, E., and Shestakov, A.V. (1999). Directly diode-pumped tunable continuous-wave room-temperature $Cr^{4+}YAG$ laser. **Optics Letters**. Vol.24: 1578-1580.

Srivastava, A.M. (1998). Luminescence of divalent bismuth in $M^{2+}BPO_5$. **Journal of Luminescence.** Vol.78: 239-243.

Srivastava, A.M. (2002). On the luminescence of Bi^{3+} in the pyrochlore $Y_2Sn_2O_7$. **Materials Research Bulletin.** Vol.37: 745-751.

Sumimiya, S., Sakida, S., Nanba,T., and Miura,Y. (2006). **Proceedings of the 46th Symposium on Glasses and Phonics Materials, P-17, Hikone, Japan**. [in Japanese].

Suzuki, T and Ohishi, Y. (2004). Broadband 1400 nm emission from Ni^{2+} in zinc-alumino-silicate glass. **Applied Physics Letters**. Vol.84: 3804-3806.

Suzuki, T., Murugan, G.S., and Ohishi, Y. (2005). Spectroscopic properties of a novel near-infrared tunable laser material Ni: $MgGa_2O_4$. **Journal of Luminescence.** Vol.113: 265-270.

Tanabe, S.,Hirao, K., and Soga, N. (1990). Upconversion fluorescences of TeO_2- and Ga_2O_3-based oxide glasses containing Er^{3+}. **Journal of Non-Crystalline Solids**. Vol.122: 79-82.

Technical University of Vienna. (2008). **X-ray Photoelectron Spectroscopy** [On-line]. Available: http://www.iap.tuwien.ac.at/~werner/qes_tut_xps.html

Trigg, George L. (Ed.). (2006). Optical networks. **The optics Encyclopedia.** Vol.4: 2127.

Van der Steen, A.C., Van Hesteren, J.J.A., and Slok, A.P. (1981). Luminescence of the Bi^{3+} Ion in Compounds $LiLnO_2$ and $NaLnO_2$ (Ln=Sc, Y, La, Gd, Lu). **Journal of the Electrochemical Society.** Vol.128: 1327-1333.

Varshneya, A.K. (1993). Glass Composition and Structure. **Fundamentals of Inorganic Glasses.** Academic press. 116.

Varshneya, A.K., Busbey, R.F., and Soules, T.F. (1985). Comparison of AlPO$_4$ and SiO$_2$ glass structures using molecular dynamics. **Journal of Non-crystalline Solids.** Vol.69: 381-385.

Wagner, C.D. et al. (1979). The Electron Spectrum Qualitative and Quantitative Interpretation. **X-ray Photoelectron Spectroscopy**. Handbook. Perkin-Elmer, Physical Electronics Division. U.S.A.

Watts, F.J. and Wolstenholme, J. (2003). **An Introduction to Surface analysis by XPS and AES.** The Atrium, Southrn Gate, Chichster, England. 71.

Wikipedia. (2007). **Optical amplifier** [On-line]. Available: http://en.wikipedia.org/ wiki/Optical_amplifier

Wikipedia. (2007). **Soda-lime glass** [on-line]. Available: http://en.wikipedia.org/wiki/ Soda-lime_glass

Wikipedia. (2008). **Electron paramagnetic resonance** [On-line]. Available: http://en. wikipedia.org/wiki/Electron_spin_resonance

Wikipedia. (2008). **X-ray Photoelectron Spectroscopy** [on-line]. Available: http://en.wikipedia.org/wiki/X-ray_photoelectron_spectroscopy

APPENDIX A

DETERMINATION OF PERCENT CRYSTALLINITY

BY XRD

Determination of percent crystallinity by XRD

Percent crystallinity is determined using Ohlberg and Strickler's method.

Percent crystallinity = 100 x (Ig - Ix) /(Ig - Ic) (A1)

Where Ig is the background intensity of glass, Ix that of the specimen and Ic that of the crystal at $2\theta = 23°$. The calibration curve is obtained using mixtures of α-Quartz and parent glass at various ratio (mechanical mixing). Results are shown below. The good linearity is obtained.

Table A1 The calculation of crystallinity using Ohlberg and Strickler's method.

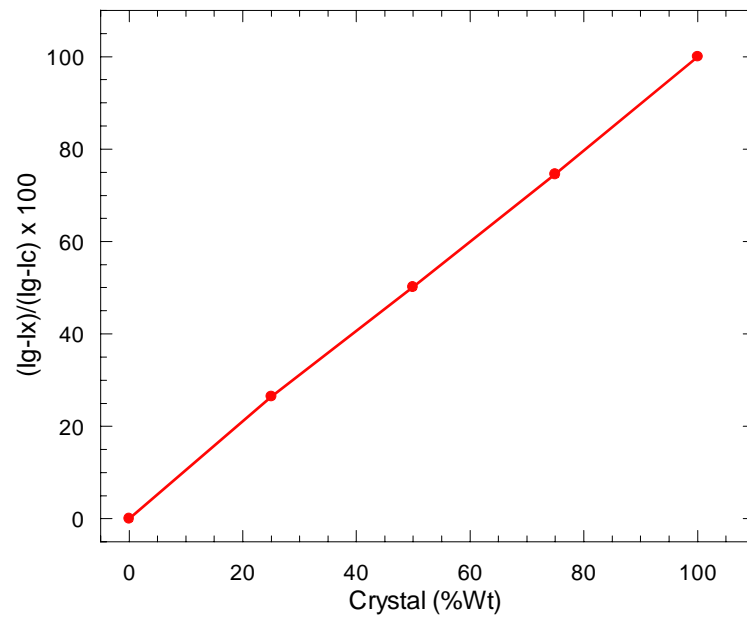| Mixture*		Ig	Ic	Ix	100 x (Ig - Ix) /(Ig - Ic)
Glass	α-Quartz				
100	0	66.7	3.5	66.7	0
75	25	66.7	3.5	19.6	26.42
50	50	66.7	3.5	35	50.16
25	75	66.7	3.5	50	74.53
0	100	66.7	3.5	3.5	100

*; mechanical mixing by wt%

Figure A1 Experimentary determines crystallinity VS calculated crystallinity for mechanical mixture of α-quartz and parent glass.

APPENDIX B

DETERMINATION OF CRYSTALLITE SIZE BY XRD

Determination of crystallite size by XRD

The crystallite size can be calculated using Scherrer's equation.

$$d = 0.9 \cdot \lambda / \beta \cdot \cos\theta \qquad\qquad (B1)$$

where d is crystallite size (Å), λ is the wavelength of X-ray (Cu-Kα, 1.54 Å), β is the true half width (radian) and θ is the diffraction angle (degree). The true half width (line broadening) can be obtained calibration curve (next page).

For example:

Observed half width (line broadening): 0.5 degree

True half width (line broadening): 0.375 degree ($0.375 \times 2\pi/360 = 0.00654$ radian)

Wavelength of X-ray: 1.54 Å (Cu-Kα)

Diffraction angle $2\theta = 26.8$ degree ($\theta = 13.4$ degree, $\cos\theta = 0.9728$)

Thus

$$d = 0.9 \times 1.54/0.00654 \times 0.9728 = 218 \text{ Å} = 22 \text{ nm}$$
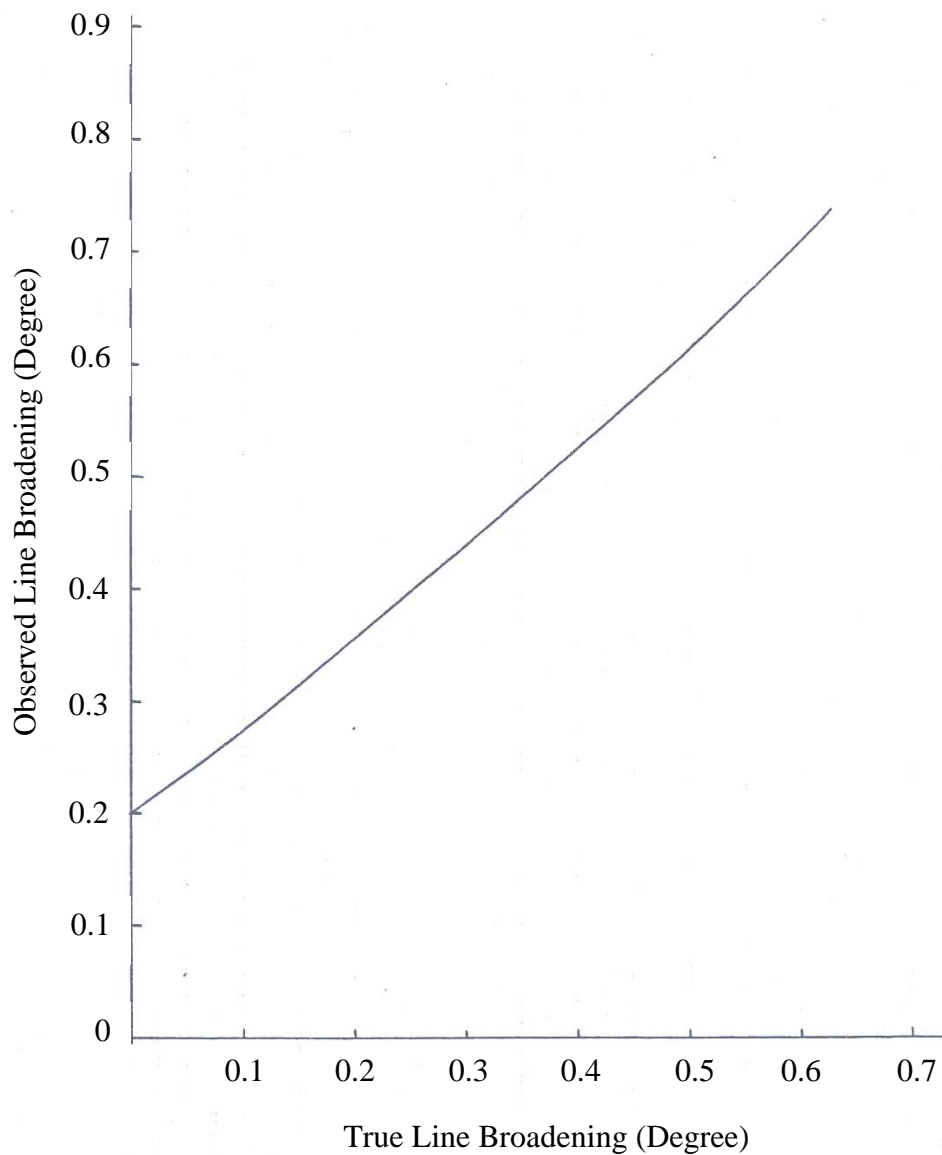
X-ray Line Broadening For AgCl Precipitated In Glass

Figure B1   Calibration curve of X-ray line broadening for AgCl precipitated in glass

by Jone's method (Nitta, 1975).

APPENDIX C

CALCULATION OF OPTICAL BASICITY

Calculation of Optical Basicity

Duffy and Ingram defined the theoretical optical basicity (Λ) as follows:

$$\Lambda = \Sigma(x_i/f_i) \qquad\qquad\qquad (C1)$$

where, x_i is the equivalent cationic fraction and f_i is the basicity moderating parameter for the constituent cation i, respectively (Key to Metals, www, 2008).

Table C1   Optical basicity, Λ for some oxides

Oxides	Λ/Duffy
P_2O_5	0.33
B_2O_3	0.42
SiO_2	0.48
Al_2O_3	0.60
MgO	0.78*
CaO	1.00
SrO	1.10*
BaO	1.15*
K_2O	1.40*
Na_2O	1.15*
FeO	1.00*

*: Reddy, 1999.

Optical basicity,Λ, of glass composition was calculated as follow:

$$\Lambda = X_A\Lambda(A)+ X_B\Lambda(B)+ \cdots\cdots.$$

X_A, X_B,…are the molar proportions contributed by the constituent oxides, A, B,… to the total oxide(-II) content of the glass (that is, the equivalent fractions) and $\Lambda(A)$, $\Lambda(B)$,… are the optical basicity values of these individual oxides (Duffy,1996).

Calculation of Λ for borate glasses

A glass of composition: $90[10Al_2O_3\cdot(80-X)B_2O_3\cdot10ZnO\cdot X\ K_2O]$

X-0; $10Al_2O_3\cdot80B_2O_3\cdot10ZnO$

($9Al_2O_3\cdot72B_2O_3\cdot9ZnO$)

The total oxygen   = (0.09x3) + (0.72x3) +0.09

= 0.27+2.16+0.09

= 2.52

Λ $= \dfrac{(0.72x3)\ (0.42)}{2.52} + \dfrac{(0.09x3)\ (0.6)}{2.52} + \dfrac{(0.09)\ (0.95)}{2.52}$

= 0.36+0.064+0.0339

= 0.4579 ≈ 0.46

X-10; $10Al_2O_3\cdot70B_2O_3\cdot10ZnO\cdot10K_2O$

($9Al_2O_3\cdot63B_2O_3\cdot9ZnO\cdot9K_2O$)

The total oxygen   = (0.09x3) + (0.63x3) +0.09+0.09

= 0.27+1.89+0.09+0.09

= 2.34

Λ $= \dfrac{(0.63x3)\ (0.42)}{2.34} + \dfrac{(0.09x3)\ (0.6)}{2.34} + \dfrac{(0.09)\ (0.95)}{2.34} + \dfrac{(0.09)\ (1.4)}{2.34}$

$$= 0.3392+0.0692+0.0365+0.0538$$

$$= 0.4987 \approx 0.50$$

X-20; $10Al_2O_3 \cdot 60B_2O_3 \cdot 10ZnO \cdot 20K_2O$

$(9Al_2O_3 \cdot 54B_2O_3 \cdot 9ZnO \cdot 18K_2O)$

The total oxygen $= (0.09 \times 3) + (0.54 \times 3) + 0.09 + 0.18$

$$= 0.27+1.62+0.09+0.18$$

$$= 2.16$$

$\Lambda \quad = \dfrac{(0.54 \times 3)(0.42)}{2.16} + \dfrac{(0.09 \times 3)(0.6)}{2.16} + \dfrac{(0.09)(0.95)}{2.16} + \dfrac{(0.18)(1.4)}{2.16}$

$$= 0.315+0.075+0.0396+0.1167$$

$$= 0.5463 \approx 0.55$$

X-30; $10Al_2O_3 \cdot 50B_2O_3 \cdot 10ZnO \cdot 30K_2O$

$(9Al_2O_3 \cdot 45B_2O_3 \cdot 9ZnO \cdot 27K_2O)$

The total oxygen $= (0.09 \times 3) + (0.45 \times 3) + 0.09 + 0.27$

$$= 0.27+1.35+0.09+0.27$$

$$= 1.98$$

$\Lambda \quad = \dfrac{(0.45 \times 3)(0.42)}{1.98} + \dfrac{(0.09 \times 3)(0.6)}{1.98} + \dfrac{(0.09)(0.95)}{1.98} + \dfrac{(0.27)(1.4)}{1.98}$

$$= 0.2864+0.0818+0.0432+0.1909$$

$$= 0.6023 \approx 0.60$$

Borate compositions: X-0; $\Lambda=0.46$

X-10; $\Lambda=0.50$

X-20; $\Lambda=0.55$

X-30; $\Lambda=0.6$

APPENDIX D

LIST OF PUBLICATIONS

List of Publications

I. Papers

Sasithorn Khonthon, Shigeki Morimoto, and Yasutake Ohishi. (2006). Absorption and Emission Spectra of Ni-Doped Glasses and Glass-Ceramics in Connection with Its Co-Ordination Number, **Journal of the Ceramic Society of Japan**. Vol.114: 791-794.

Sasithorn Khonthon, Shigeki Morimoto, Yusuke Arai, and Yasutake Ohishi. (2007). Luminescence Characteristics of Te-and Bi-Doped Glasses and Glass-Ceramics. **Journal of the Ceramic Society of Japan.** Vol.115: 259-263.

Sasithorn Khonthon, Shigeki Morimoto, and Yasutake Ohishi. (2007)**.** Luminescence Characteristics of Ni^{2+} Ion-Doped Glasses and Glass-Ceramics in Relation to its Coordination Number. **Journal of Solid Mechanics and Materials Engineering**. Vol.1: 439-446.

Yusuke Arai, Takenobu Suzuki, Yasutake Ohishi, Shigeki Morimoto, and Sasithorn Khonthon (2007). Ultrabroadband near-infrared emission from a colorless Bi-doped glass. **Applied Physics Letters.** Vol.90: 261110.

Sasithorn Khonthon, Shigeki Morimoto, Yusuke Arai, and Yasutake Ohishi. (2007). Near Infrared Luminescence from Bi-Doped Soda-Lime-Silicate Glasses. **Suranaree Journal of Science and Technology**. Vol.14, No.2: 141-146.

Shigeki Morimoto, Sasithorn Khonthon, and Yasutake Ohishi. (2008). Optical Properties of Cr^{3+} ion in lithium metasilicate $Li_2O \cdot SiO_2$ transparent glass-ceramics. **Journal of Non-Crystalline Solids.** Vol.354: 3343-3347.

Sasithorn Khonthon, Penprapa Punpai, Shigeki Morimoto, Yusuke Arai, Takenobu Suzuki, and Yasutake Ohishi. (2008). On the near-infrared luminescence from TeO_2 containing borate glasses. **Journal of the Ceramic Society of Japan**. Vol.116: 829-831.

Penprapa Punpai, Shigeki Morimoto, Sasithorn Khonthon, Yusuke Aria, Takenobu Suzuki, and Yasutake Ohishi. Effect of carbon addition and TeO2 concentration on the NIR luminescence characteristics of Te-doped soda-lime-silicate glasses. **Journal of Non-Crystalline Solids**. Accepted: 4/08/2008. To be published.

II. Presentations

Sasithorn Khonthon*, Shigeki Morimoto, and Yasutake Ohishi. (2006). Luminescence Characteristics of Ni^{2+} Ion-Doped Glasses and Glass-Ceramics in Relation to its Coordination Number. **Asian Symposium on Materials and Processing 2006.** Proceedings A-16, 9-10/Nov./2006, Bangkok, Thailand [Oral presentation]

Shigeki Morimoto*, Sasithorn Khonthon, and Yasutake Ohishi. (2006). Luminescence Characteristics of Se-, Te- and Bi-Doped Glasses and Glass-Ceramics. **Asian Symposium on Materials and Processing 2006.** Proceedings A-16, 9-10/Nov./2006, Bangkok, Thailand [Oral presentation]

Shigeki Morimoto*, Sasithorn Khonthon, Yusuke Arai, and Yasutake Ohishi. (2006). Luminescence Characteristics of Te- and Bi-Doped Glasses and Glass-Ceramics. **The 47th Symposium on Glasses and Photonics Materials, Glass Division of the Ceramic Society of Japan.** Proceedings 2A-09, 21-22/Nov./2006, Noda, Japan [Oral presentation]

Sasithorn Khonthon, Shigeki Morimoto, Yusuke Arai, and Yasutake Ohishi. (2006). Luminescence Characteristics of Se-Doped Glass. **The 47th Symposium on Glasses and Photonics Materials, Glass Division of The Ceramic Society of Japan**. Proceedings P1, 21-22/Nov./2006, Noda, Japan [Poster presentation]

Shigeki Morimoto, Sasithorn Khonthon, and Yasutake Ohishi. (2006). Is tetrahedrally coordinated Cr^{3+} ion possible in glasses and glass-ceramics. **The 47th Symposium on Glasses and Photonics Materials, Glass Division of The Ceramic Society of Japan.** Proceedings P2, 21-22/Nov./2006, Noda, Japan [Poster presentation]

Sasithorn Khonthon, Shigeki Morimoto*, Yusuke Arai, and Yasutake Ohishi. (2007). Melting temperature and glass composition dependence on the NIR luminescence characteristics of Bi-containing borate glasses. **The 48th Symposium on Glasses and Photonics Materials, Glass Division of The Ceramic Society of Japan**. Proceedings 1A-02, 29-30/Nov./2007, Toyohashi, Japan [Oral presentation]

Sasithorn Khonthon, Penprapa Punpai*, Shigeki Morimoto, Yusuke Arai, and Yasutake Ohishi. (2007). Near-infrared luminescent center of Te-doped glasses. **The 48th Symposium on Glasses and Photonics Materials, Glass Division of The Ceramic Society of Japan.** Proceeding P06, 29-30/Nov./2007, Toyohashi, Japan [Poster presentation]

Sasithorn Khonthon, Shigeki Morimoto*, Yusuke Arai, Takenobu Suzuki, and Yasutake Ohishi. (2008). On the near-infrared luminescence characteristics of Bi-containing borate glasses. **The 3rd Siam Physics Congress 2008 (SPC2008).** Proceedings PA-28, 20-22/March/2008, Khao Yai, Thailand. [Poster presenta tion]

Penprapa Punpai*, Shigeki Morimoto, Sasithorn Khonthon, Yusuke Arai, and Yasutake Ohishi. (2008). Near-infrared luminescent center of Te-doped soda-lime-silicate glasses. **The 3rd Siam Physics Congress 2008 (SPC2008).** Proceedings A-5, 20-22/March/2008, Khao Yai, Thailand. [Oral presentation]

BIOGRAPHY

Sasithorn Khonthon was born on March 23, 1970 in Suphanburi Province, Thailand. She earned her Bachelor Degree in Ceramic Technology from Phranakhon Teachers' College in 1992. After graduation, she was a lecturer at Kanchanaburi Teachers' College from 1992 to 1997. Since 1997 to present, she has been a lecturer of Faculty of Industrial Technology at Phranakhon Rajabhat University and earned her Master Degree in Industrial Technology from Phranakhon Rajabhat University in year 2000. In year 2004, she furthered the study for Doctoral Degree, supported by Phranakhon Rajabhat University, in Ceramic Engineering at School of Ceramic Engineering, Institute of Engineering at Suranaree University of Technology from year 2004 to 2008. During her Doctoral Degree study, she had nine paper presentations and seven paper-published in international journals and one paper published in Suranaree Journal of Science and Technology.